NASA CR-2299

NASA CONTRACTOR REPORT

NASA CR-2299



# PRESSURE RECOVERY PERFORMANCE OF CONICAL DIFFUSERS AT HIGH SUBSONIC MACH NUMBERS

*by Francis X. Dolan and Peter W. Runstadler, Jr.*

*Prepared by*
CREARE INCORPORATED
Hanover, N.H. 03755
*for Lewis Research Center*

NATIONAL AERONAUTICS AND SPACE ADMINISTRATION • WASHINGTON, D. C. • AUGUST 1973

| 1. Report No. NASA CR-2299 | 2. Government Accession No. | 3. Recipient's Catalog No. |
|---|---|---|
| 4. Title and Subtitle PRESSURE RECOVERY PERFORMANCE OF CONICAL DIFFUSERS AT HIGH SUBSONIC MACH NUMBERS | | 5. Report Date July 1973<br>6. Performing Organization Code |
| 7. Author(s) Francis X. Dolan and Peter W. Runstadler, Jr. | | 8. Performing Organization Report No. TN-165<br>10. Work Unit No. |
| 9. Performing Organization Name and Address Creare Incorporated P. O. Box 71 Hanover, New Hampshire 03755 | | 11. Contract or Grant No. NAS 3-15331<br>13. Type of Report and Period Covered Contractor Report |
| 12. Sponsoring Agency Name and Address National Aeronautics and Space Administration Washington, D. C. 20546 | | 14. Sponsoring Agency Code |

15. Supplementary Notes

Project Manager, Jerry R. Wood, NASA Lewis Research Center and U. S. Army Air Mobility R&D Laboratory, Cleveland, Ohio

16. Abstract

The pressure recovery performance of conical diffusers has been measured for a wide range of geometries and inlet flow conditions. The approximate level and location (in terms of diffuser geometry) of optimum performance were determined. Throat Mach numbers from low subsonic ($M_t = 0.2$) through choking ($M_t = 1.0$) were investigated in combination with throat blockage $B_t$ from 0.03 to 0.12. For fixed Mach number, performance was measured over a fourfold range of inlet Reynolds number. Maps of pressure recovery are presented as a function of diffuser geometry for fixed sets of inlet conditions. The influence of inlet blockage, throat Mach number, and inlet Reynolds number is discussed.

| 17. Key Words (Suggested by Author(s)) | 18. Distribution Statement | | |
|---|---|---|---|
| Conical diffusers<br>Diffuser performance<br>Pipe diffusers | Unclassified - unlimited | | |
| 19. Security Classif. (of this report) Unclassified | 20. Security Classif. (of this page) Unclassified | 21. No. of Pages 145 | 22. Price* $3.00 |

* For sale by the National Technical Information Service, Springfield, Virginia 22151

TABLE OF CONTENTS

## SUMMARY

A parametric investigation has been made of the pressure recovery performance of conical diffusers. Geometric variables examined were area ratio and length to throat diameter ratio. Throat Mach numbers from near incompressible ($M_t$ = 0.2) through choking ($M_t$ = 1.0) were studied in combination with throat blockages $B_t$ from 0.03 to 0.12. Inlet Reynolds number $Re_D$ was also included as a variable, and for fixed $M_t$ performance was measured over a fourfold range in $Re_D$.

The primary results are presented as maps of pressure recovery performance as a function of diffuser geometry for fixed sets of inlet conditions. The influences of $B_t$, $M_t$ and $Re_D$ on diffuser performance are discussed.

As in the study of other diffuser types, inlet blockage is the single most important variable affecting conical diffuser pressure recovery performance. All other conditions held constant, a change in $B_t$ from 0.03 to 0.12 can result in a 15 to 20 point drop in pressure recovery. Mach number and Reynolds number have a less pronounced effect on performance.

The performance of the conical diffuser and the square entry, single-plane-divergence diffuser, as measured by their respective highest recoveries, is almost identical for the same inlet conditions.

Extension of the experimental data to the design of diffusers for centrifugal compressors is discussed.

A corollary program was undertaken to determine the influence of wall shape on the performance of diffusers of circular cross section. Four diffusers having both bell and trumpet shapes were tested over the full subsonic Mach number range and with inlet blockages ranging from 0.03 to 0.12. The pressure recovery of conical, bell and trumpet shapes is compared for the same inlet conditions. There is little performance gain to be realized as a consequence of wall contouring of circular cross-section diffusers.

## INTRODUCTION

Diffusing passages, in one form or another, have always played a vital role in obtaining good performance from turbo-machinery and many other flow devices. For example, the small, high pressure ratio centrifugal compressor has undergone extensive development during the last decade. The efficiency of these centrifugal stages has been steadily improved by advancing the performance of all of the stage components. Significant further improvement in efficiency, however, will only be gained by improving the pressure recovery characteristics of the diffusing elements of these machines (Reference 1). It is axiomatic that the diffusers of these high pressure ratio centrifugal stages incorporate multiple parallel diffusing passages. These passages may be any one of a variety of geometric shapes the choice of which depends upon the design intent. In some cases, a particular configuration is dictated by manufacturing costs or other considerations.

While all diffuser geometries are conceptually simple, their performance characteristics, whether it be diffuser static pressure recovery, velocity diffusion, flow unsteadiness, etc., are complicated functions of diffuser geometry, flow inlet conditions and, in some cases, flow exit conditions. The selection of an optimum channel diffuser for a particular task is difficult since it must be chosen from an almost infinite number of cross sectional shapes and wall configurations.

Unfortunately, our analytical tools today are not sufficient to calculate the optimum performance characteristics of passage or channel diffusers over the range of geometries and inlet conditions of interest to the designer. While the prediction of diffuser performance for some inlet conditions and geometries has been shown possible, the performance predicted, in general lies below that of optimum diffusers. Further, although some analytical approaches are successful in part in predicting the optimum geometry for a given class of diffusers, the correlation techniques of necessity must include empirical measurements, e.g. see Reference 2.

Very few diffuser configurations have been investigated in sufficient detail to permit the selection of an optimum diffuser. Of the many classes of diffuser shapes possible, only the pressure recovery performance of the straight-wall, single-plane-divergence diffuser has been surveyed in detail as a function of diffuser geometry and flow inlet variables. Reference 3 reports the final results of such a study and presents diffuser maps which describe to the designer how to select optimum performance diffusers (in terms of pressure recovery) over a wide range of geometric and flow variables.

A novel centrifugal compressor diffuser employing conical channel shapes has recently received much attention. In the literature this diffuser is called the "pipe" diffuser. This configuration appears to offer advantages over other diffuser shapes because tolerances and dimensions can be readily controlled and it is easy to manufacture. There has been some speculation that the "pipe" geometry provides diffuser performance better than that obtained with other channel diffuser shapes. Recent interest has also been shown in the performance of the basic conical diffuser shape because turbine exit diffusers for advanced concept small turbomachinery can be developed around a diffuser geometry of annular cross-section (Reference 4). The purpose of the present program was to provide empirical performance data for a family of conical (and near-conical) diffusing passages over a sufficiently wide range of geometric parameters and fluid dynamic inlet conditions to be able to define the maximum pressure recovery for this basic diffuser configuration.

The important inlet conditions included for study were the range of throat Mach numbers from near incompressible flow to throat choke. Inlet flow blockage and throat Reynolds numbers germane to current small centrifugal compressor diffuser designs were used in the program.

The work reported presents the measured pressure recovery of these conical diffusers in the form of the diffuser performance maps that display pressure recovery performance for the conical diffuser as a function of the inlet flow conditions.

## TECHNICAL APPROACH

The straight-wall, conical diffuser geometry studied in this program is shown in the figure below.

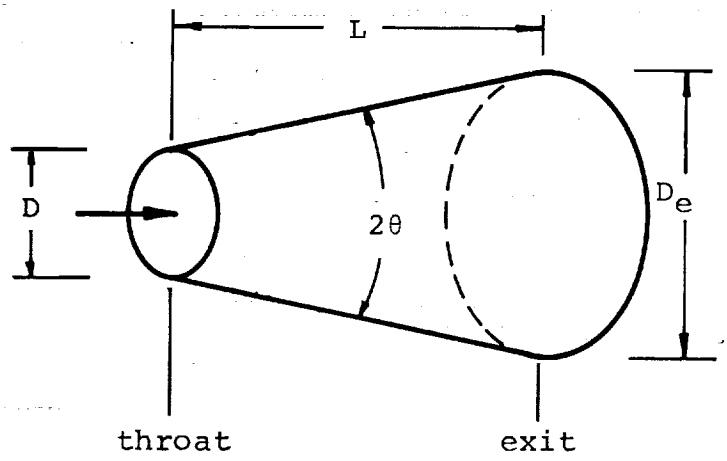


This geometry can be described in terms of two non-dimensional parameters:

AR = area ratio = diffuser exit area to inlet area ratio
L/D = channel centerline length to channel throat diameter ratio

A third diffuser geometry variable:

2θ = diffuser included divergence angle

is often employed in describing diffuser geometry. Diffuser divergence angle 2θ can be prescribed in terms of AR and L/D as follows:

$$\tan\theta = \frac{\sqrt{AR} - 1}{2\ L/D} \qquad (1)$$

The straight-centerline, conical diffuser is geometrically a simpler configuration than other diffusers. Straight-channel, single-plane-divergence diffusers, reported in Reference 3, require three non-dimensional parameters to describe their geometry:

AR = area ratio

L/W = channel centerline length to throat width ratio

AS = throat aspect ratio

The conical diffuser is equivalent, in effect, to a single aspect ratio of the single-plane-divergence diffuser family. As a result, the number of tests required to define the performance of the entire conical diffuser family is reduced to the number required for one aspect ratio of the single-plane-divergence diffuser family.

In defining its characteristics, the diffuser can be treated as a unit flow component. While the characteristics of the diffuser component are determined by a large number of parameters, it is useful for the purposes of this report to classify these parameters into two general groups:

1) geometric parameters
2) inlet flow parameters

For the conical diffuser, the number of separate geometric (non-dimensional) parameters required to define Group 1 above is two: any combination of area ratio, dimensionless length, or equivalent cone angle will specify the diffuser geometry.

The important inlet flow parameters (Group 2) are given in Table I.

Of the variables in Table I, this study has been limited to a consideration of Mach number, throat blockage and Reynolds number. When the inlet velocity profile distribution into the channel diffuser is nearly uniform and the flow has thin boundary layers, experiments have shown that diffuser performance correlates on throat blockage, defined as

$$B_t = 1 - \frac{A_{effective}}{A_{geometric}} \qquad (2)$$

TABLE I - INLET FLOW PARAMETERS

1. Throat blockage
2. Throat Reynolds number
3. Throat Mach number
4. Inlet swirl
5. Inlet flow spatial distortion
   a. stream
   b. wall
6. Inlet flow temporal distortion
   a. turbulence level and form
   b. pulsations in the bulk flow
   c. wake interactions
   d. acoustic interactions

Throat blockage is believed to be the most important inlet parameter affecting conical diffuser performance. Mach number and Reynolds number were investigated to determine if the morphology of the pressure recovery performance maps was significantly altered over the range of diffuser throat Mach number and Reynolds number anticipated in small centrifugal compressors.

Therefore, this study has measured the pressure recovery characteristics of the conical diffuser over a range of values of the following independent parameters:

AR = area ratio
L/D = non-dimensional length parameter
$B_t$ = inlet blockage
$M_t$ = inlet Mach number
$Re_D$ = inlet Reynolds number

The experimental program and procedures structured to do the foregoing are described next.

## EXPERIMENTAL PROGRAM

Discussed in this section are the apparatus and instrumentation used in the test program, and the procedures followed

in acquiring, reducing, and presenting the diffuser pressure recovery data.

## Flow Loop and Pressure, Flow and Temperature Control

A closed loop wind tunnel was used to provide and maintain a flow of clean, dry air to the diffuser test section at controlled pressure and temperature levels. Figure 1 is a schematic diagram of the loop and its pressure, flow and temperature controls.

A single stage, screw compressor circulated air around the loop. Foam filled tanks and Helmholtz branch resonators were installed on the inlet and discharge piping of the compressor to minimize the level of pressure fluctuations transmitted to the test section from the compressor. The temperature of the air leaving the compressor was reduced to approximately the level of the surroundings in a water-cooled heat exchanger before being passed to the flow metering nozzle. Following the heat exchanger, a bypass line and control valve were used to return cooled, excess air to the compressor inlet.

Makeup air, used to compensate for leaks in the main compressor piping and for initially filling the system, was provided from an auxiliary compressor. An oil mist filter and water desiccator were used to reduce oil levels in the makeup air to less than two parts per million, and to depress the dew point of the makeup air to about -35°C.

A calibrated flow nozzle was placed just upstream of the diffuser test section for measuring the flow rate of air entering the diffusers. The nozzle and its upstream and downstream piping and pressure taps were designed in accordance with standard practice (Reference 5). Calibration of the nozzle was performed by the Colorado Engineering Experiment Station, Inc., in June 1971, and again in June 1972 at extended inlet Reynolds number ranges. The results of these calibrations are shown in Figure 2 as a plot of nozzle discharge coefficient $C_d$ versus nozzle throat Reynolds number $Re_d$. A least squares curve fitting procedure was used to fit a third order polynomial expression to the data. The fitted equation is shown as a solid line through the data points. The variance of the data from the analytical expression lies within an uncertainty band of $2\sigma = 0.0017$ around the mean line.

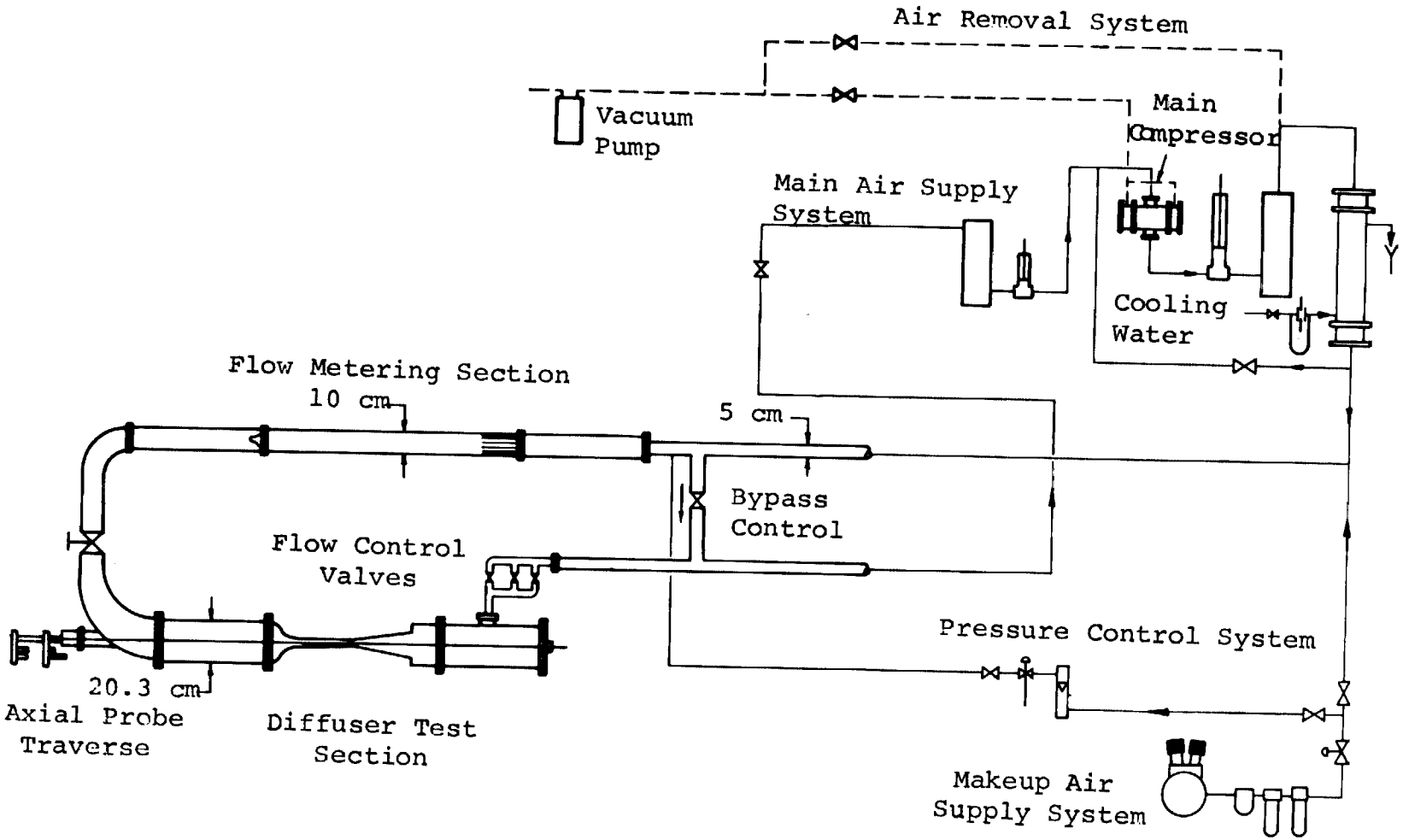


Figure 1 - Conical Diffuser Test Loop

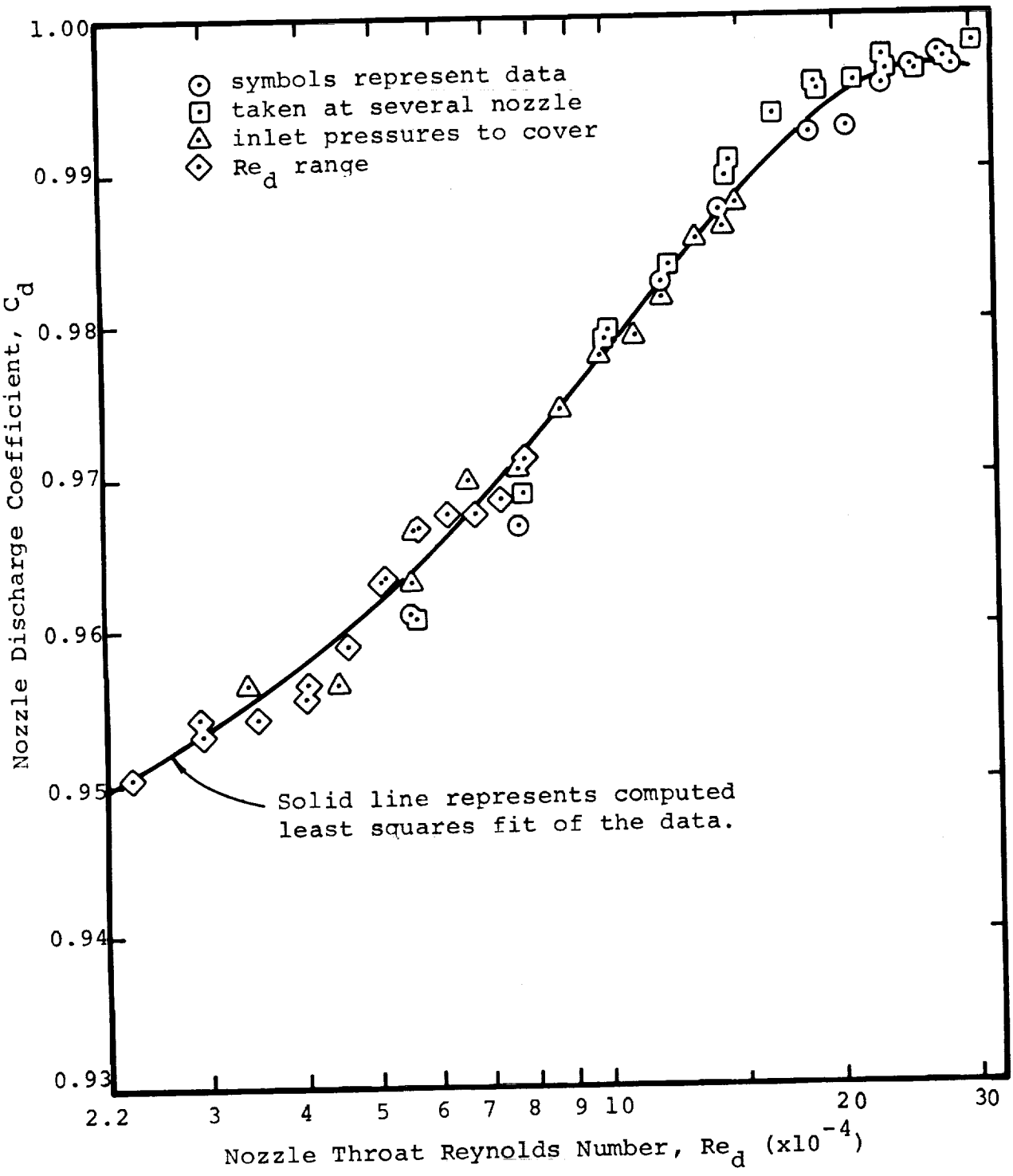


Figure 2 - Flow Metering Nozzle Calibration

A 20.3 cm diameter inlet plenum six diameters in length was located downstream of the flow meter. A nozzle was used to accelerate the flow from this plenum to the inlet of the diffuser test section. The design of the nozzle and the inlet and diffuser blocks will be discussed in greater detail in the next section. The diffuser flow passage was terminated by "dumping" the flow into a downstream plenum or collector, also 20.3 cm in diameter. The discharge dump area ratio varied from 20 to 160. From this point the flow passed through a set of control valves and was returned to the inlet of the main compressor.

The desired throat stagnation pressure $p_{ot}$ was set and maintained by continuously removing air from the system, either to the inlet of a vacuum pump or to atmosphere (depending on the level of $p_{ot}$) and by supplying makeup air through a precision pressure regulator. This regulator had a rated sensitivity of 0.07 $kN/m^2$ ; i.e. it was designed to respond to this small a deviation from the set point. In practice it was found that $p_{ot}$ could be held within this specification by controlling the makeup air supply rate through the regulator.

The flow rate of air through the diffuser test section, and therefore the throat Mach number, was set by manually adjusting the bypass control valve and the throttle valves at the outlet of the downstream plenum, while maintaining a fixed $p_{ot}$. This combination of controls permitted operation with diffuser throat stagnation pressures from 54.5 $kN/m^2$ absolute to 218 $kN/m^2$ absolute and over the full range of subsonic diffuser throat Mach numbers from 0.2 to 1.0.

## Test Section and Diffuser Design

The main test section, shown in cross section in Figure 3, consisted of an inlet nozzle, boundary layer growth blocks, the diffuser assembly and a dump plenum. All components manufactured for this program were fabricated from aluminum.

Inlet nozzle and boundary layer growth blocks. Available air pumping capacity and inlet stagnation pressure levels dictated the use of a 1.27 cm diffuser throat diameter.

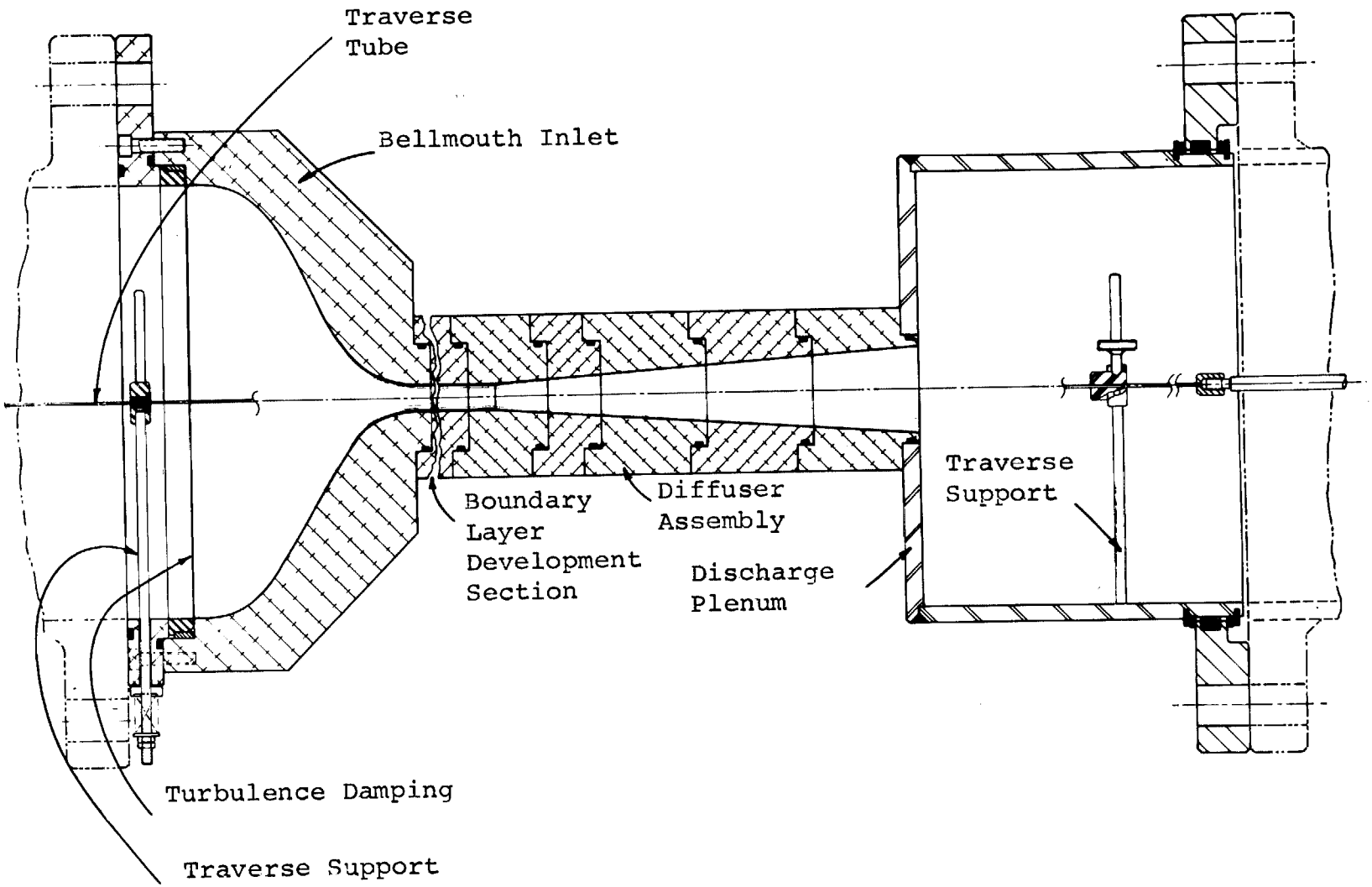


Figure 3 - Main Test Section Components

Thus, an inlet nozzle was required to provide an acceleration of the flow from the 20.3 cm diameter plenum to the 1.27 cm constant diameter boundary layer growth section. The nozzle profile was laid out as shown in the sketch below.

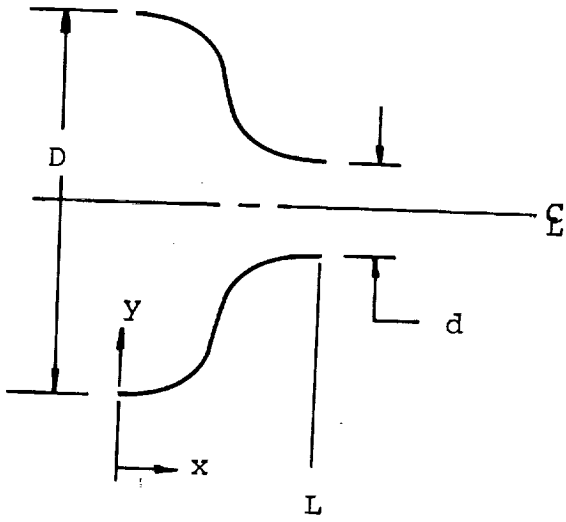


$$y = \left(\frac{D-d}{2}\right)\frac{x}{L} - \left(\frac{D-d}{4\pi}\right)\sin 2\pi\frac{x}{L} \qquad (3)$$

The inlet nozzle also contained a support for an axial traverse probe. A fine mesh wire screen (stainless steel, square-weave with 0.055 mm wires on 0.125 mm centers) was placed at the beginning of the nozzle contraction to reduce the level of turbulence of the inlet flow.

At the exit of the nozzle was a 2.54 cm long block (1.27 cm diameter flow passage) having a machined circumferential groove, 0.75 mm deep by 3.2 mm wide. This groove was provided to promote transition of the boundary layer from laminar to turbulent flow as it entered the boundary layer growth section. (A discussion of the effectiveness of this trip is given beginning on page 103.)

Throat blockage is defined as unity minus the ratio of the effective flow area to the geometric flow area. For an axisymmetric passage of diameter D, blockage can be expressed as a function of the boundary layer displacement thickness $\delta^*$:

$$B_t = 4\frac{\delta^*}{D}\left(1 - \frac{\delta^*}{D}\right) \qquad (4)$$

An increase in inlet boundary layer displacement thickness through the constant diameter inlet section is approximately proportional to the passage length x, and inversely proportional to some power of the unit Reynolds number $Re_x$:

$$\delta^* \propto x(Re_x)^{-n} \qquad (5)$$

So, by adjusting the length of the inlet section, for a fixed flow rate and $p_{ot}$, the displacement thickness at the diffuser throat was controlled to provide the range of throat blockage values from 0.03 to 0.12.

The boundary layer growth blocks were designed to permit variations in the length of this section. Five different combinations of inlet blocks were used, providing a total inlet length of from one to twelve times the inlet diameter. The inlet lengths listed in various tables and figures in this report are the lengths of the constant diameter (1.27 cm) flow passage following the boundary layer trip block.

Conical diffuser design. The diffusers were installed immediately downstream of the inlet section. All diffusers were assembled from a series of truncated conical sections of constant divergence angle $2\theta$. Various ratios of diffuser length to throat diameter, and so area ratios, were obtained by assembling appropriate mating conical sections. The first block in each assembly, called the throat block, included a 1.27 cm long constant diameter (1.27 cm) section which was followed by a sharp entry into the diverging passage. Table II lists the several diffuser and inlet geometry combinations tested.

All of the geometry sections were designed and manufactured to maintain a straight centerline when assembled together. The final boring operation of the diffusing channel was done simultaneously on all blocks of a common divergence angle. This resulted in a smooth transition between adjacent sections with no detectable step. Radial misalignment was minimized by having a very tight fit between mating sections. Also, locating pins were used to ensure that the blocks were assembled for testing such that their relative positions were the same as when manufactured. The diffuser and inlet blocks were joined together by longitudinal tie rods passing through

the walls of the blocks and terminating in a threaded connection in the inlet nozzle.

TABLE II - CONICAL DIFFUSER GEOMETRIES AND INLET LENGTHS

| Divergence Angle 2θ | Length to Throat Diameter Ratio L/D | Inlet Lengths (cm) |
|---|---|---|
| 3° | 16, 25 | 1.27,4.45,7.95,12.05,15.55 |
| 4° | 4*, 8, 12, 16, 25 | " |
| 6° | 25 | " |
| 8° | 2*, 4, 8, 12, 16 | " |
| 12° | 2*, 4, 8, 12 | " |
| 16° | 2*, 4, 8 | " |

* these L/D values used only at $p_{ot}$ = 109 kN/m$^2$

Static pressure taps (0.3 mm diameter) were drilled perpendicular to the walls of the diffuser sections, in a straight line from the throat region to the exit plane. Four taps were placed in the vicinity of the geometric throat (two upstream, one at the throat and one downstream). These taps covered a lengthwise span of 9.5 mm and were used to help locate the position of the minimum pressure used in defining the diffuser "throat". The remaining taps in the diffuser were spaced such that at least six additional wall pressure readings were available for each L/D tested. At the diffuser exit, four taps were located around the circumference and 1.0 mm upstream of the true exit plane. All four taps were read during the testing and the average used to calculate the exit pressure. The maximum spread among these four readings was never greater than 0.25% of the mean value.

Axial traverse probe. In addition to the wall taps, a traversing pressure probe was located along the centerline of the test section. The probe was made from a 1.27 mm diameter tube (stainless steel, hypodermic grade tubing, 0.2 mm wall thickness) one meter in length. Two 0.33 mm holes were drilled into the tube wall with an axial spacing between the holes of 20 cm. A plug was located in the tube between holes. This probe could be traversed over a 25 cm range and, by selecting either of the two pressure taps in the tube, the static pressure was measured at the channel centerline over a span some 45 cm in length. The axial location of the holes relative to a fixed point in the flow channel, e.g. the diffuser throat, could be determined to an accuracy of 0.13 mm. The probe was accurately centered in the flow passage by means of support spiders in the upstream and downstream plenums. An axial tensioning system was used to minimize the deflection of the tube, such as might be caused by vibrations, over its unsupported length.

For each test run, the probe was traversed in the vicinity of the geometric throat in order to locate the minimum pressure. This minimum pressure location was then defined as the aerodynamic throat. Additional measurements were made with the traverse probe (at the beginning of the program) of the pressure profile from the inlet section and on through the diffuser.

Discharge plenum. The flow from the diffusers was "dumped" into a 20.3 cm diameter discharge plenum chamber. This chamber was bolted tightly to the final diffuser block and, by means of a flexible coupling, was fixed to the downstream piping.

Non-conical diffuser design. Several diffusers were tested in this program which, though circular in cross-section, were of a non-conical area schedule. Two general classes of these non-conicals were examined: trumpet-shape and bell-shape. The area ratio variation for these diffusers closely follows the practice adopted by Carlson, et al (Reference 6) in their investigation of two dimensional diffusers.

$$AR(x) = 1 + (AR-1) \frac{x}{L} \left[1 + \alpha \left(1 - \frac{x}{L}\right)\right] \qquad (6)$$

The sketch below shows the general wall shapes produced by this relationship.

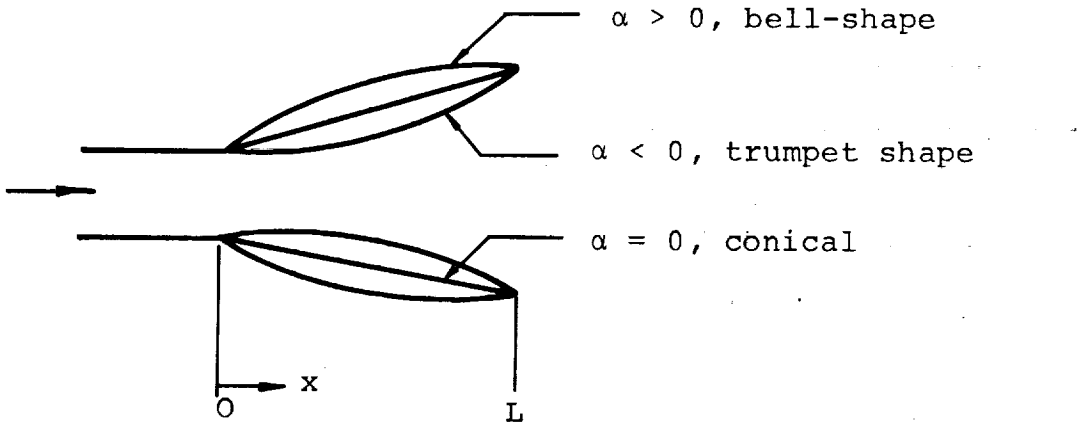


In Equation (6), AR is the area ratio defined by the square of the ratio of exit and inlet diameters, and $\alpha$ is a geometry parameter defining the general wall shape. For the present study, this parameter was chosen as + 1.0 for the bell shapes and - 1.0 for the trumpets. All of the conicals tested have $\alpha = 0$, by definition.

Within each general class, two non-conicals were fabricated and tested. The area ratios selected corresponded to those for a conical diffuser of $2\theta = 6°$ and for L/D = 8 and 12, resulting in area ratios of 3.4 and 5.1, respectively. These four diffusers were tested at a single throat total pressure level ($p_{ot}$ = 109 kN/m$^2$ absolute) and over the full range of subsonic Mach numbers and throat blockages from 0.03 to 0.12.

## Instrumentation

Following is a discussion of the instruments used for measuring the data needed to calculate the diffuser performance variables. Also presented is their method of use and calibration and an estimate of their uncertainty, where appropriate.

Temperature measurements. Dial type, insertion stem thermometers were used to measure the temperature of the air at the inlet to the flow meter and again in the plenum upstream of the test section.

The temperature of the air leaving the compressor was controlled such that it approached the ambient temperature in the test laboratory. By controlling the air temperature in this fashion, heat transfer to or from the surroundings had a minimal effect on the temperature of the flow loop. As a result, indicated temperatures in the loop were always within $\pm$ 2°C of room temperature which was measured with a secondary standard mercury thermometer.

This laboratory standard thermometer was checked at the ice and boiling points of water and was found to repeatedly correctly indicate these temperatures. The dial-stem thermometers were calibrated against this standard over the narrow range of expected ambient conditions (15°C to 25°C) and were found to differ from the standard by less than $\pm$ 1.5°C at any point. Consequently, all temperature measurements were recorded directly from the dial thermometers since the indicated errors were small in relation to the absolute temperature levels.

Pressure measurements. During the testing program, all pressure data (except atmospheric pressure) that were used to calculate diffuser performance were measured with calibrated transducers. Two transducers were of the strain gauge type with differential pressure ranges of $\pm$ 17.3 kN/m$^2$ and $\pm$ 138 kN/m$^2$. The third transducer was a sensitive, variable reluctance unit with a differential range of $\pm$ 3.45 kN/m$^2$. The output from these transducers was recorded on a digital millivoltmeter with resolution to 10 microvolts.

A mercurial barometer was used for measuring atmospheric pressure as a reference data point at the beginning of each testing sequence.

Due to the great number of pressure taps in place in the diffusers and through the flow loop (as many as 40 for some configurations) a system of wafer-type pneumatic switches was employed to facilitate routing of the pressures to any of the three transducers. This system also permitted referencing each pressure against either atmospheric pressure or

the inlet plenum pressure. The differential pressure across the flow meter was read directly without referencing to a third pressure, to minimize errors. Final recorded data were always measured on the most sensitive transducer for which the range of the transducer was not exceeded. As a check, the same pressure was sometimes recorded on the transducer with the next higher sensitivity, and the results compared.

A combination of water and mercury manometers were utilized for calibrating the pressure transducers and for checking the calibrations over the course of the program. Miscellaneous pressure gauges were used to assist in setting flow conditions and for monitoring the operation of the main compressor. No final data were recorded from any of these gauges.

Barometer calibration. The barometer used had a vernier scale which permitted readings as small as 0.1 mm of mercury. Atmospheric pressures recorded on this instrument were checked against the readings with similar barometers at Dartmouth College and at the U. S. Army Cold Regions Research and Engineering Laboratory, both located in Hanover, N. H. After suitable corrections for altitude differences, the three instruments agreed to within 0.5 mm of mercury, and this has been used as the uncertainty (at 20:1 odds) in the observed barometric pressure.

Transducer calibration. The three pressure transducers were each calibrated several times during the course of the test program, and were checked from time to time to ensure that they were following the prescribed calibration curves.

For calibration purposes, the standards used were water and mercury manometers. These were considered to be secondary standards with probable uncertainties (consisting primarily of a capillary error, see Reference 7) of 3.0 mm of water and 2.0 mm of mercury, respectively.

The digital voltmeter used was calibrated by an outside laboratory and certified to be within the manufacturers specifications, 0.05% of reading, plus or minus 10 micro-volts. This calibration is traceable to the National Bureau of Standards.

A typical calibration involved the application of a differential pressure to the transducer and to the appropriate

reference manometer simultaneously. The transducer excitation voltage was set by adjusting a bridge resistance and all future uses of the transducer were referenced to this excitation level. Output voltage and manometer deflection and temperature were recorded at each calibration point. Both positive and negative differentials were applied with as many as 50 readings constituting a calibration. These data were reduced and a straight line fit applied, using a least squares method. The calibration data were compared to the resultant expression in order to calculate the variance of the data and to assign an uncertainty to the fitted expressed. The total uncertainties for each transducer calibration (including manometer and voltmeter errors) are listed in Table III.

TABLE III - ESTIMATED UNCERTAINTY BAND FOR TRANSDUCERS EMPLOYED IN TEST PROGRAM

| Transducer | Range ($kN/m^2$) | Total Uncertainty ($kN/m^2$) |
|---|---|---|
| Low Range | 0.5 - 3.5 | 0.033 |
| Medium Range | 3.5 - 17.0 | 0.039 |
| High Range | 17.0 - 130.0 | 0.38 |

These instrument errors were used to estimate the uncertainty in the reported primary experimental data.

## Data Acquisition

The methods of acquiring diffuser performance data are best understood by discussing the procedures followed in the test program:

1. The desired inlet and diffuser geometry was assembled and installed in the test section. All pressure taps from the diffuser were connected to the appropriate locations in the pneumatic switching system.

2. After closing up the test section, the loop was evacuated and then repressurized with dried, oil-

free air from the makeup compressor. At this point the test section was checked for leaks; from the flow meter through the discharge plenum a leak-tight condition was maintained. The main compressor was brought on line and the desired throat total pressure $p_{ot}$ set by means of the pressure control system.

3. While $p_{ot}$ was being controlled, the flow rate was set to give the desired throat Mach number $M_t$. This was determined by monitoring and adjusting to a predetermined level the static pressure level (for fixed $p_{ot}$) just upstream of the diffuser geometric throat. Using this approach, it was possible to set $M_t$, as measured by the traverse tube static pressure, very close to the specified values of 0.2, 0.4, 0.6, 0.8 and 1.0.

4. After the system had reached equilibrium ($p_{ot}$ and $T_{ot}$ steady and $M_t$ set as desired) all data were recorded on a standard format. The axial pressure probe was traversed to determine the minimum pressure. The location and indicated pressure of the traverse tube then defined the aerodynamic "throat" conditions.

5. Following the recording of the data, the operator changed the flow rate to achieve a new $M_t$ while maintaining $p_{ot}$ constant and step 4 was repeated until all five $M_t$ values had been run. These five tests constituted a "run" and the data were reduced as a set.

6. The next step in the testing procedure involved changing $p_{ot}$ (to change inlet Reynolds number) and repeating steps 3, 4 and 5. In all, three $p_{ot}$ levels were used, resulting in 15 data points for pressure recovery for each combination of inlet and diffuser geometry. Table IV lists the Reynolds number for each $p_{ot}$ and $M_t$ combination.

7. When all tests for the particular geometry were completed, the loop was shut down and the geometry changed. Five different inlet configurations were used, in combination with twenty diffuser geometries. These various geometry and flow combinations resulted in some 1100 data points, excluding repeat runs.

In addition, wall static pressure readings were measured and recorded for each test run. This information was collected mainly as a check on the operation of the loop and only in a few cases have pressure profiles been reduced and plotted from the raw data.

TABLE IV - DIFFUSER THROAT REYNOLDS NUMBER

| Throat Total Pressure $P_{ot}$ | Throat Mach Number $M_t$ | Throat Reynolds Number $Re_D$ |
|---|---|---|
| 54.5 kN/m$^2$ | 0.2 | 30,000 |
| | 0.4 | 57,000 |
| | 0.6 | 78,000 |
| | 0.8 | 93,000 |
| | 1.0 | 101,000 |
| 109 kN/m$^2$ | 0.2 | 60,000 |
| | 0.4 | 114,000 |
| | 0.6 | 156,000 |
| | 0.8 | 186,000 |
| | 1.0 | 202,000 |
| 218 kN/m$^2$ | 0.2 | 120,000 |
| | 0.4 | 227,000 |
| | 0.6 | 312,000 |
| | 0.8 | 371,000 |
| | 1.0 | 404,000 |

The data needed to determine diffuser pressure recovery performance were the barometric pressure, stagnation pressure and temperature in the inlet plenum, and throat and exit plane static pressures. To determine throat blockage, the temperature and pressure at the flow meter inlet and flow meter differential were required.

## Data Reduction

The results of this test program are presented in terms of the measured pressure recovery $C_p$ for fixed throat Mach number $M_t$, blockage $B_t$, and inlet Reynolds number $Re_D$.

Static pressure recovery. The static pressure recovery coefficient is defined as the increase in measured static pressure between the throat and exit plane, divided by the total dynamic head at the throat.

$$C_p = \frac{p_e - p_t}{p_{ot} - p_t} \tag{7}$$

In this study, $p_e$ was measured on the wall at the exit plane and $p_t$ is measured along the diffuser centerline, and is the minimum pressure recorded in the vicinity of the geometric throat. Throat total pressure, $p_{ot}$, is measured as the total pressure in the upstream plenum; i.e. an isentropic core flow is assumed to exist from the inlet plenum to the throat.

Throat Mach number. The throat Mach number was calculated from the measured throat static and total pressures, again assuming an isentropic core flow from the inlet to the throat.

$$M_t^2 = \frac{2}{k-1}\left[\left(\frac{p_{ot}}{p_t}\right)^{\frac{k-1}{k}} - 1\right] \tag{8}$$

For all data reported in this study, the diffuser throat location is defined as the point of minimum pressure in the region of the geometric throat, as determined from the traverse pressure probe measurements.

Throat blockage. Blockage at the diffuser throat is defined in terms of the ratio of the actual mass flow through the diffuser throat to the ideal, one-dimensional flow for a passage with the same geometric area, throat stagnation temperature and pressure and measured throat static pressure.

$$B = 1 - \frac{\dot{m}_{actual}}{\dot{m}_{ideal}} \tag{9}$$

The actual mass flow, $\dot{m}_{actual}$, is measured with the calibrated flow meter upstream of the test section. The ideal mass flow, $\dot{m}_{ideal}$, is calculated from one-dimensional, isentropic flow considerations:

$$\dot{m}_{ideal} = \sqrt{\frac{k}{R}} \frac{p_{ot} A_t}{\sqrt{T_{ot}}} \frac{M_t}{\left(1+\frac{k-1}{2} M_t^2\right)^{\frac{k+1}{2(k-1)}}} \tag{10}$$

Throat Reynolds number. The diffuser throat Reynolds number is defined by

$$Re_D = \frac{VD}{\nu} \tag{11}$$

where:

V is the throat core velocity
D is the diameter of the throat
$\nu$ is the fluid kinematic viscosity at the throat conditions.

The throat core velocity is calculated from the previously determined throat Mach number:

$$V = \frac{M_t}{\sqrt{1 + \frac{k-1}{2} M_t^2}} \sqrt{kRT_{ot}} \tag{12}$$

Calculated pressure recovery coefficient. A second diffuser performance parameter was also determined and given the name "calculated" pressure recovery $C_{pc}$ to distinguish it from the measured performance $C_p$.

$$C_{pc} = \frac{p_e - p_t}{\bar{p}_{ot} - p_t} \tag{13}$$

where:

$\bar{p}_{ot}$ is a "mass-averaged" throat stagnation pressure; i.e. the throat stagnation pressure which would have to exist given the measured mass flow ($\dot{m}_{actual}$) and throat static pressure and stagnation temperature and throat geometric area.

The ratio of the calculated to measured pressure recovery coefficients is very closely given by the expression

$$\frac{C_{pc}}{C_p} \simeq \frac{1}{(1-B_t)^2} \tag{14}$$

with only a small compressibility factor error. A more detailed derivation of $C_{pc}$ is found in Appendix A along with a graphical relationship among $C_p$, $C_{pc}$, $B_t$ and $M_t$. All of the data are reported in terms of the measured pressure recovery coefficient; however, given the measured blockage values, a simple conversion can be made, if desired.

## Data Processing

Because of the large amount of data generated in this program, a routine procedure was adopted for processing the data from the "raw" form all the way through to the plotting of the final performance maps.

A digital computer was used in the first stage of this procedure to calculate throat Mach number, the actual and ideal mass flow rates, throat blockage, the measured and calculated pressure recovery coefficients and throat Reynolds

number. The computer printout from a typical run is shown in Figure 4.

The remaining steps in the data reduction process involve plotting, tabulating, and cross-plotting of the reduced performance data in the following sequence:

1. Pressure recovery $C_p$ is plotted as a function of throat Mach number for fixed inlet and diffuser geometries (Figure 5). All measured blockage data for a fixed inlet length and Reynolds number (combination of $p_{ot}$ and $M_t$) are averaged together. The averaged $B_t$ vs $M_t$ data are shown in Figures 6, 7 and 8. Further discussion of the handling and interpretation of the blockage data and interpolation of the $B_t$ vs $M_t$ curve is found in Appendix B.

2. Values of $C_p$ at $M_t$ = 0.2, 0.4, 0.6, 0.8 and 1.0 are tabulated from the plots, for constant inlet length and diffuser geometry and fixed $p_{ot}$. From the averaged values of $B_t$ vs $M_t$, throat blockages at the five $M_t$ levels are tabulated.

3. Cross-plots of $C_p$ vs $B_t$ are made for each diffuser geometry combination (2θ and L/D), throat Mach number and inlet Reynolds number. From these curves, $C_p$ values are tabulated at throat blockages, $B_t$ = 0.03, 0.06, 0.09 and 0.12. Figure 9 shows $C_p$ vs $B_t$ curves for two diffuser geometries at identical inlet conditions.

4. Using the tabulated $C_p$ values, cross-plots of $C_p$ vs divergence angle 2θ and $C_p$ vs length to throat diameter ratio L/D are made for constant inlet conditions of $M_t$, $B_t$ and $Re_D$. Typical examples of these geometry cross plots are shown in Figures 10 and 11.

CONICAL DIFFUSER STUDY

I. DIFFUSER GEOMETRY
   1) DOUBLE ANGLE = 8 DEGREES
   2) L/D RATIO = 16
   3) BLOCKAGE LENGTH = 1.27 CM
   4) AREA RATIO = 10.577

II. HIGH LEVEL REYNOLDS NUMBER TESTS (RE=400,000 @ M=1)

III. SUMMARY OF REDUCED DATA FOR 8/ 15/ 72

| RUN NOS. | $\dot{M}_A$ (KG/SEC) | $\dot{M}_T$ | MACH NO. | BLOCK | CP-1 MEAS | CP-2 CALC | REY NO. |
|---|---|---|---|---|---|---|---|
| 81603. .2 | .021 | .0218 | .201 | .036 | .783 | .841 | 121510. |
| 81603. .4 | .0395 | .0404 | .399 | .024 | .776 | .816 | 229059. |
| 81603. .6 | .0516 | .0537 | .59 | .039 | .769 | .835 | 312582. |
| 81603. .8 | .0594 | .0619 | .789 | .04 | .76 | .828 | 373872. |
| 81603. 1 | .0624 | .0645 | 1.002 | .033 | .763 | .819 | 408888. |

```
3000  DATA 5,2,8,15,72,31.6
3001  DATA 81603.,.2,71,65,70,29.504,19.15,2,57.47,3
3002  DATA 18.83,2,-14.31,1,-39.99,-39.9,-39.99,-39.99,3
3003  DATA 81603.,.4,71,64.5,70,29.504,19.8,2,15.19,1
3004  DATA 18.83,2,-3.6,2,-12.01,-12.02,-12,-12.01,1
3005  DATA 81603.,.6,71,64.5,69,29.504,20.48,2,25.77,1
3006  DATA 18.82,2,-7.26,2,-25.04,-24.96,-24.98,-25.01,1
3007  DATA 81603.,.8,71,66,69,29.504,21.06,2,34.25,1
3008  DATA 18.86,2,-11.69,2,-2.8,-2.8,-2.8,-2.8,2
3009  DATA 81603.,1,71,66,69,29.504,21.29,2,37.83,1
3010  DATA 18.85,2,-16.4,2,-3.88,-3.88,-3.88,-3.87,2

END
```

Figure 4 - Computer Output from Typical Test

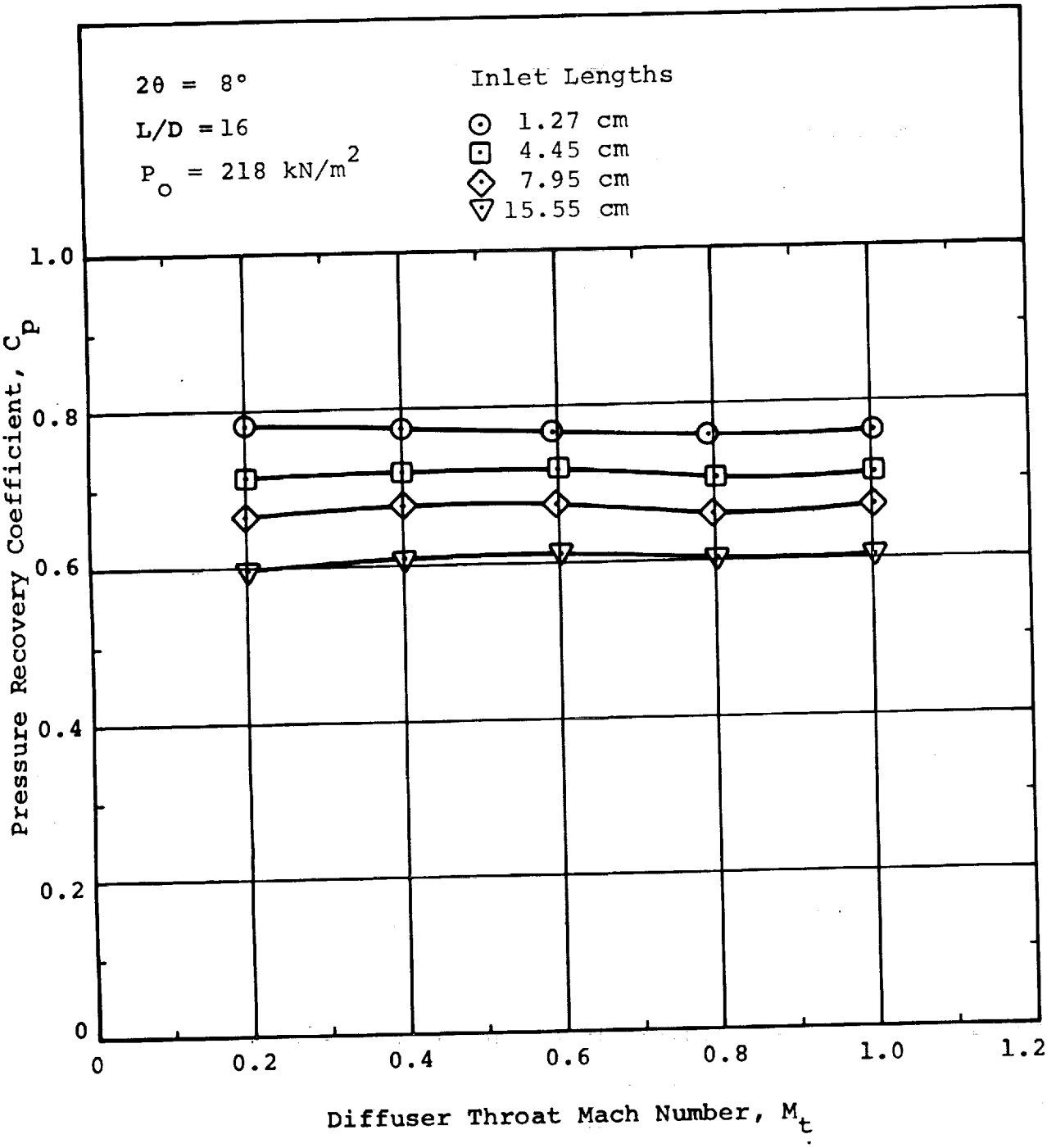


Figure 5 - Diffuser Pressure Recovery Versus Mach Number

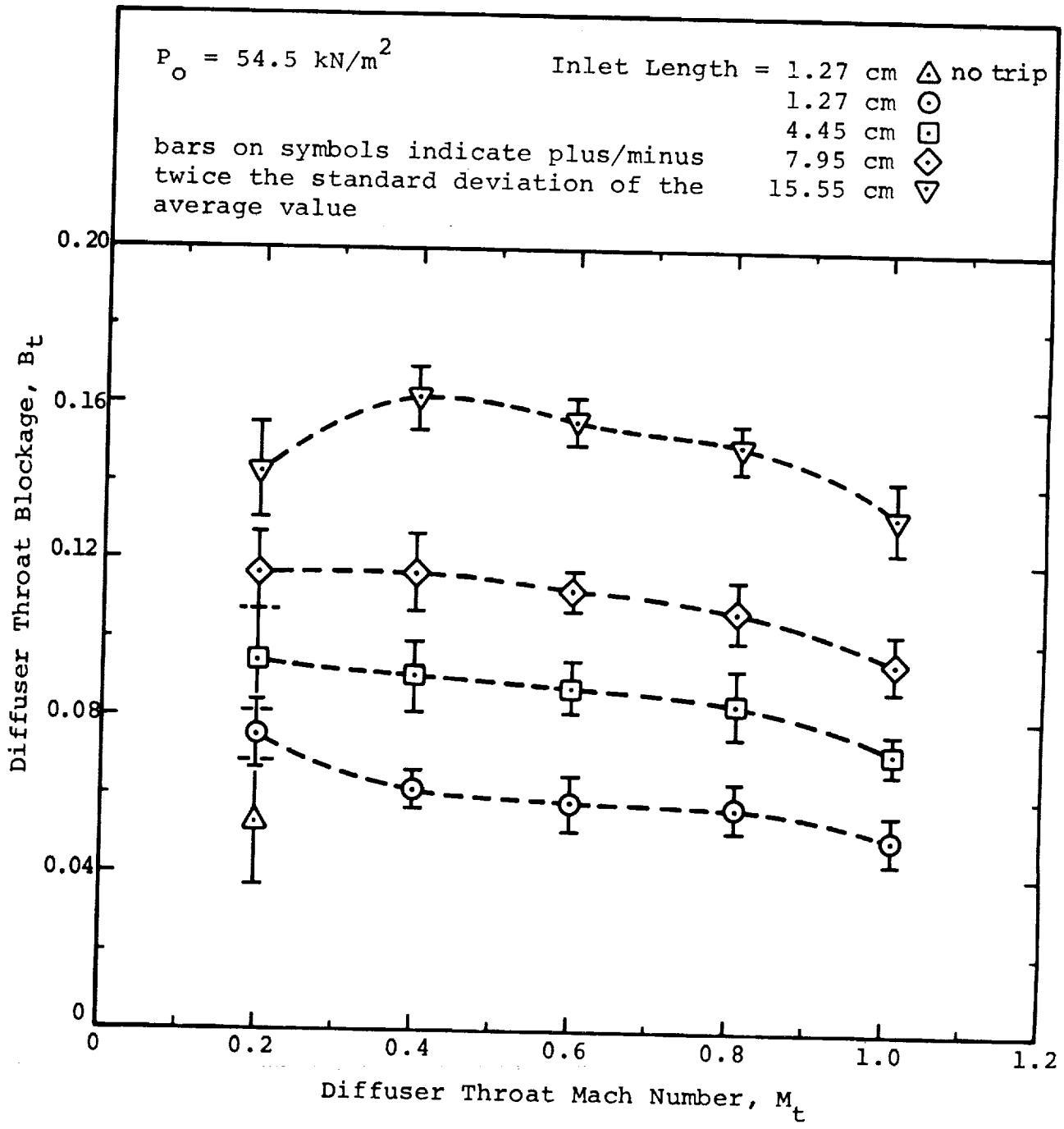


Figure 6 - Blockage Versus Mach Number - $p_{ot}$ = 54.5 kN/m$^2$

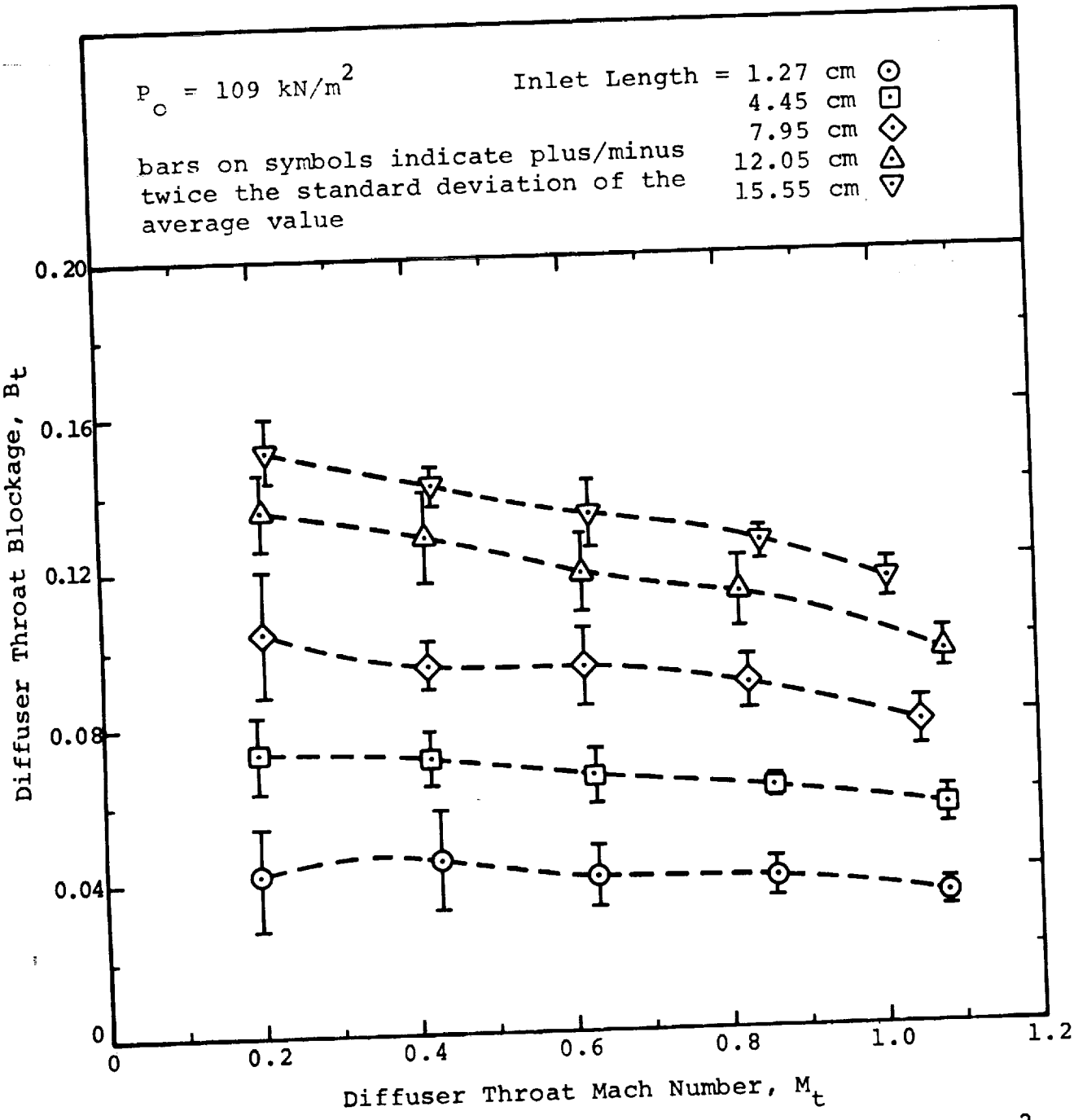


Figure 7 - Blockage Versus Mach Number - $P_{ot}$ = 109 kN/m$^2$

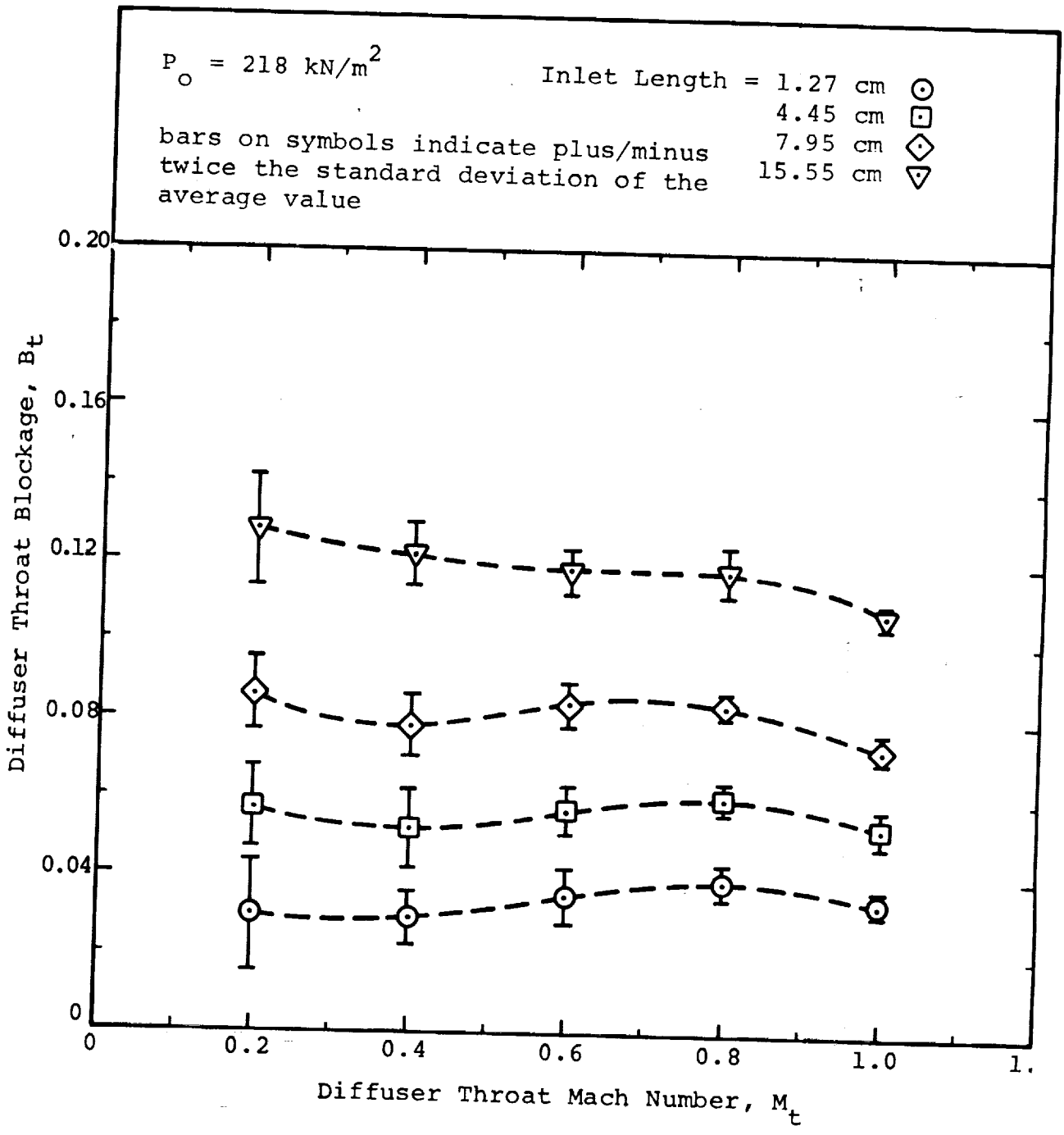


Figure 8 - Blockage Versus Mach Number - $p_{ot}$ = 218 kN/m$^2$

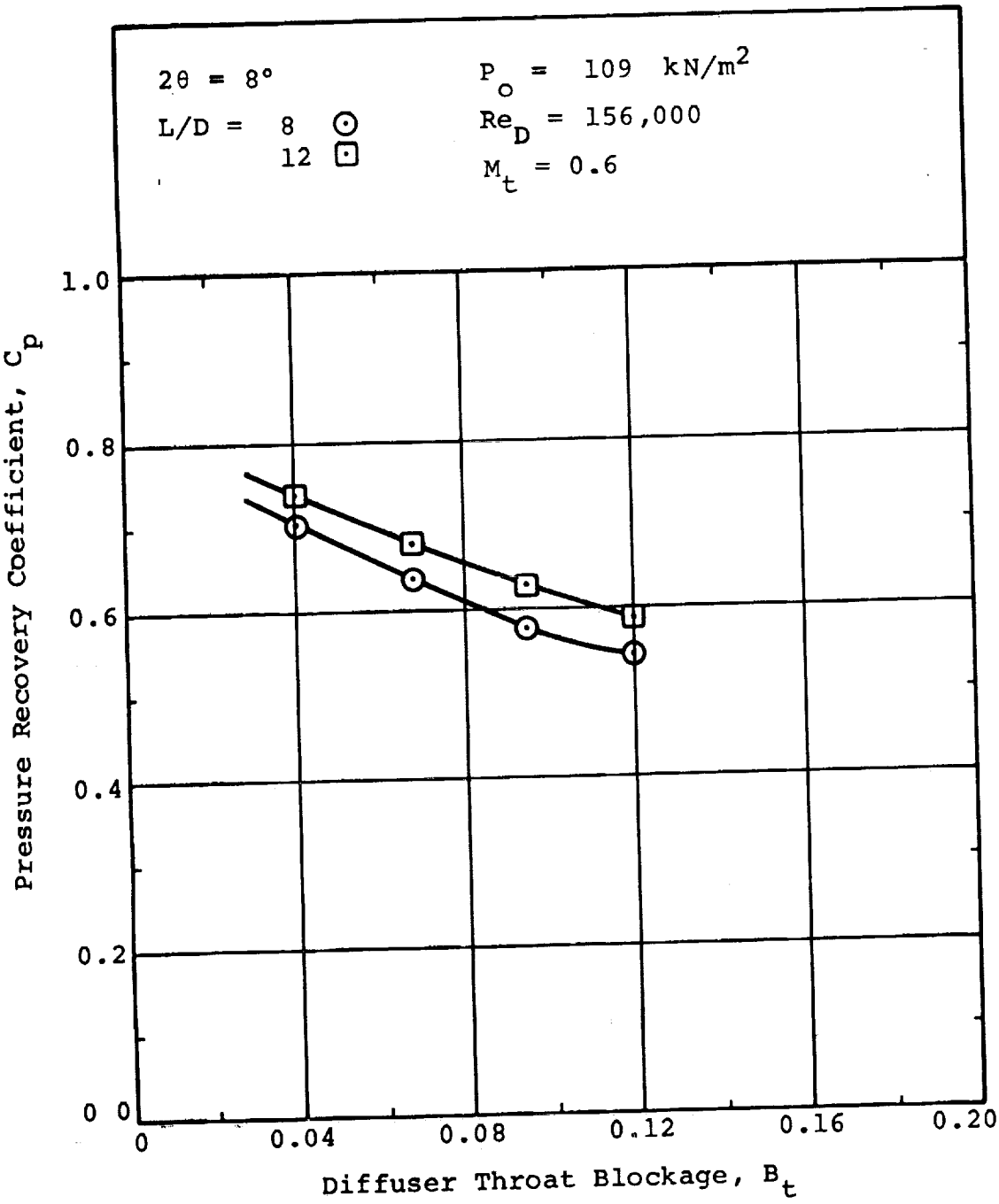


Figure 9 - Pressure Recovery Versus Blockage

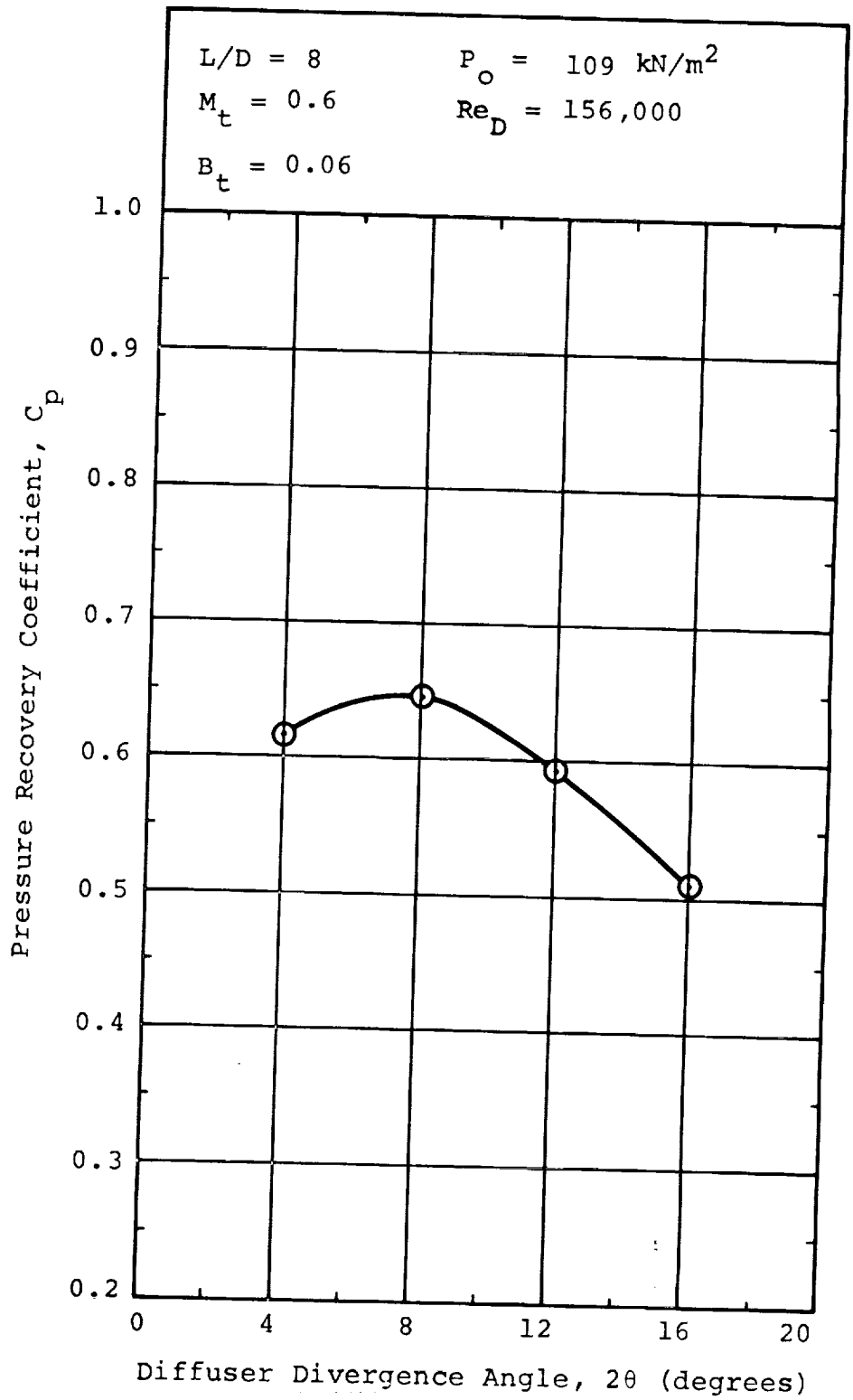


Figure 10 - Pressure Recovery Versus Divergence Angle

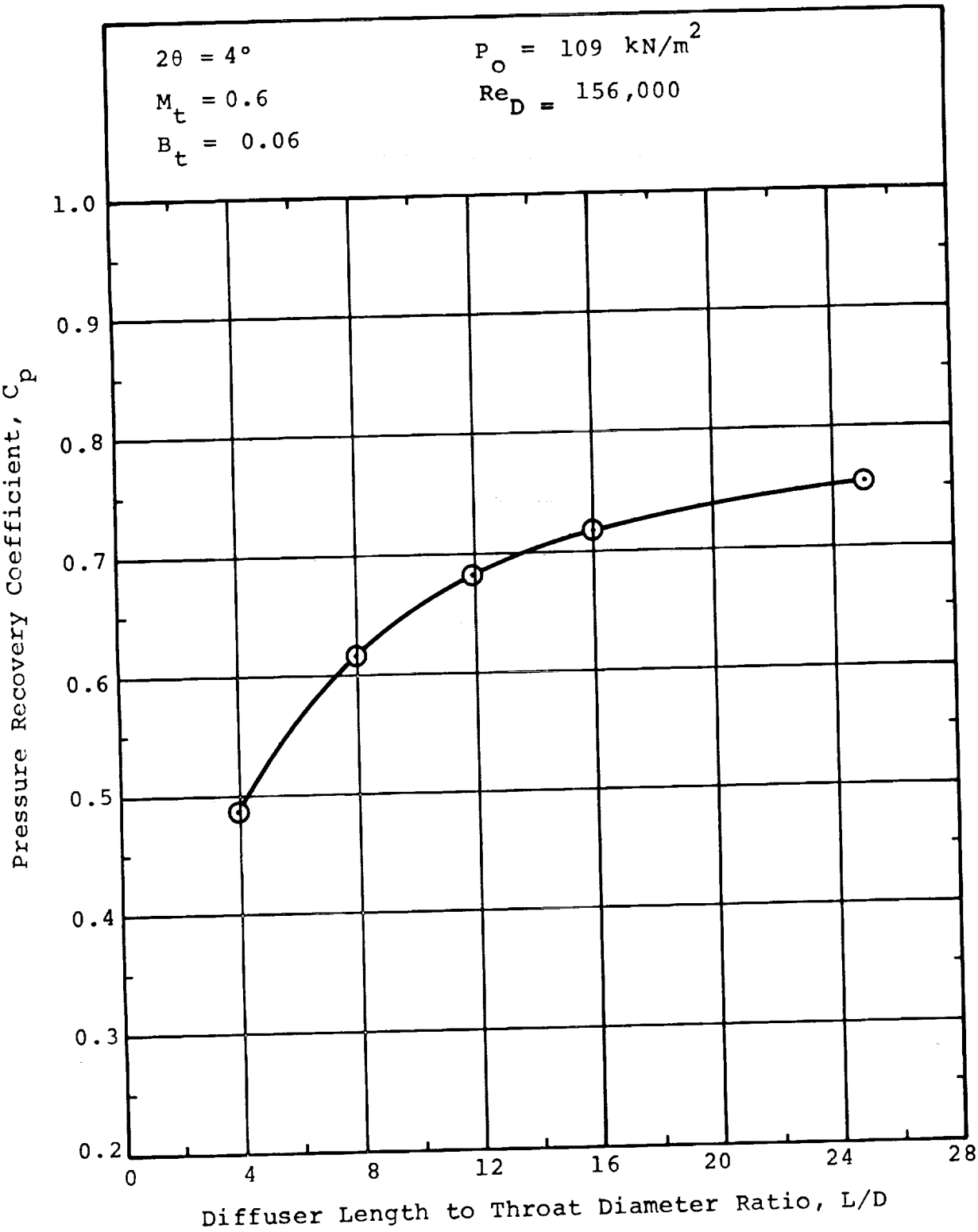


Figure 11 - Pressure Recovery Versus Diffuser Length

5. Finally, tabulations are made from the $C_p$ vs $2\theta$ and $C_p$ vs L/D curves for plotting of the conical diffuser perfomance "maps". These maps show contours of constant $C_p$ drawn on a plot of diffuser geometry, and they form the heart of the results of this program. On the average, each map contains about 50 data points.

## Experimental Uncertainty

In any study of this nature, the "accuracy" of the reported data can be as important to the user as the quoted absolute values. This is particularly true when the results of primary interest, i.e. $C_p$, are strongly affected by some independent parameter, such as throat blockage. The analysis here reviews the definitions of uncertainty for the variables of major interest. For a more complete discussion see Reference 3.

The uncertainties in pressure recovery, throat Mach number, Reynolds number and blockage (each expressed as a fraction of the absolute value) are presented below.

$$\frac{\Delta C_p}{C_p} = \left\{ \left[ \frac{1}{C_p} - 1 \right]^2 \left[ \frac{\Delta (p_{ot} - p_t)}{p_{ot} - p_t} \right]^2 + \left[ 1 - \frac{1}{C_p} \right]^2 \left[ \frac{\Delta (p_{ot} - p_e)}{p_{ot} - p_e} \right]^2 \right\}^{1/2} \tag{15}$$

$$\frac{\Delta M_t}{M_t} = \frac{1}{kM_t^2} \left( \frac{p_{ot}}{p_t} \right)^{\frac{k-1}{k}} \frac{\Delta (p_{ot}/p_t)}{p_{ot}/p_t} \tag{16}$$

$$\frac{\Delta Re_D}{Re_D} = \left\{ \left[ \frac{1}{1 + \frac{k-1}{2} M_t^2} \frac{\Delta M_t}{M_t} \right]^2 + \left[ \frac{\Delta D}{D} \right]^2 + \left[ \frac{1}{2} \frac{\Delta T_{ot}}{T_{ot}} \right]^2 \right\}^{1/2} \quad (17)$$

$$\frac{\Delta B_t}{B_t} = \frac{1-B_t}{B_t} \left\{ \left[ \frac{\Delta \dot{m}_a}{\dot{m}_a} \right]^2 + \left[ \frac{\Delta \dot{m}_i}{\dot{m}_i} \right]^2 \right\}^{1/2} \quad (18)$$

Four additional definitions are required in order to solve for the uncertainty in these primary quantities.

$$\frac{\Delta (p_{ot}/p_t)}{p_{ot}/p_t} = \left\{ \left[ (1 - \frac{p_{ot}}{p_t}) (\frac{\Delta p_{ot}}{p_{ot}}) \right]^2 + \left[ (\frac{p_{ot}}{p_t} - 1) \ (\frac{\Delta (p_{ot}-p_t)}{p_{ot}-p_t}) \right]^2 \right\}^{1/2} \quad (19)$$

$$\frac{\Delta p_{ot}}{p_{ot}} = \left\{ \left[ \frac{\Delta p_{atm}}{p_{atm}} \right]^2 + \left[ \frac{\Delta (p_{ot}-p_{atm})}{p_{ot} - p_{atm}} \right]^2 \right\}^{1/2} \quad (20)$$

$$\frac{\Delta \dot{m}_a}{\dot{m}_a} = \left\{ \left[ \frac{\Delta C_D}{C_D} \right]^2 + \left[ \frac{1}{2} \frac{\Delta T_{inlet}}{T_{inlet}} \right]^2 + \left[ \frac{1}{2} \frac{\Delta (p_{inlet}-p_{atm})}{p_{inlet} - p_{atm}} \right]^2 + \left[ \frac{1}{2} \frac{\Delta (\Delta p_{nozzle})}{\Delta p_{nozzle}} \right]^2 \right\}^{1/2} \quad (21)$$

$$\frac{\Delta \dot{m}_i}{\dot{m}_i} = \left\{ \left[ \frac{\Delta A_t}{A_t} \right]^2 + \left[ \frac{1}{2} \frac{\Delta T_{ot}}{T_{ot}} \right]^2 + \left[ \frac{1 - M_t^2}{1 + \frac{k-1}{2} M_t^2} \frac{\Delta M_t}{M_t} \right]^2 + \left[ \frac{\Delta p_{ot}}{p_{ot}} \right]^2 \right\}^{1/2} \quad (22)$$

The estimated uncertainty for several of these secondary quantities above are fixed (or very small) and are listed below.

$$\frac{\Delta C_D}{C_D} = 0.0043; \quad \frac{\Delta T_{inlet}}{T_{inlet}} = \frac{\Delta T_{ot}}{T_{ot}} = 0.0057$$

$$\frac{\Delta A_t}{A_t} = 0; \quad \frac{\Delta p_{atm}}{p_{atm}} = 0.00065$$

The remaining uncertainties in Equations 15 through 22 are solely dependent upon which of the three pressure transducers was used to make the particular measurement.

In Table V are estimated values of uncertainty in $M_t$, $Re_D$, and $B_t$ for the three pressure levels $p_{ot}$ used. The uncertainty in $C_p$ for the range of $C_p$ values attained at the given inlet conditions is also tabulated. These estimates are based on the uncertainty values assigned to each transducer (Table III) and the miscellaneous uncertainties listed above.

## RESULTS AND DISCUSSION

The principal result of this program is the measured conical diffuser pressure recovery performance, $C_p$. These data are presented in summarized form, Figures 12-71, as performance maps for the conical diffusers. The maps display the

TABLE V - ESTIMATED UNCERTAINTY FOR REPORTED DIFFUSER INLET CONDITIONS AND PERFORMANCE DATA

| Stagnation Pressure $p_{ot_2}$ ($kN/m^2$) | Mach Number $M_t$ | $\frac{\Delta M_t}{M_t}$ (%) | Reynolds Number $Re_D$ | $\frac{\Delta Re_D}{Re_D}$ (%) | Throat Blockage $B_t$ | $\frac{\Delta B_t}{B_t}$ (%) | Pressure Recovery $C_p$ | $\frac{\Delta C_p}{C_p}$ (%) |
|---|---|---|---|---|---|---|---|---|
| 54.5 | 0.4 | 0.74 | 57,000 | 0.77 | 0.03 | 51 | 0.6 | 1.08 |
| | | | | | | | 0.7 | 0.88 |
| | | | | | | | 0.8 | 0.73 |
| | | | | | 0.12 | 12 | 0.4 | 1.80 |
| | | | | | | | 0.5 | 1.37 |
| | | | | | | | 0.6 | 1.08 |
| | | | | | | | 0.7 | 0.88 |
| | 1.0 | 1.30 | 101,000 | 1.11 | 0.03 | 37 | 0.5 | 1.50 |
| | | | | | | | 0.6 | 1.04 |
| | | | | | | | 0.7 | 0.68 |
| | | | | | | | 0.8 | 0.43 |
| | | | | | 0.13 | 8.5 | 0.4 | 2.30 |
| | | | | | | | 0.5 | 1.50 |
| | | | | | | | 0.6 | 1.04 |

TABLE V - Continued

| Stagnation Pressure $p_{ot_2}$ ($kN/m^2$) | Mach Number $M_t$ | $\frac{\Delta M_t}{M_t}$ (%) | Reynolds Number $Re_D$ | $\frac{\Delta Re_D}{Re_D}$ (%) | Throat Blockage $B_t$ | $\frac{\Delta B_t}{B_t}$ (%) | Pressure Recovery $C_p$ | $\frac{\Delta C_p}{C_p}$ (%) |
|---|---|---|---|---|---|---|---|---|
| 109 | 0.4 | 0.33 | 114,000 | 0.43 | 0.03 | 29.6 | 0.5 | 0.78 |
| | | | | | | | 0.6 | 0.63 |
| | | | | | | | 0.7 | 0.48 |
| | | | | | | | 0.8 | 0.43 |
| | | | | | 0.12 | 6.75 | 0.4 | 1.02 |
| | | | | | | | 0.5 | 0.78 |
| | 1.0 | 0.63 | 202,000 | 0.59 | 0.03 | 23.2 | 0.6 | 0.63 |
| | | | | | | | 0.5 | 1.66 |
| | | | | | | | 0.6 | 1.34 |
| | | | | | | | 0.7 | 0.34 |
| | | | | | | | 0.8 | 0.21 |
| | | | | | 0.12 | 5.28 | 0.4 | 2.18 |
| | | | | | | | 0.5 | 1.66 |
| | | | | | | | 0.6 | 1.34 |

TABLE V - Concluded

| Stagnation Pressure $p_o$ ($kN/m^2$) | Mach Number $M_t$ | $\frac{\Delta M_t}{M_t}$ (%) | Reynolds Number $Re_D$ | $\frac{\Delta Re_D}{Re_D}$ (%) | Throat Blockage $B_t$ | $\frac{\Delta B_t}{B_t}$ (%) | Pressure Recovery $C_p$ | $\frac{\Delta C_p}{C_p}$ (%) |
|---|---|---|---|---|---|---|---|---|
| 218 | 0.4 | 0.92 | 228,000 | 0.935 | 0.03 | 33.7 | 0.6 | 1.16 |
| | | | | | | | 0.7 | 0.76 |
| | | | | | | | 0.8 | 0.47 |
| | | | | | 0.12 | 7.8 | 0.4 | 2.55 |
| | | | | | | | 0.5 | 1.71 |
| | | | | | | | 0.6 | 1.16 |
| | 1.0 | 0.375 | 404,000 | 0.423 | 0.03 | 22.9 | 0.6 | 0.67 |
| | | | | | | | 0.7 | 0.56 |
| | | | | | | | 0.8 | 0.47 |
| | | | | | 0.12 | 5.2 | 0.4 | 1.09 |
| | | | | | | | 0.5 | 0.83 |
| | | | | | | | 0.6 | 0.67 |

pressure recovery as a function of the non-dimensional geometry parameters and the inlet parameters. They show contours of constant pressure recovery $C_p$ on a geometry map which relates area ratio AR, length to throat diameter ratio L/D and divergence angle $2\theta$. Each map is drawn for one combination of inlet flow variables, Mach number $M_t$, throat blockage $B_t$, and inlet Reynolds number $Re_D$.

The maps are grouped together such that the first twenty maps (Figures 12-31) cover the Mach number and blockage combinations for the lowest Reynolds number data ($Re_D$ = 101,000 at $M_t$ = 1.0). Similarly, Figures 32-51 cover the middle Reynolds number range ($Re_D$ = 202,000 at $M_t$ = 1.0) and Figures 52-71 show the high Reynolds number data ($Re_D$ = 404,000 at $M_t$ = 1.0). The data are presented for four values of throat blockage ($B_t$ = 0.03, 0.06, 0.09, and 0.12) and five values of throat Mach number ($M_t$ = 0.2, 0.4, 0.6, 0.8 and 1.0). Within each group, the maps are arranged so that four tabulated $B_t$ values appear together at one $M_t$, and then another set of four $B_t$ values at the next higher $M_t$ until all five $M_t$ values are covered. Figure 75 may be used to determine if the boundary layer at the throat is laminar or turbulent for a particular combination of $B_t$, $M_t$ and $p_{ot}$.

The three groups of maps cover the range of Mach number and throat blockage surveyed in this study over a range of Reynolds number differing by a factor of four at each Mach number. These data thus permit a separate evaluation of Reynolds number and Mach number effects on conical diffuser performance, within the range of values of Reynolds numbers studied.

## Effect of Geometry on Performance

All 60 performance maps display very similar characteristics. The maximum pressure recovery (highest value of pressure recovery $C_p$, for each map) occurs in the upper right hand corner of the map. For each map this occurs at the highest value of length to throat diameter ratio studied (L/D = 25). Divergence angle corresponding to maximum recovery is on the order of $2\theta$ = 3.5° to 5°.

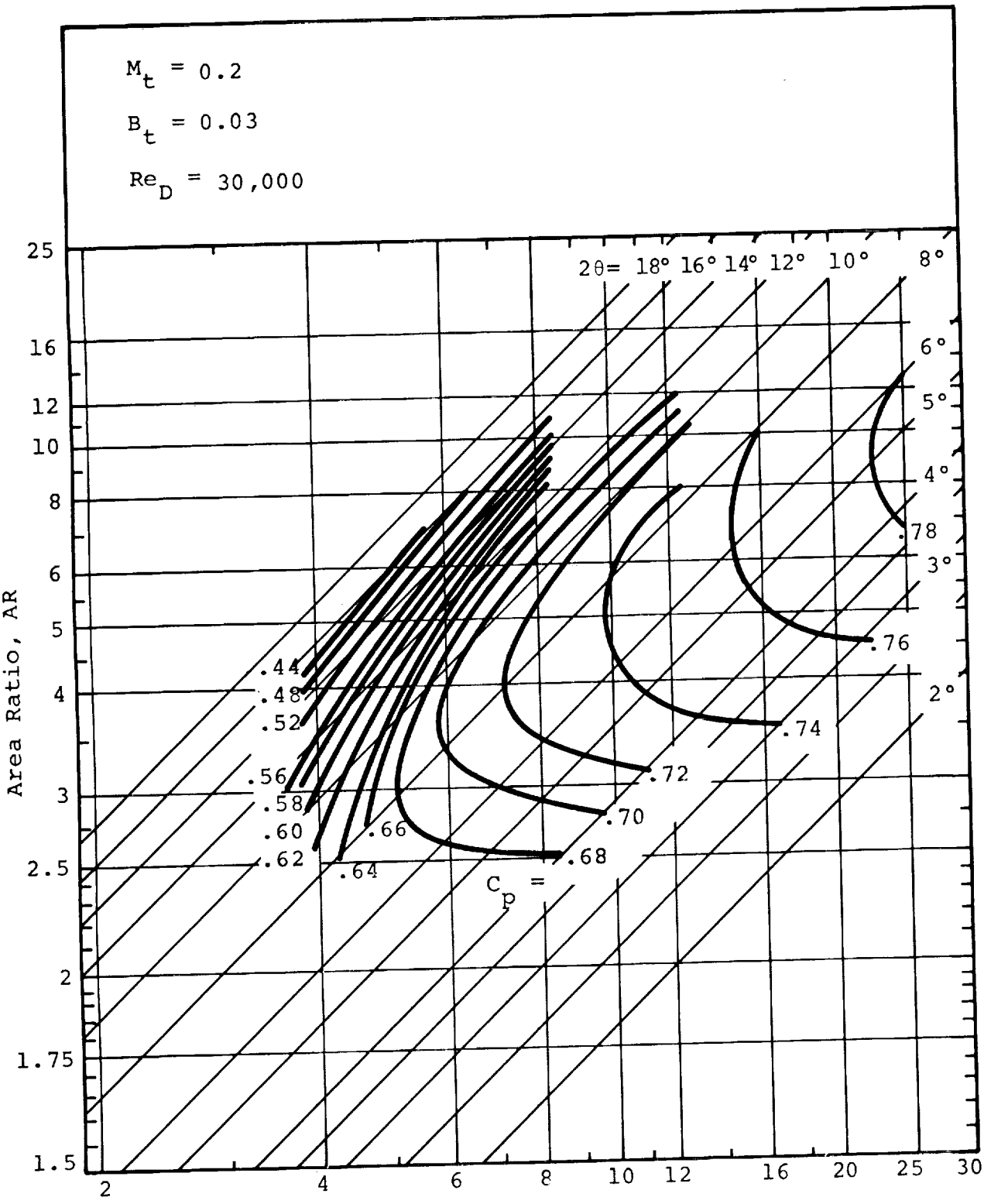


Figure 12 - Conical Diffuser Performance Map - $p_{ot}$ = 54.5 kN/m$^2$

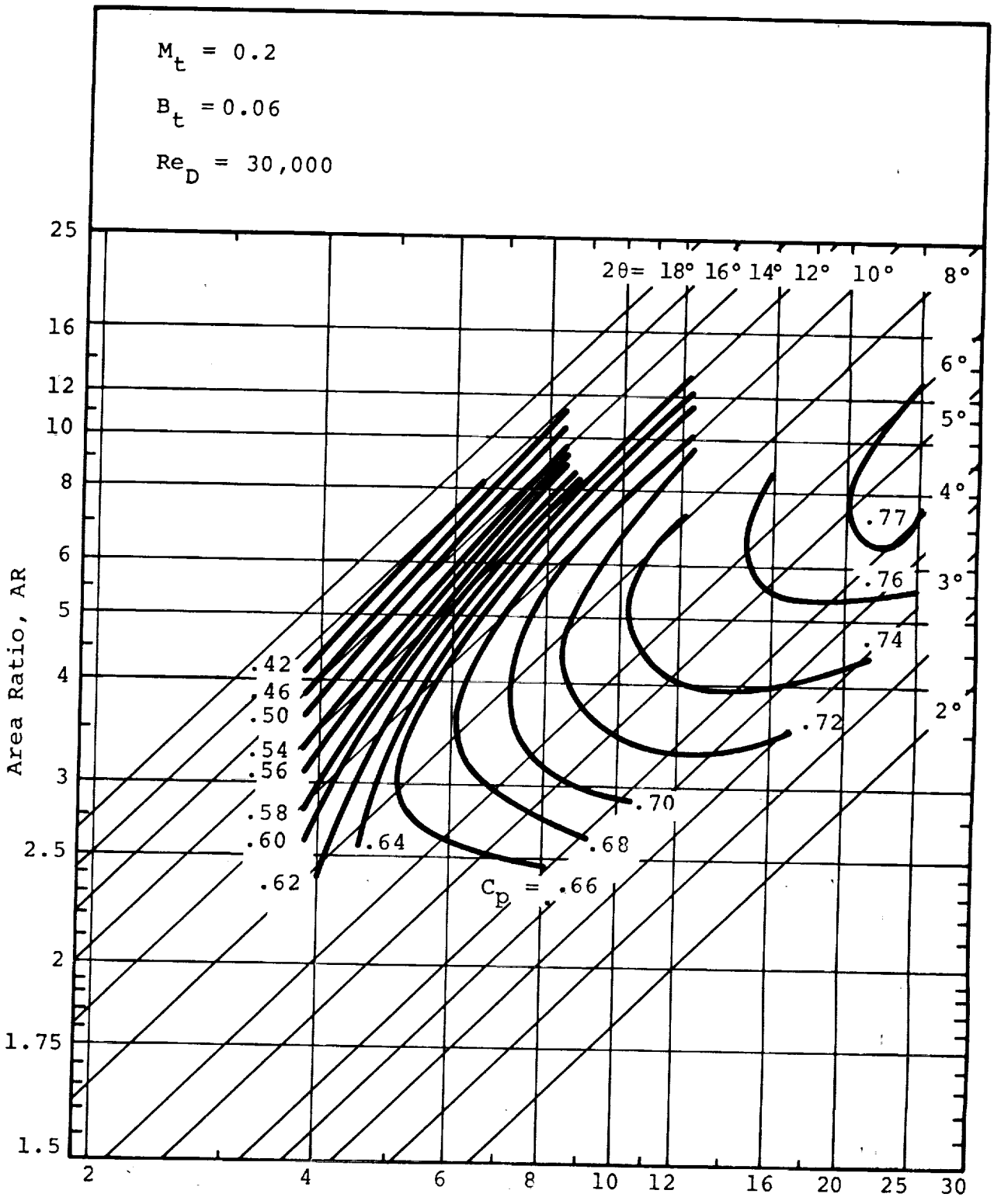


Figure 13 - Conical Diffuser Performance Map - $p_{ot}$ = 54.5 kN/m$^2$

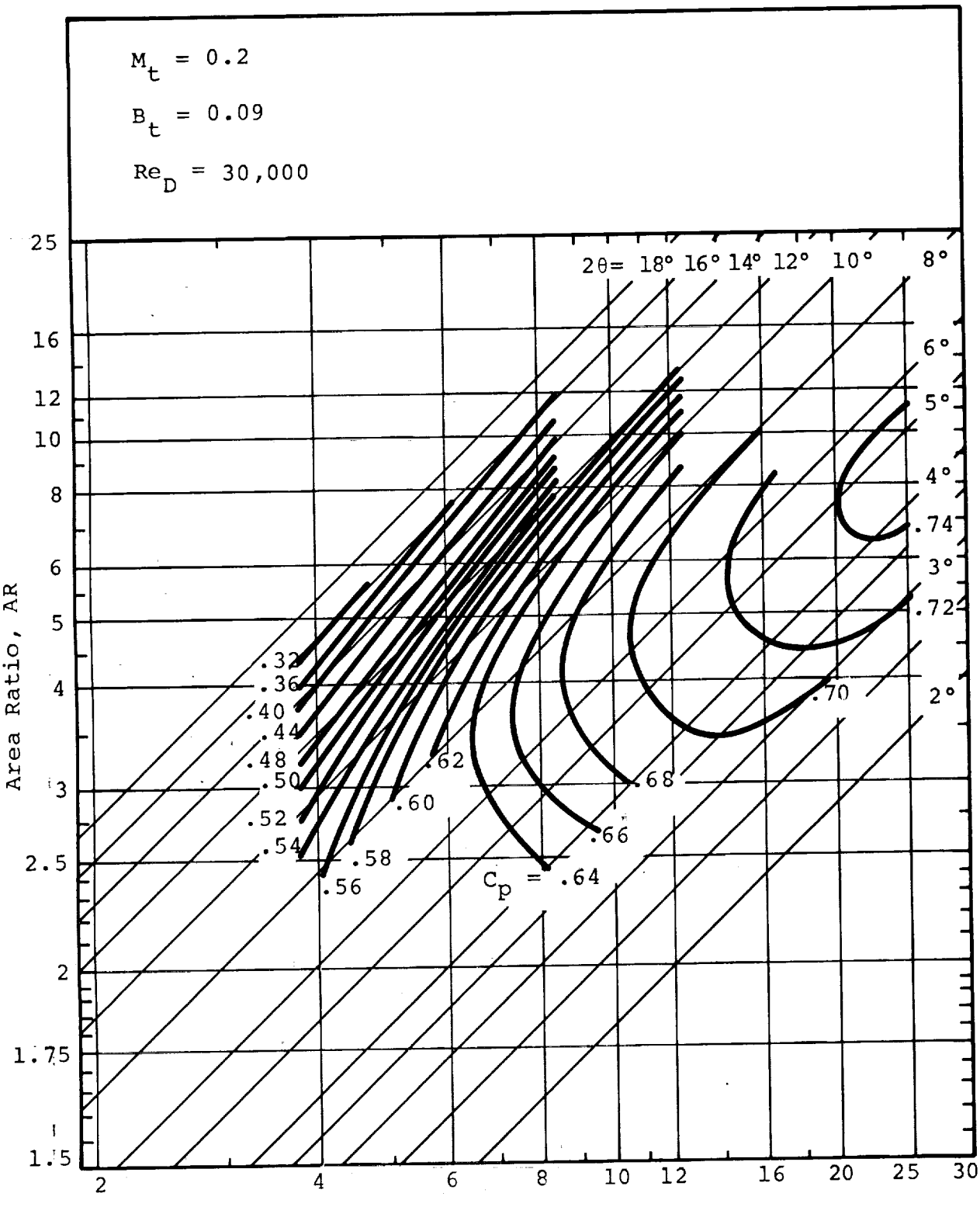


Figure 14 - Conical Diffuser Performance Map - $p_{ot}$ = 54.5 kN/m$^2$

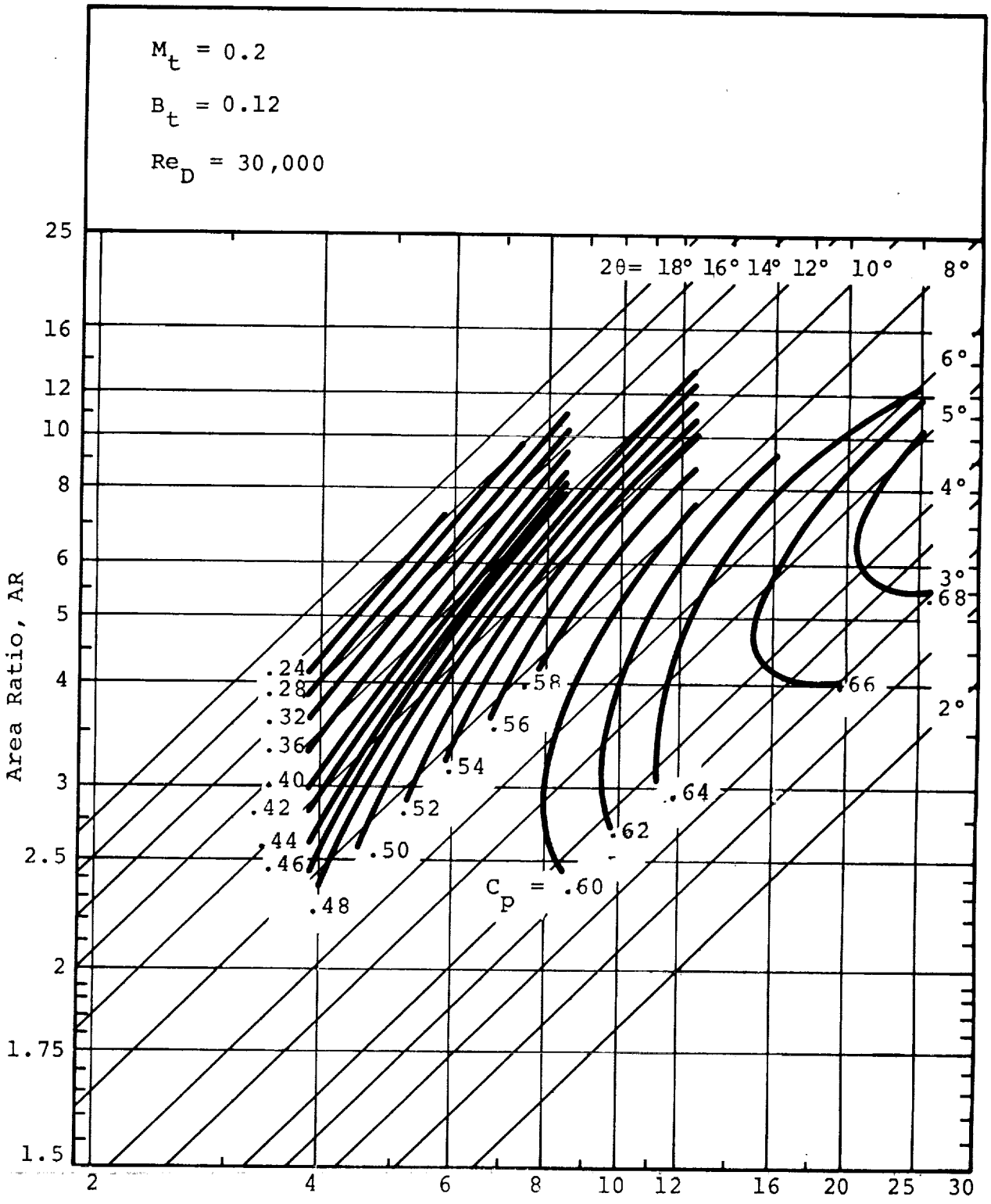


Figure 15 - Conical Diffuser Performance Map - $p_{ot}$ = 54.5 kN/m$^2$

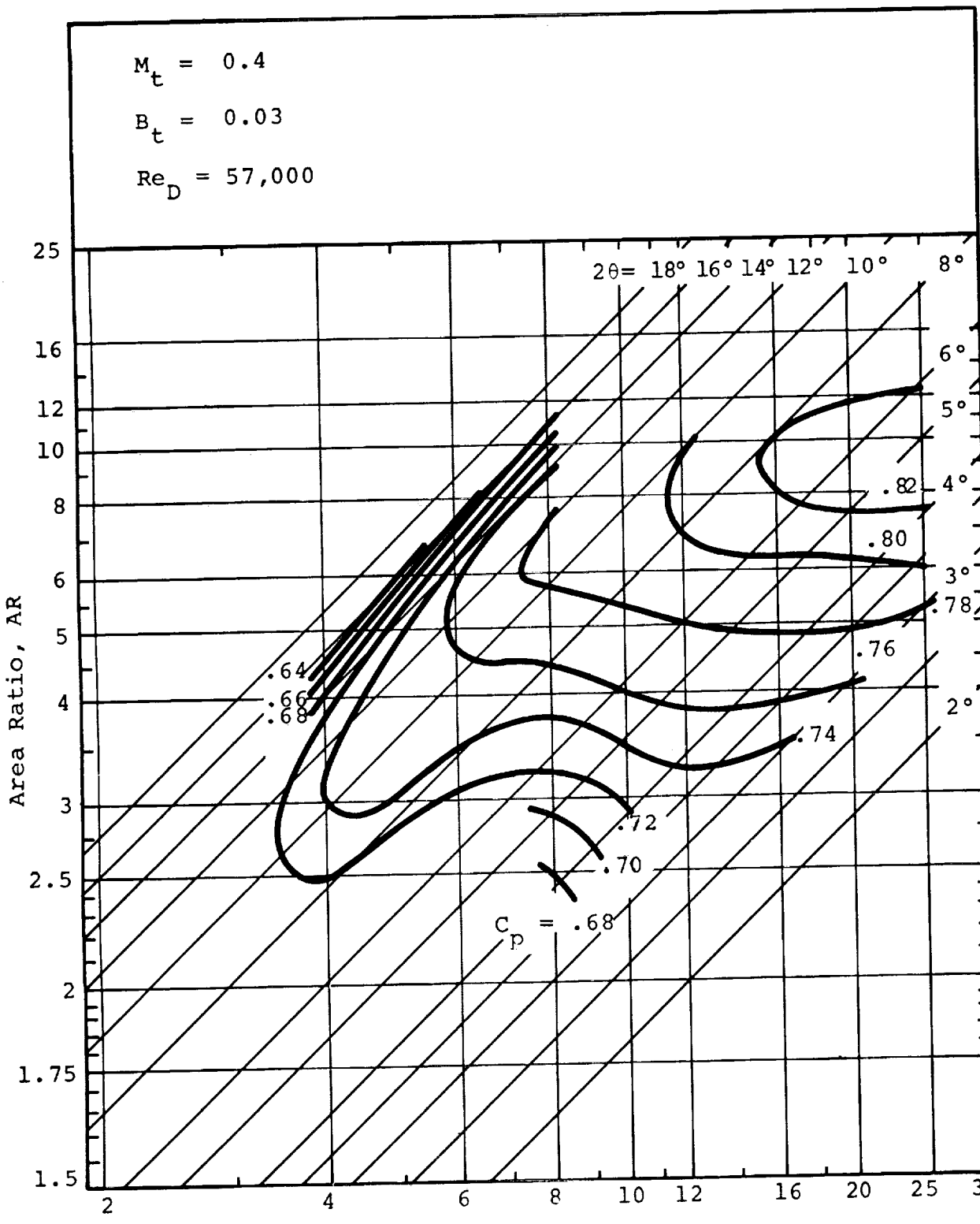


Figure 16 - Conical Diffuser Performance Map - $p_{ot}$ = 54.5 kN/m$^2$

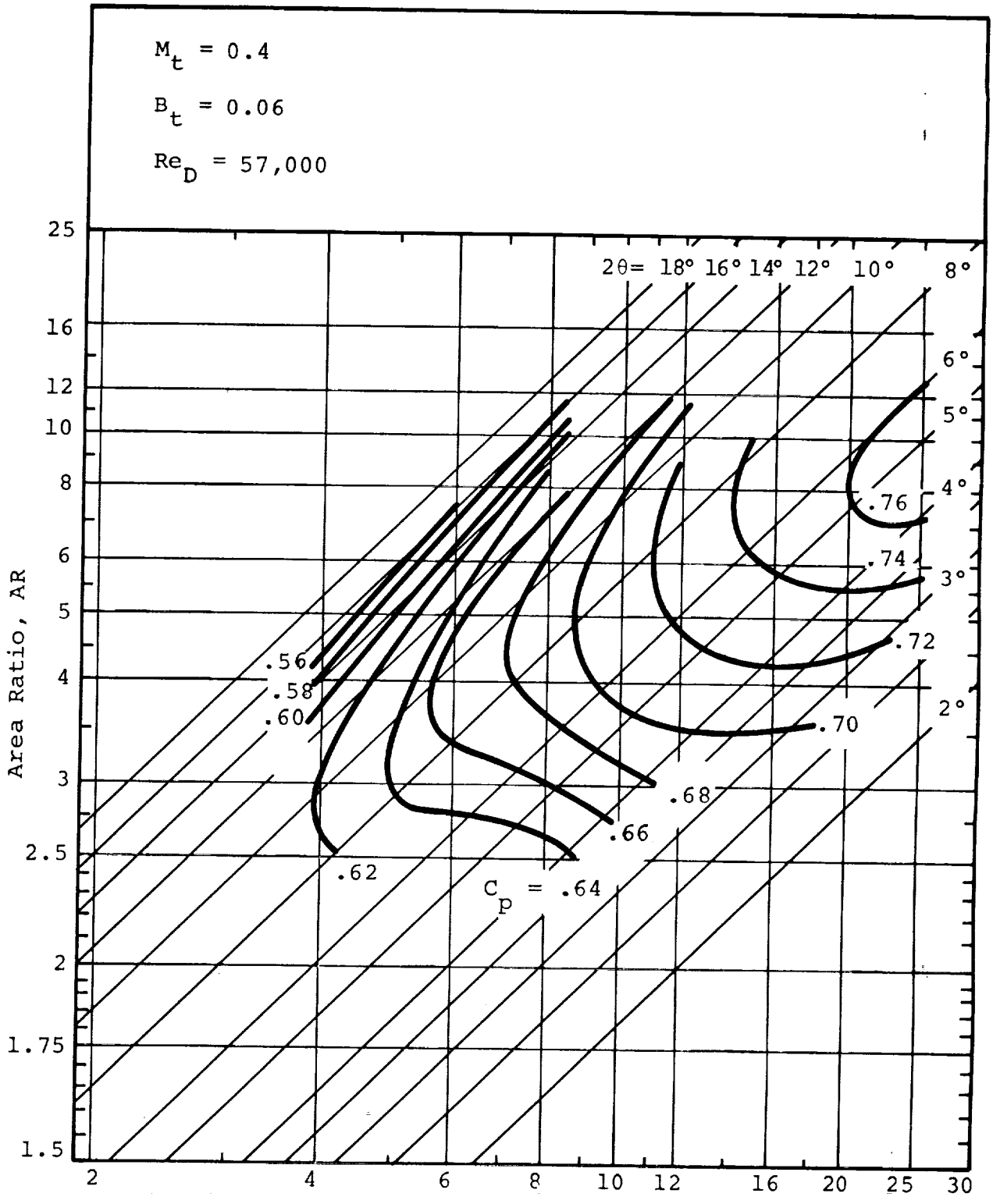


Figure 17 - Conical Diffuser Performance Map - $p_{ot}$ = 54.5 kN/m$^2$

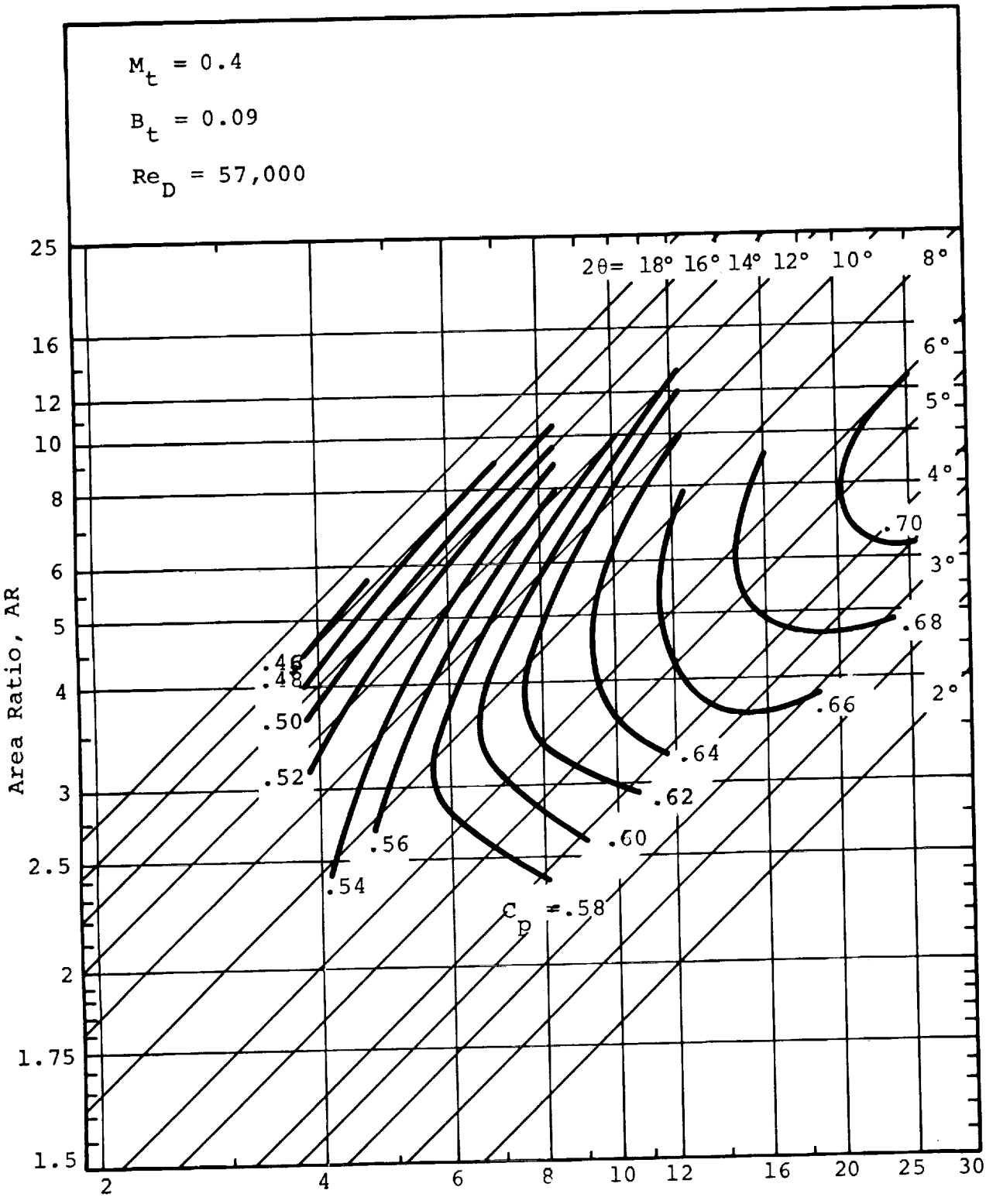


Figure 18 - Conical Diffuser Performance Map - $p_{ot}$ = 54.5 kN/m$^2$

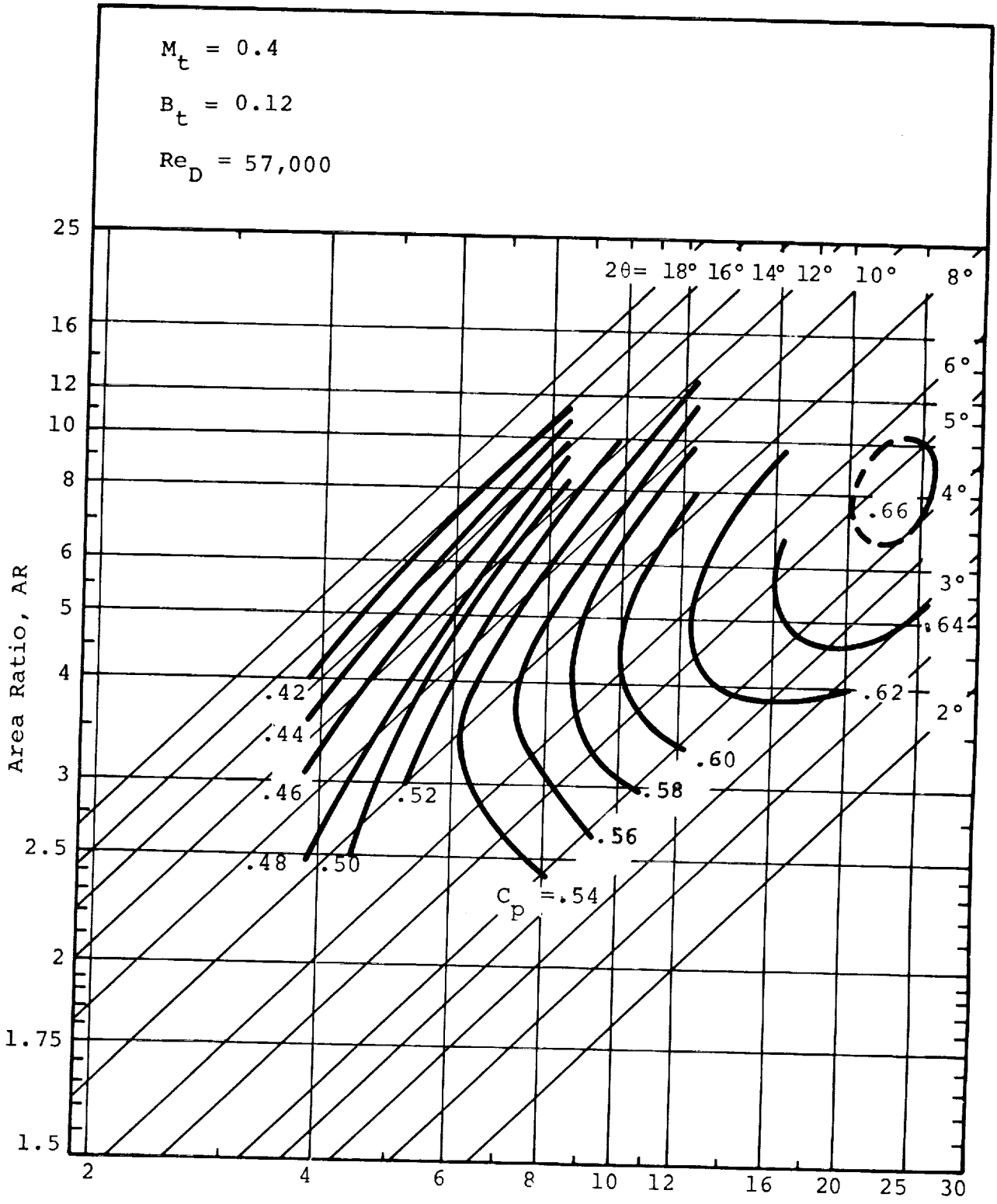


Figure 19 - Conical Diffuser Performance Map - $p_{ot}$ = 54.5 kN/m$^2$

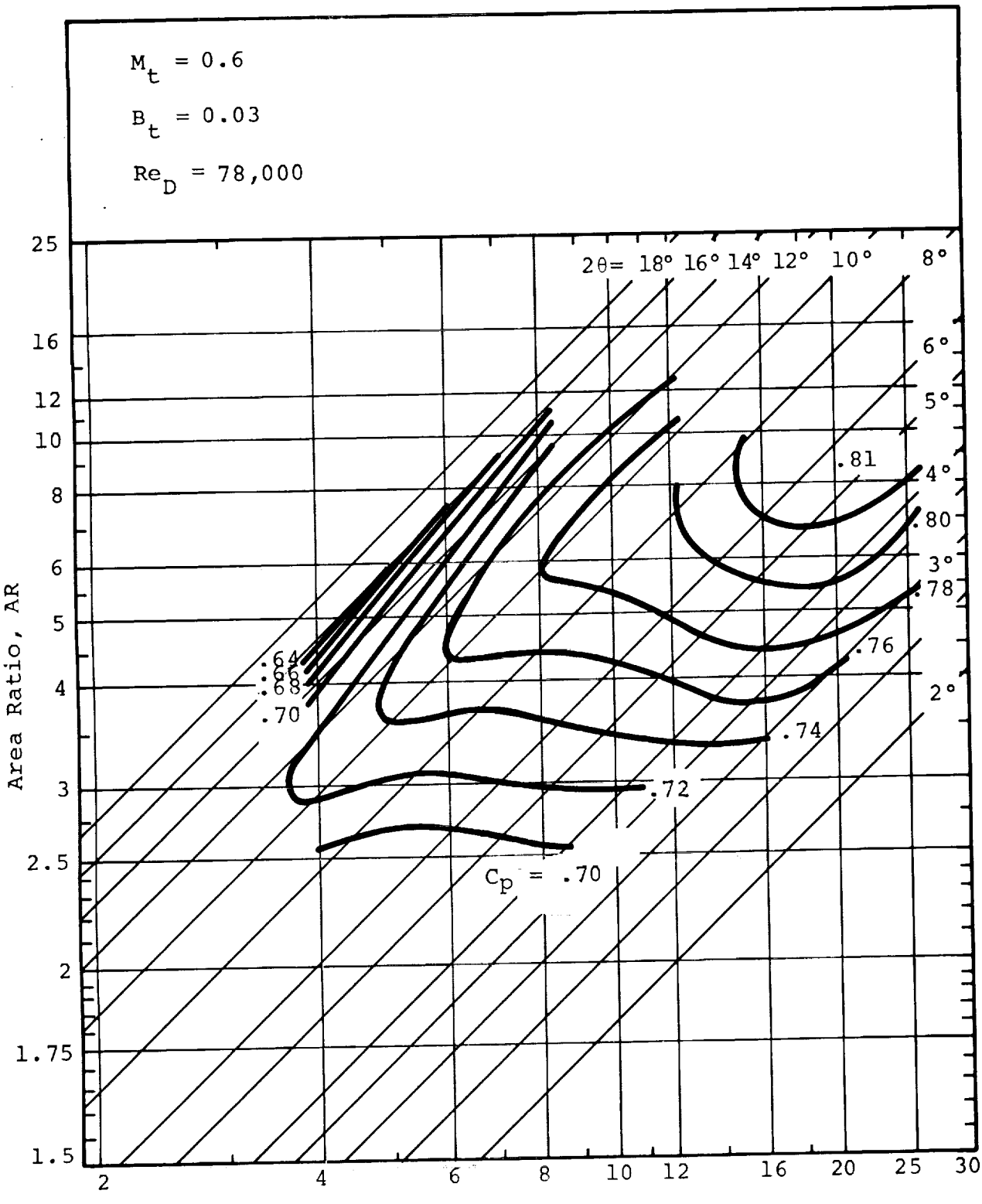


Figure 20 - Conical Diffuser Performance Map - $p_{ot}$ = 54.5 kN/m$^2$

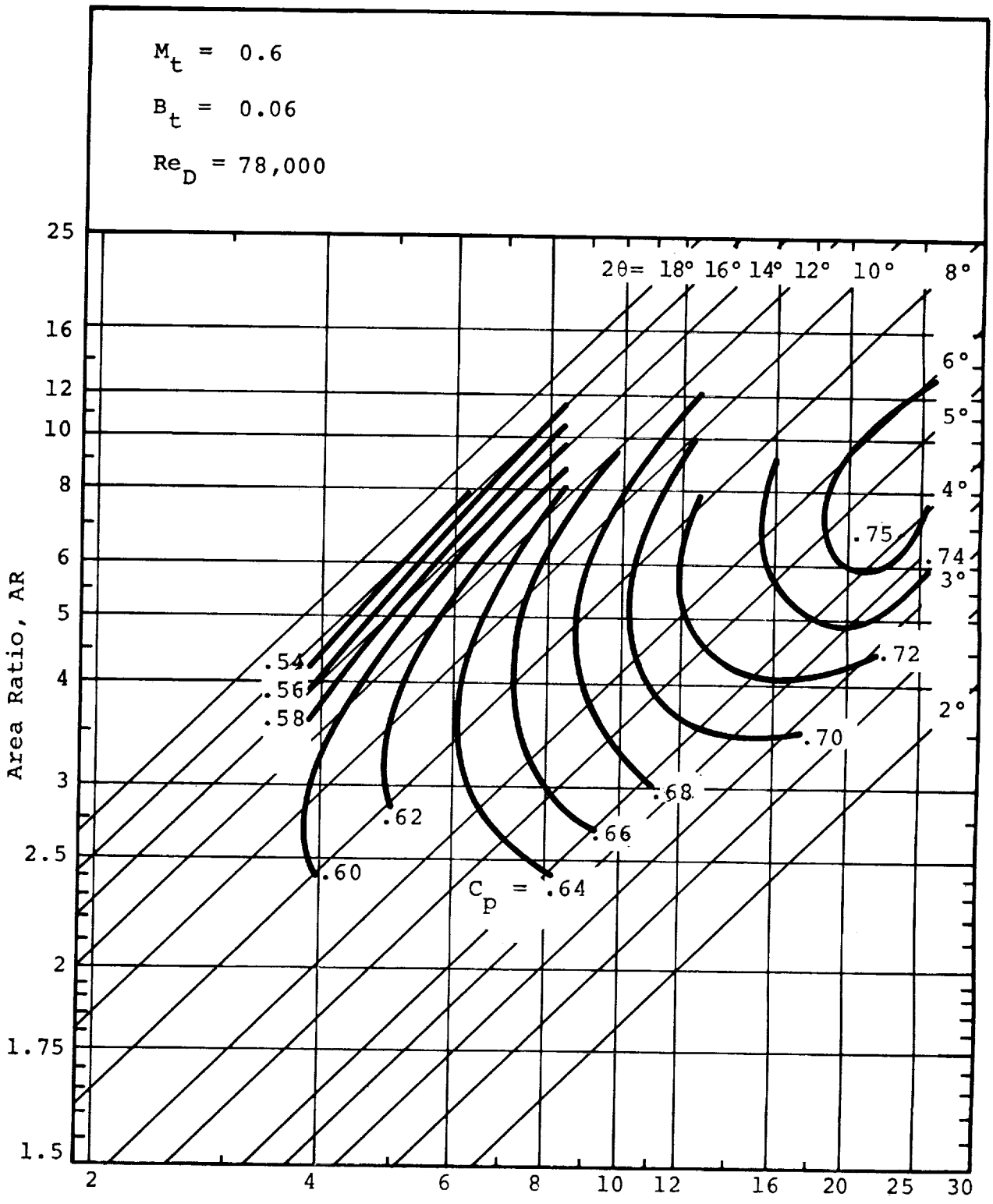


Figure 21 - Conical Diffuser Performance Map - $p_{ot}$ = 54.5 kN/m$^2$

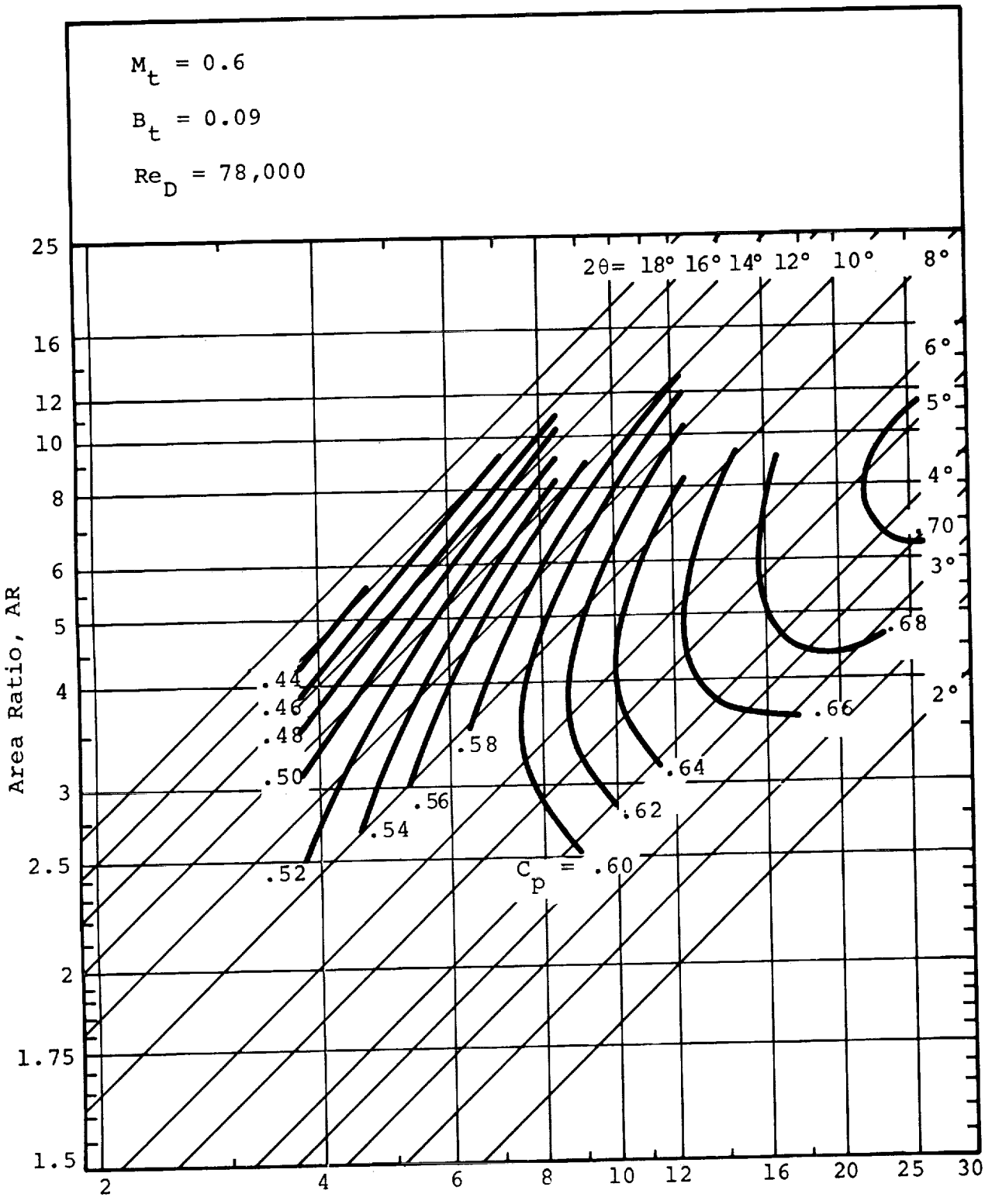


Figure 22 - Conical Diffuser Performance Map - $p_{ot}$ = 54.5 kN/m$^2$

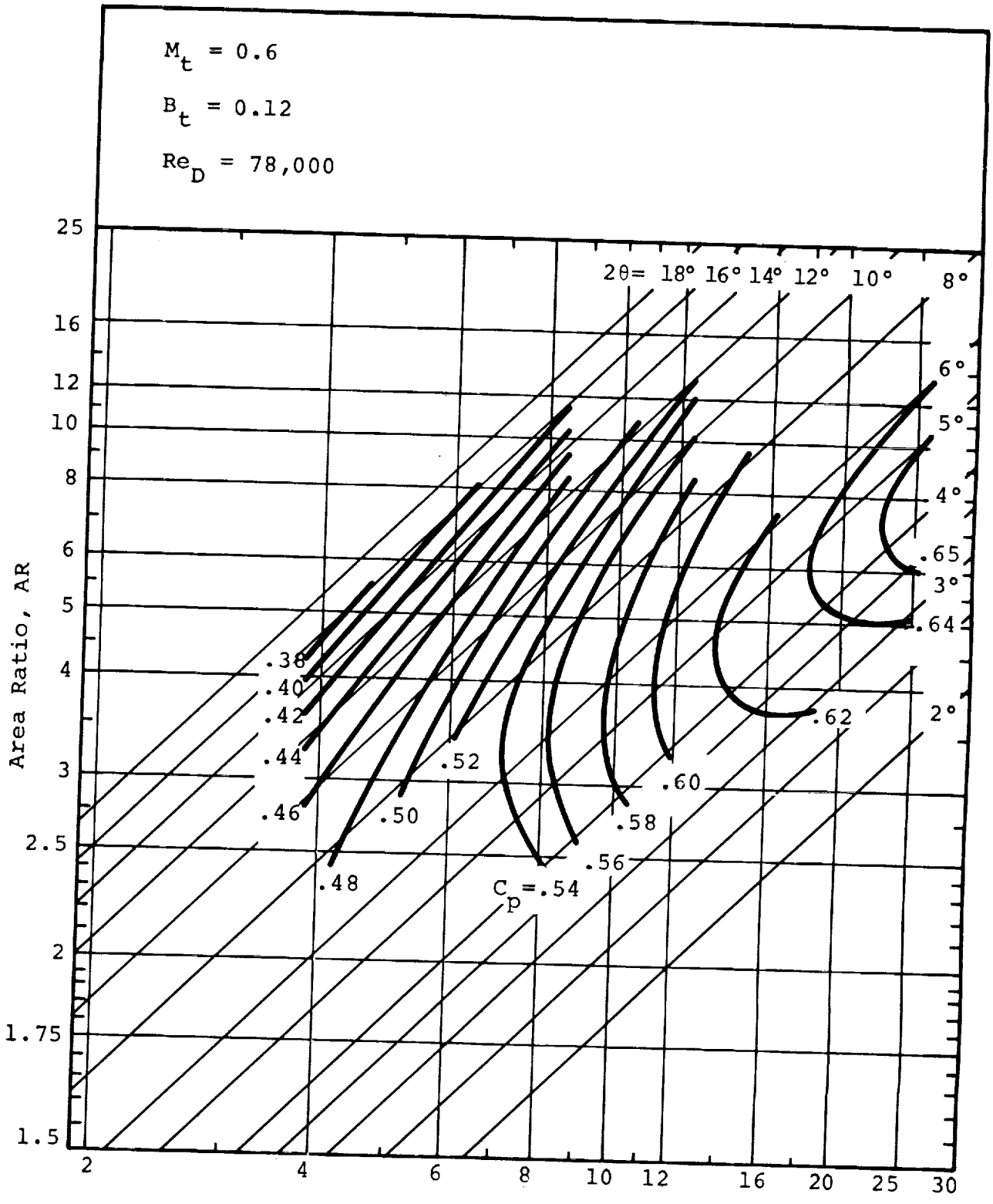


Figure 23 - Conical Diffuser Performance Map - $p_{ot}$ = 54.5 kN/m$^2$

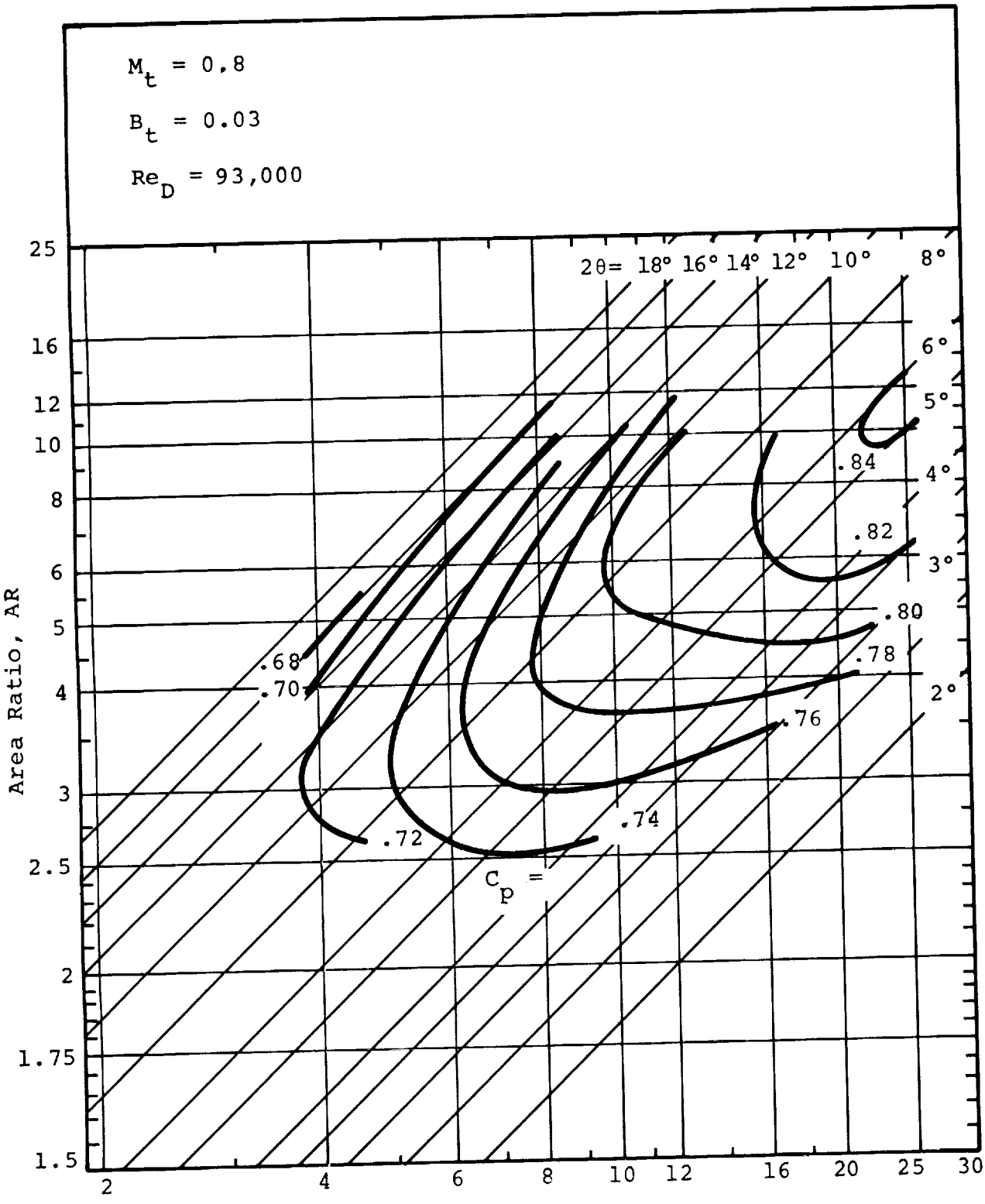


Figure 24 - Conical Diffuser Performance Map - $p_{ot}$ = 54.5 kN/m$^2$

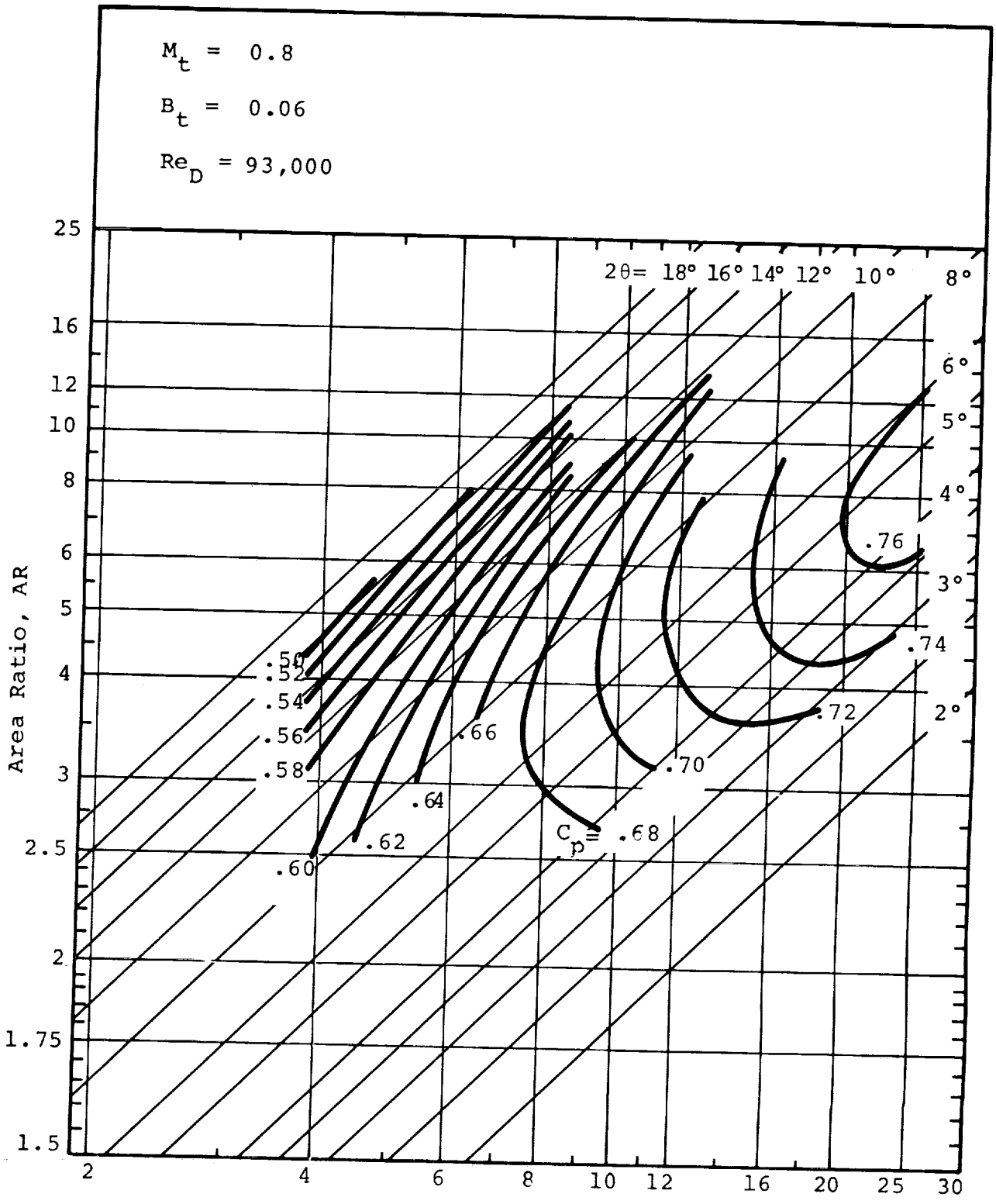


Figure 25 - Conical Diffuser Performance Map - $p_{ot}$ = 54.5 kN/m$^2$

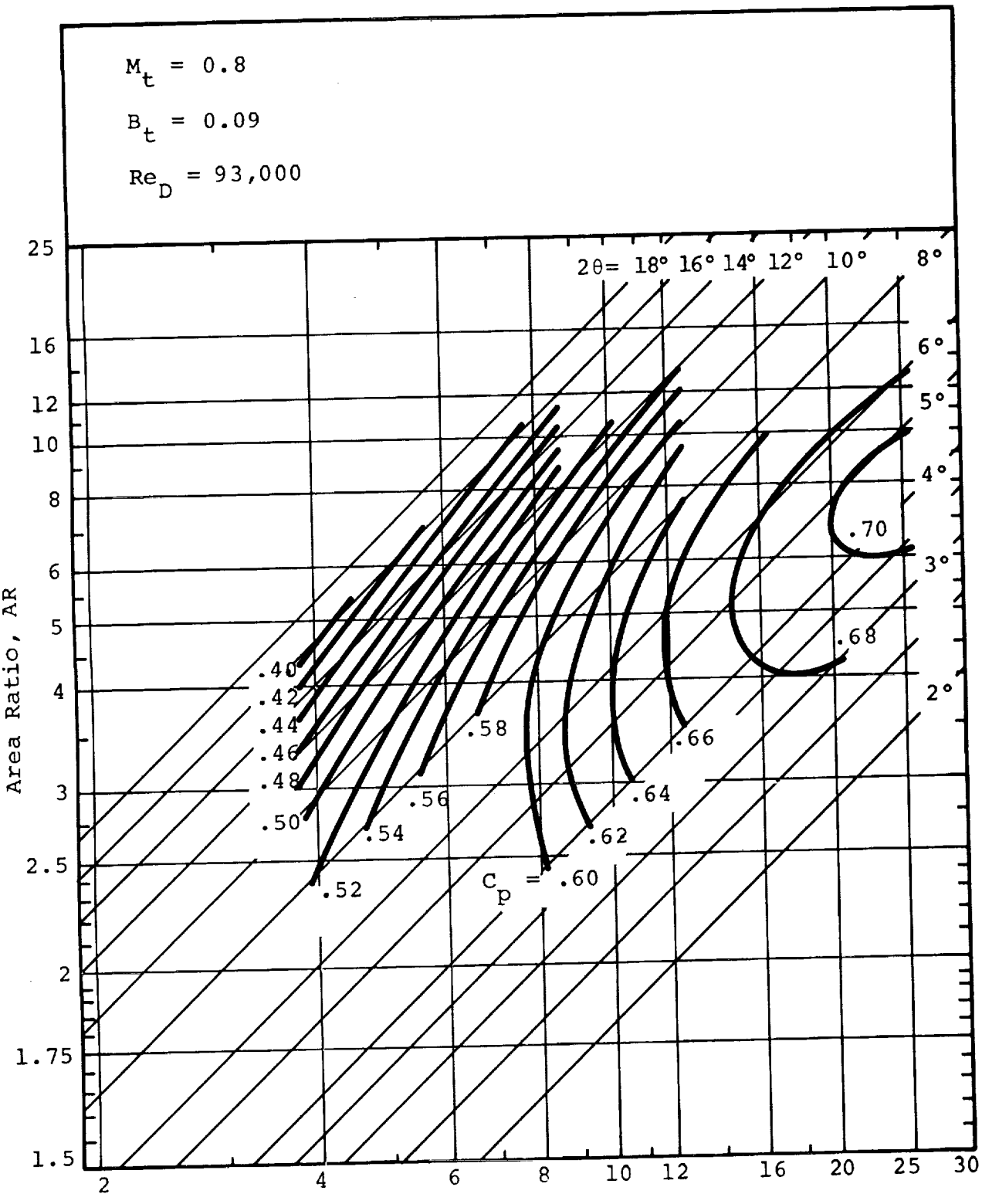


Figure 26 - Conical Diffuser Performance Map - $p_{ot}$ = 54.5 kN/m$^2$

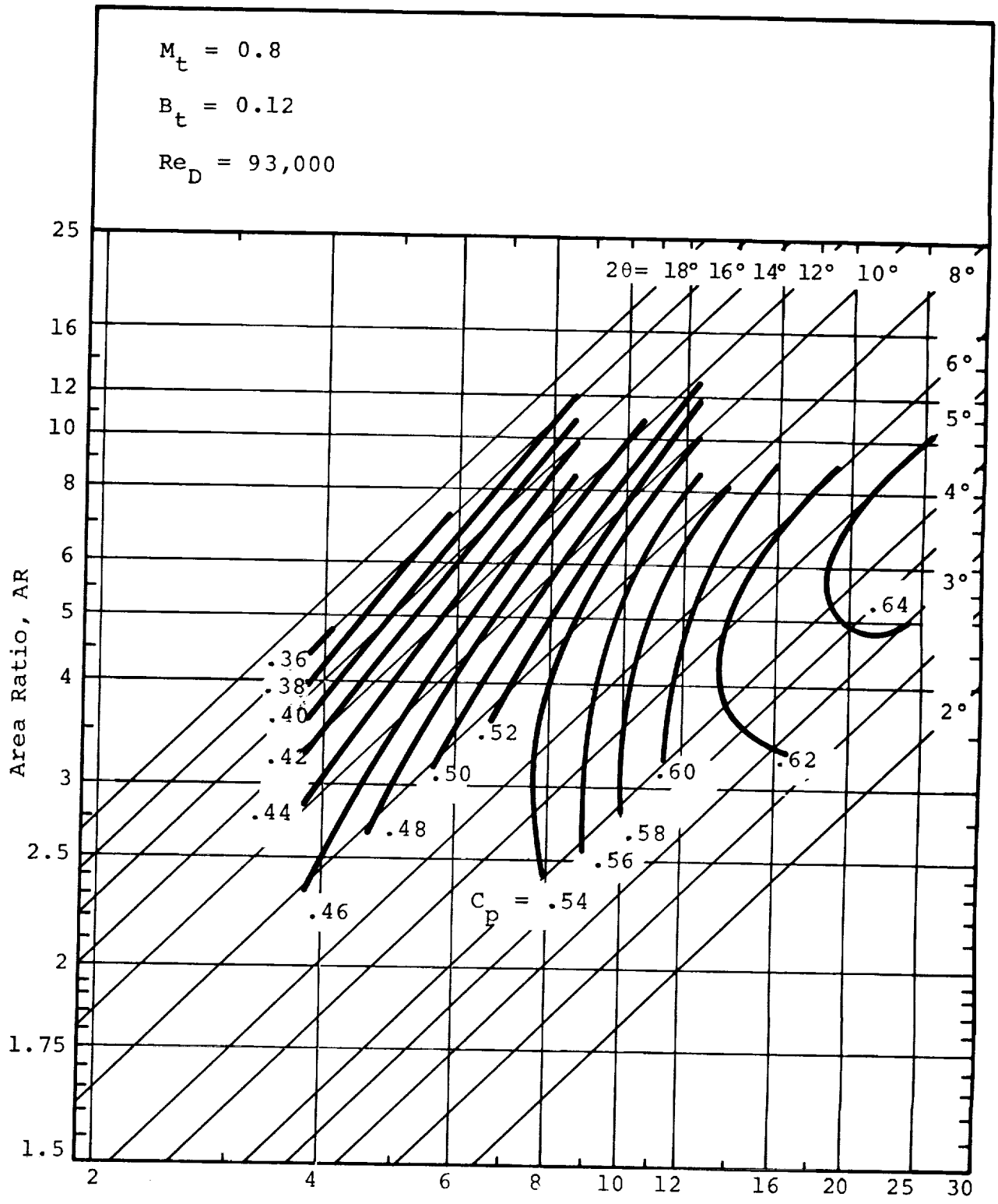


Figure 27 - Conical Diffuser Performance Map - $p_{ot}$ = 54.5 kN/m$^2$

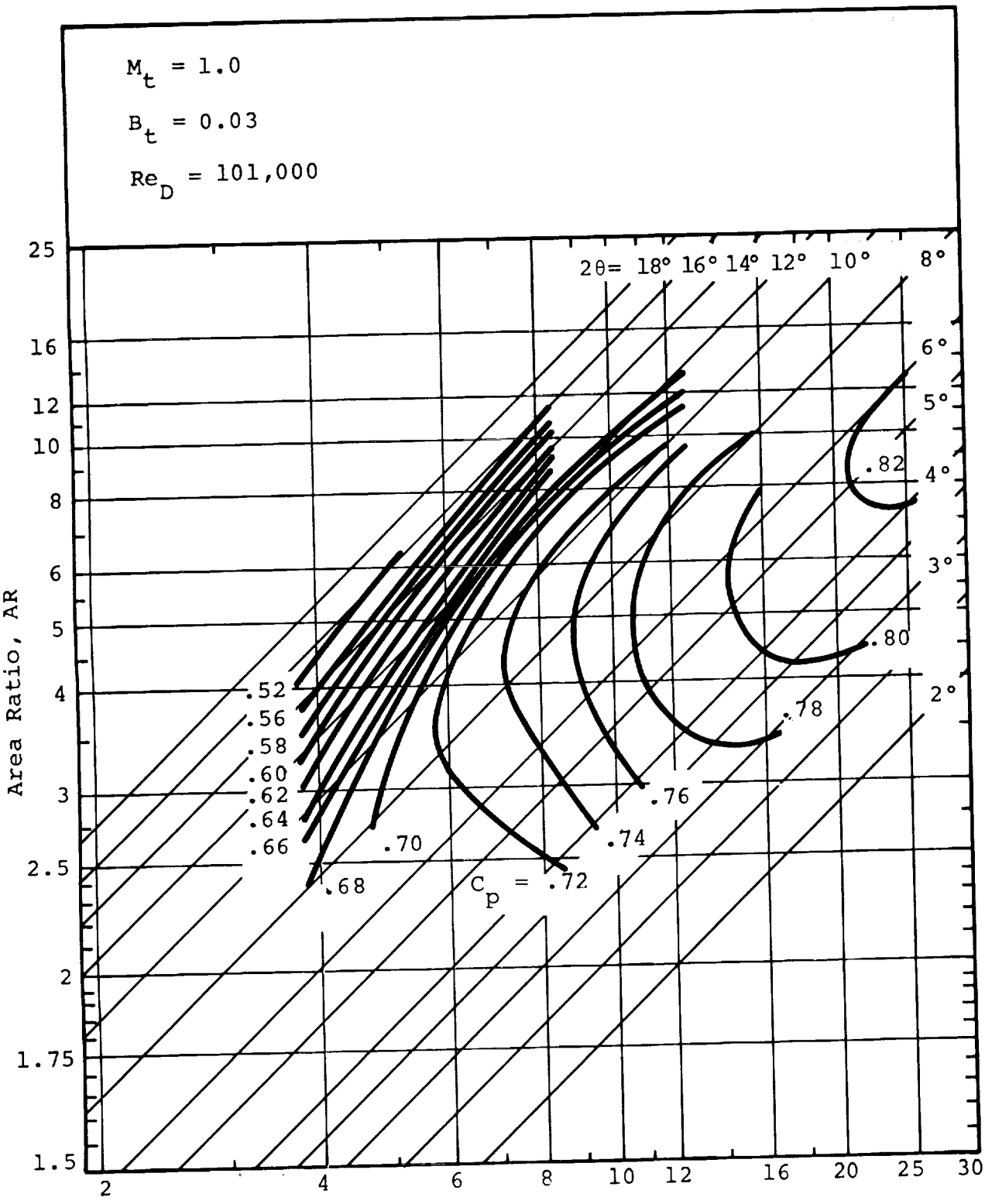


Figure 28 - Conical Diffuser Performance Map - $P_{ot}$ = 54.5 kN/m$^2$

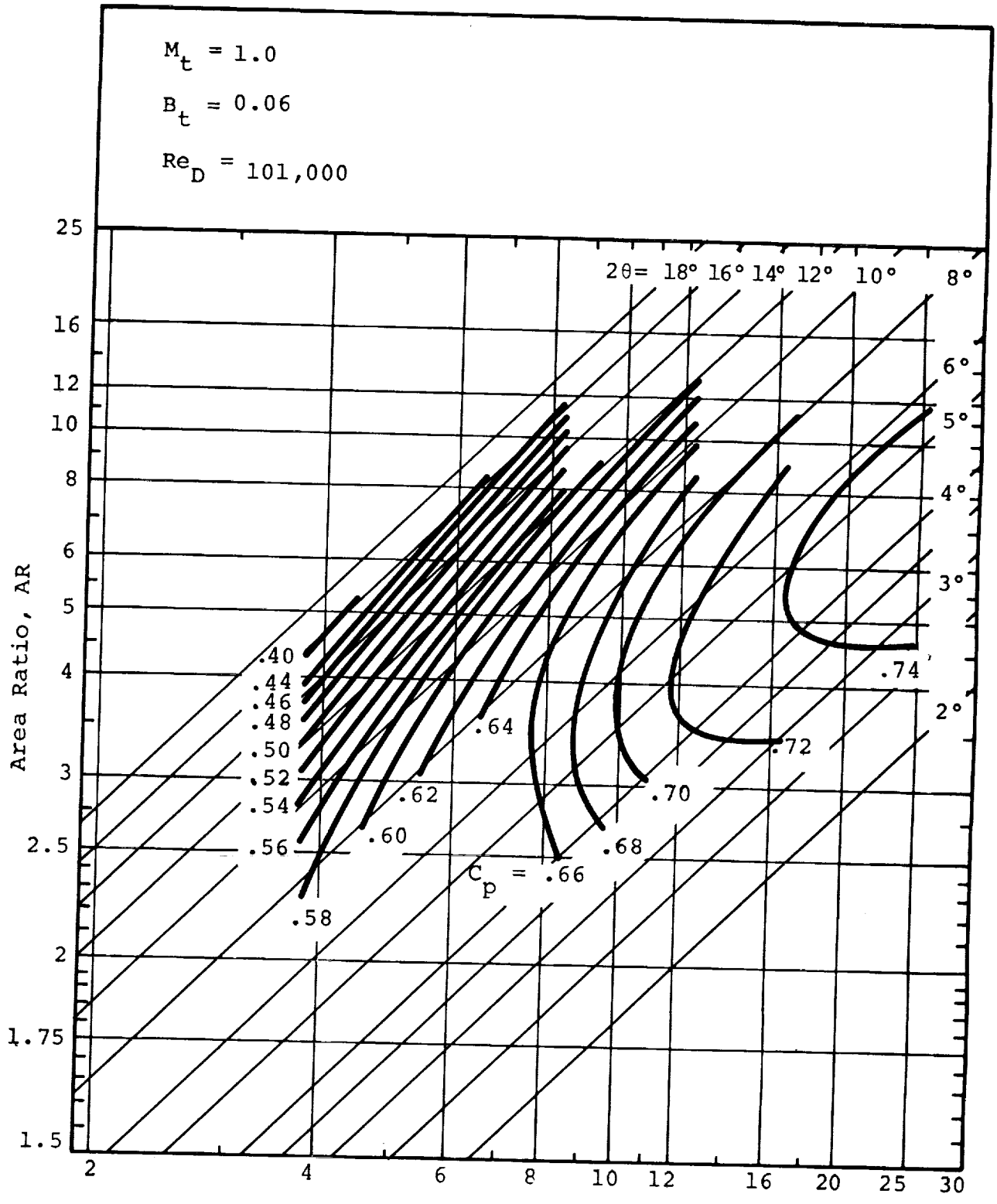


Figure 29 - Conical Diffuser Performance Map - $p_{ot}$ = 54.5 kN/m$^2$

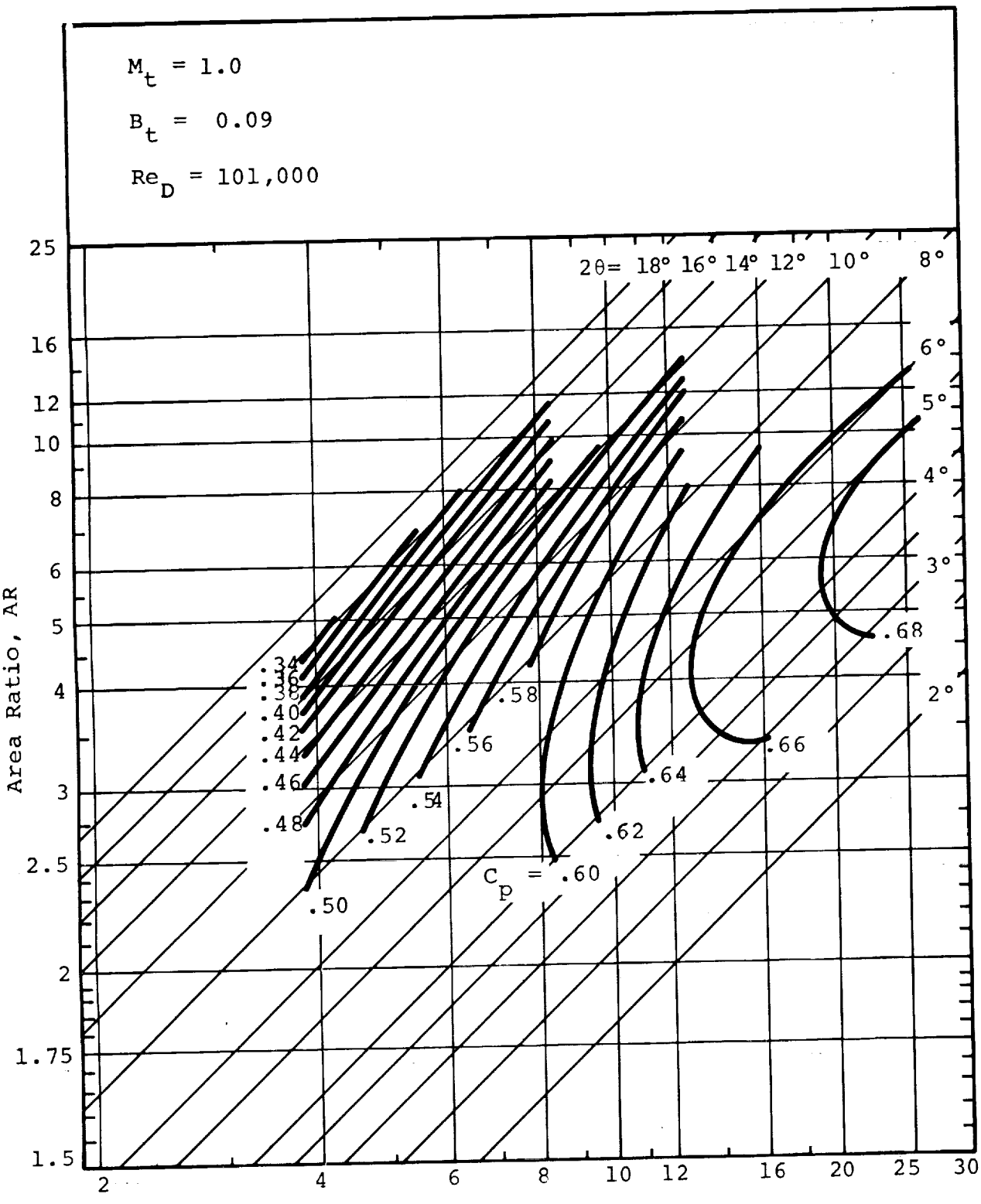


Figure 30 - Conical Diffuser Performance Map - $P_{ot}$ = 54.5 kN/m$^2$

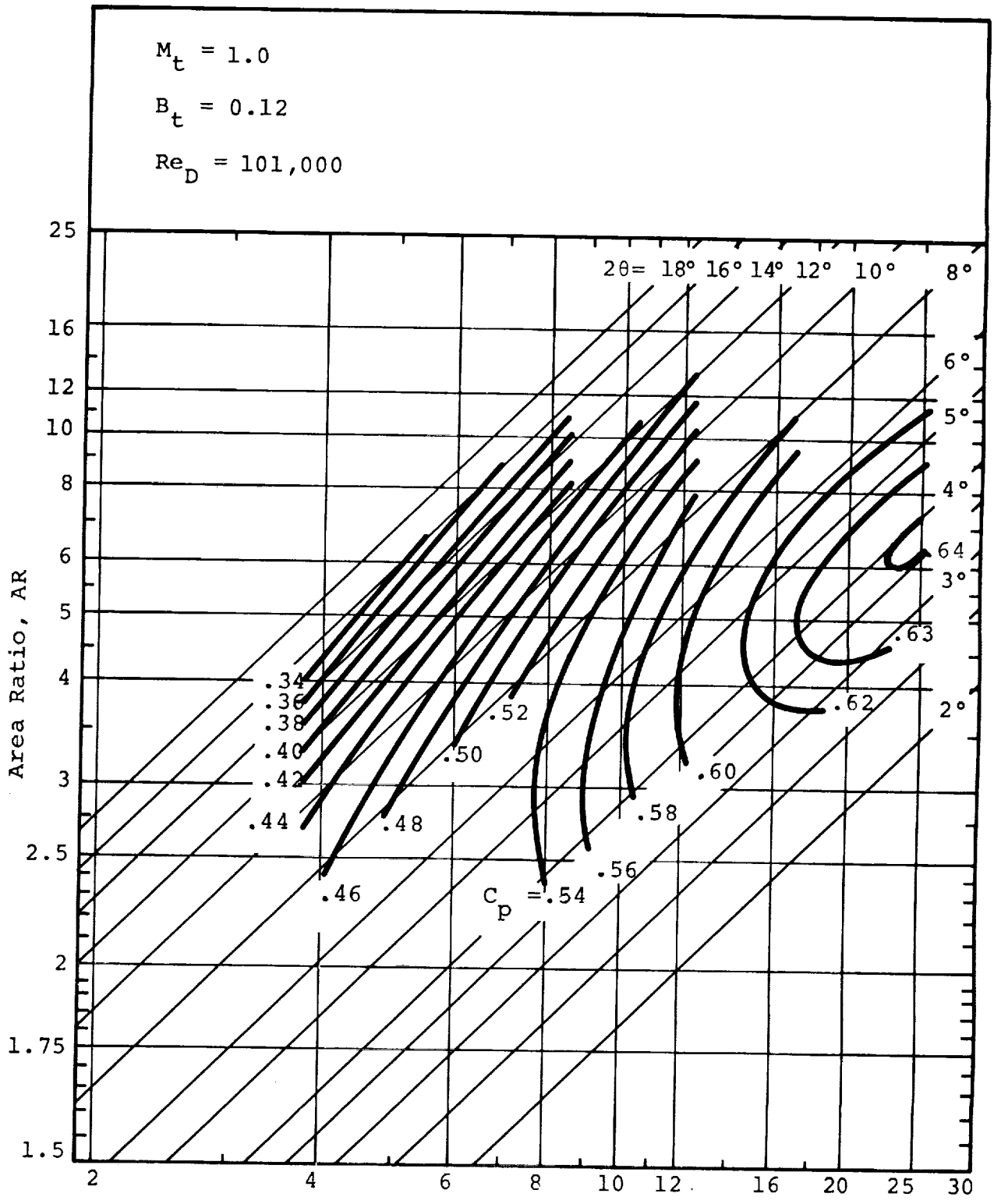


Figure 31 - Conical Diffuser Performance Map - $p_{ot}$ = 54.5 kN/m$^2$

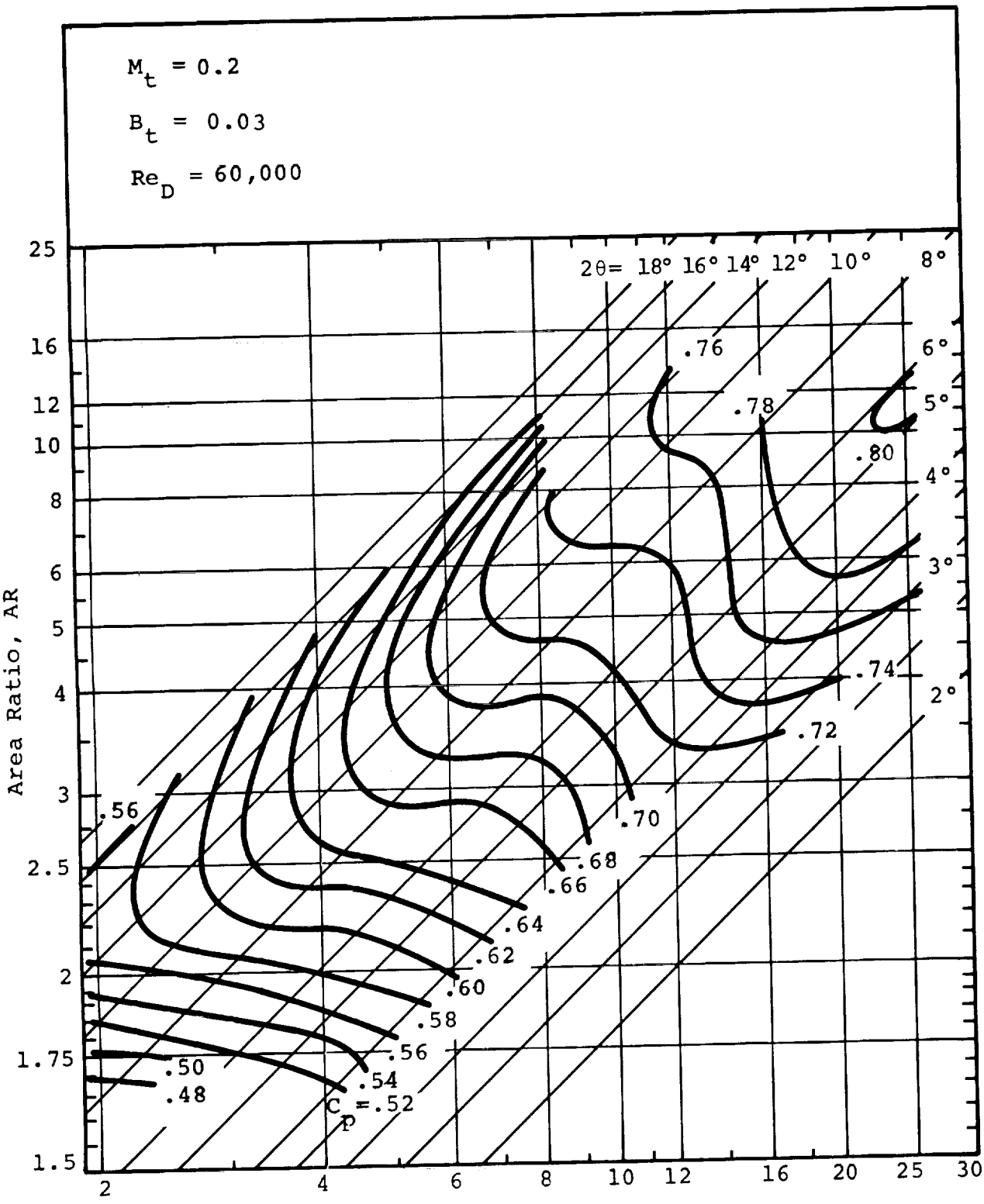


Figure 32 - Conical Diffuser Performance Map - $P_{ot}$ = 109 kN/m$^2$

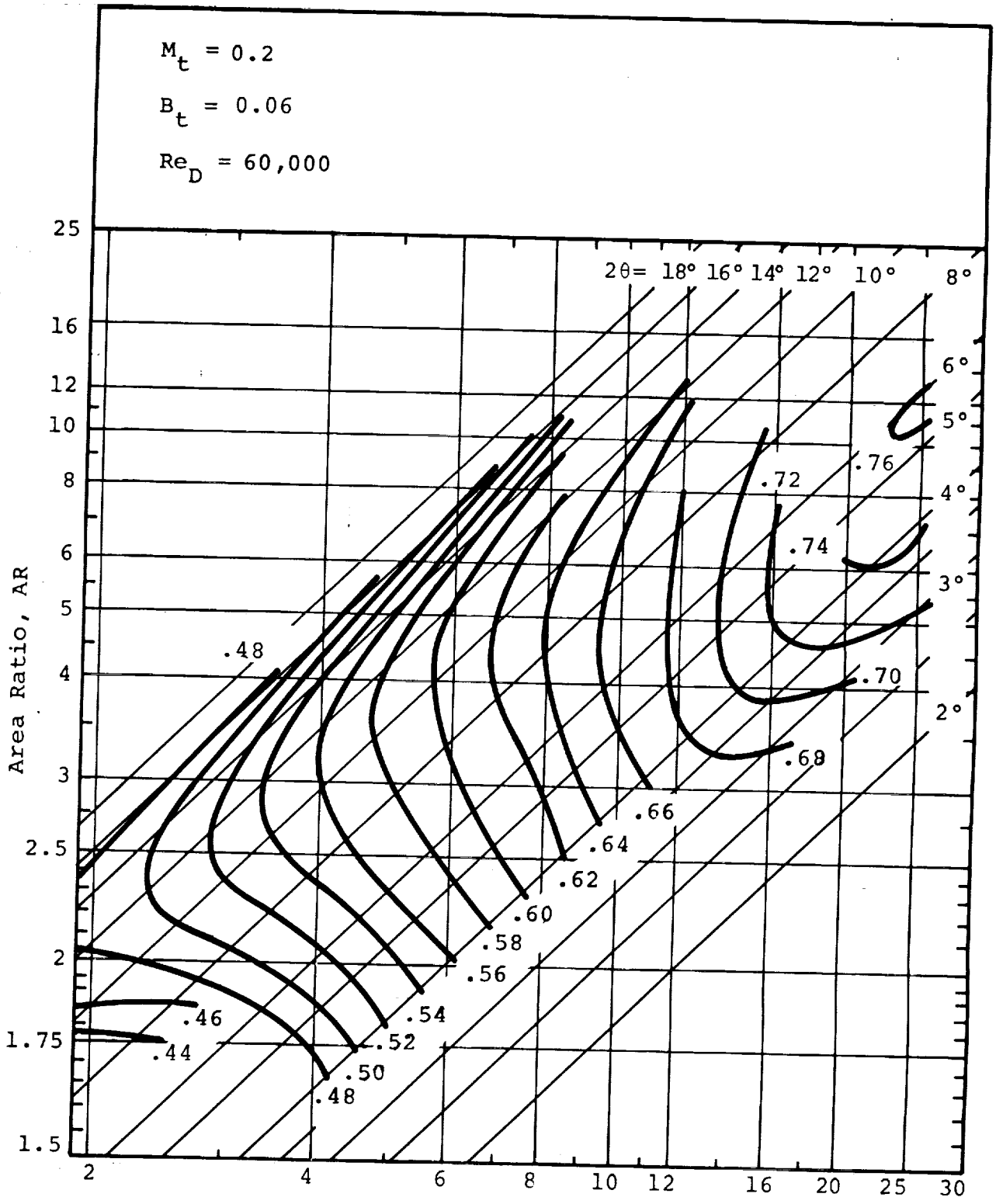


Figure 33 - Conical Diffuser Performance Map - $p_{ot}$ = 109 kN/m$^2$

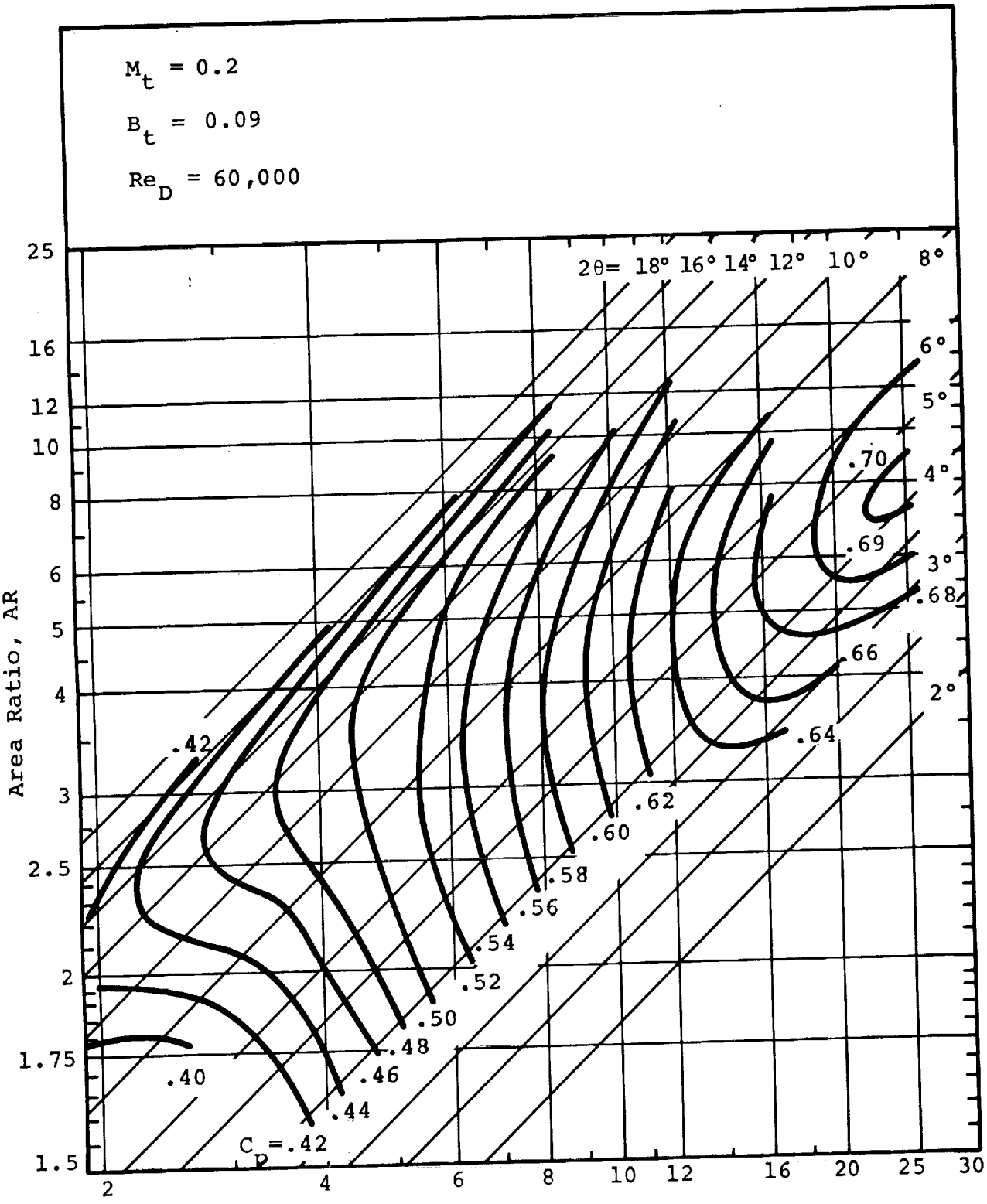


Figure 34 - Conical Diffuser Performance Map - $P_{ot}$ = 109 kN/m$^2$

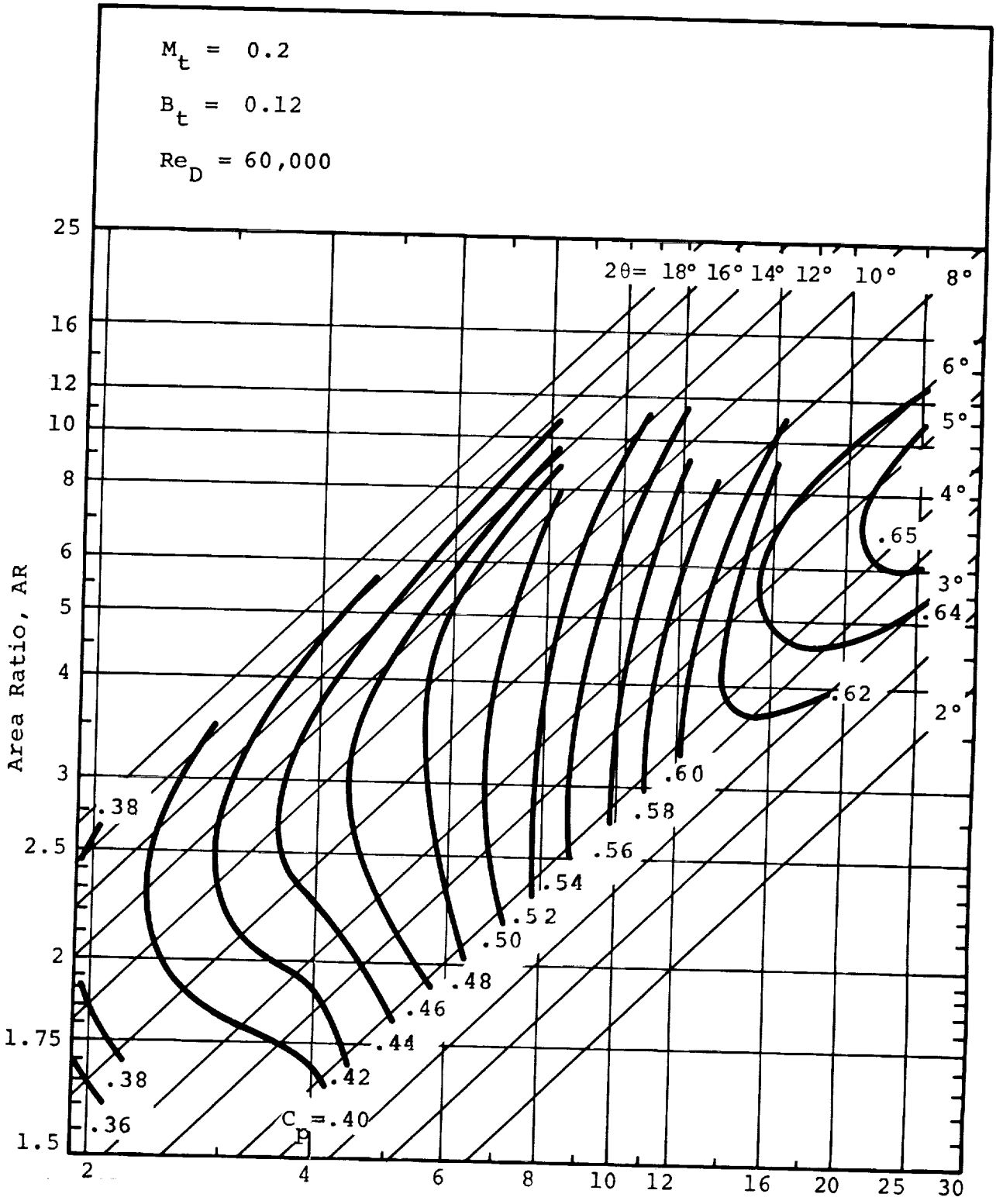


Figure 35 - Conical Diffuser Performance Map - $p_{ot}$ = 109 kN/m$^2$

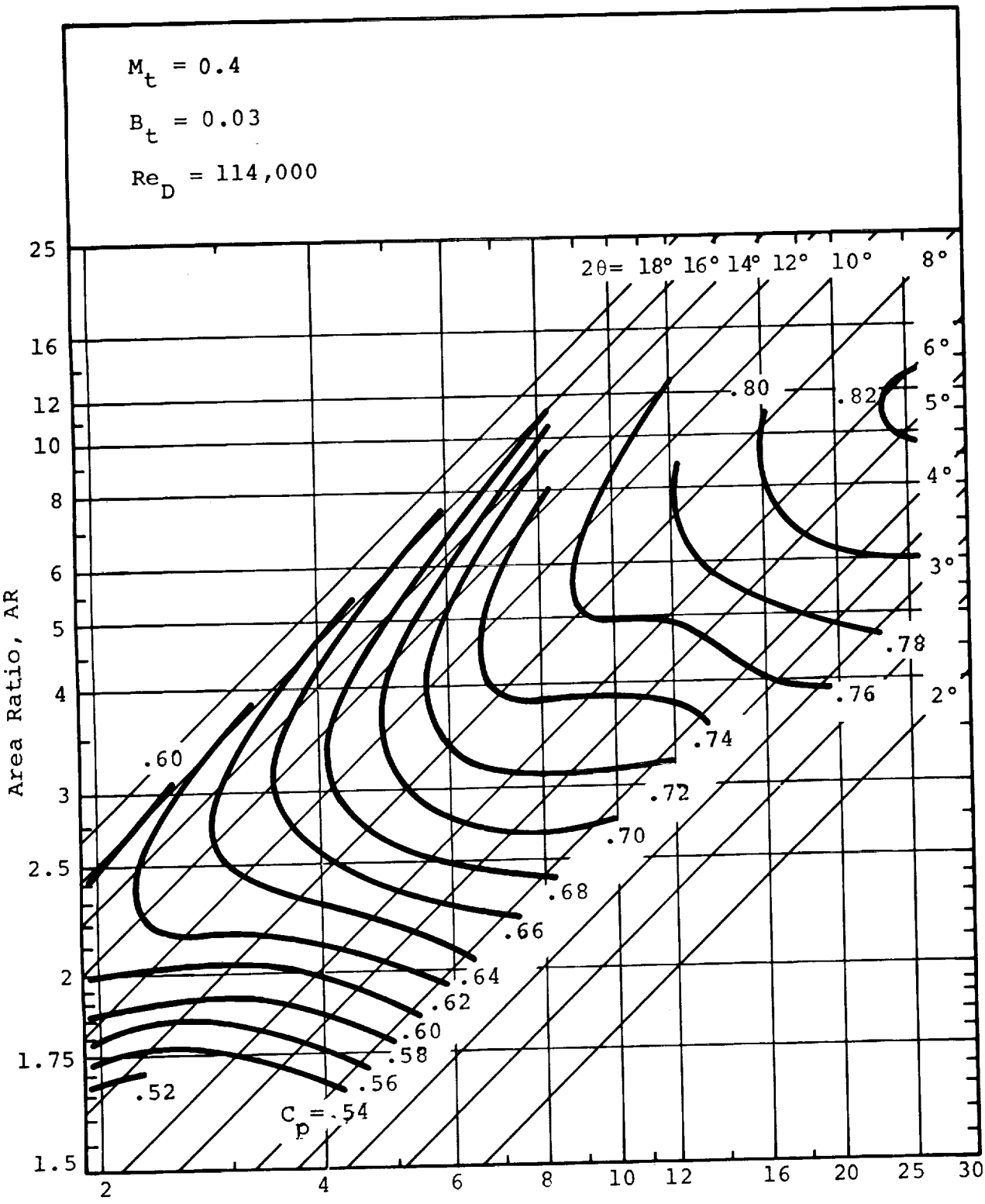


Figure 36 - Conical Diffuser Performance Map - $p_{ot}$ = 109 kN/m$^2$

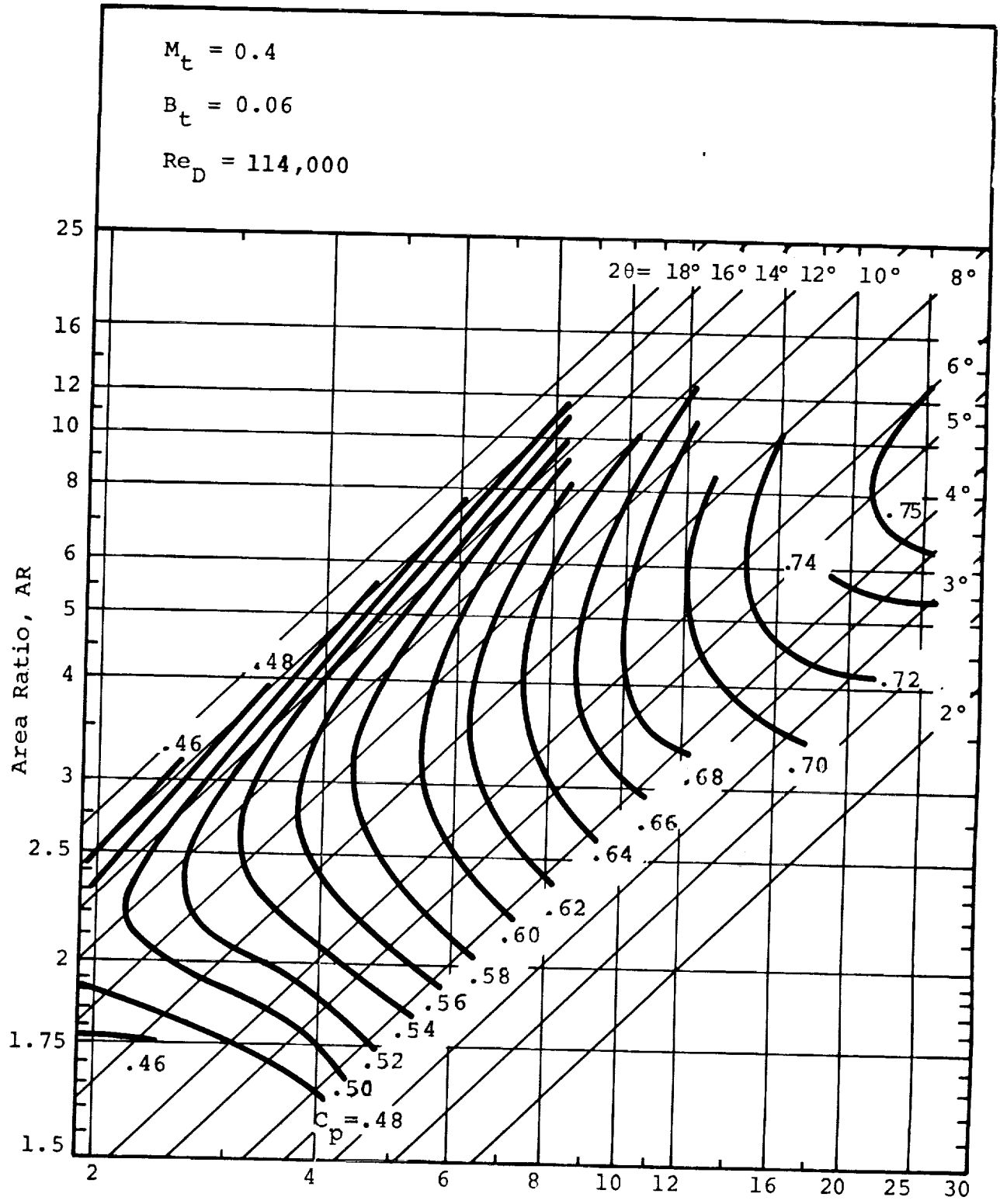


Figure 37 - Conical Diffuser Performance Map - $p_{ot}$ = 109 kN/m$^2$

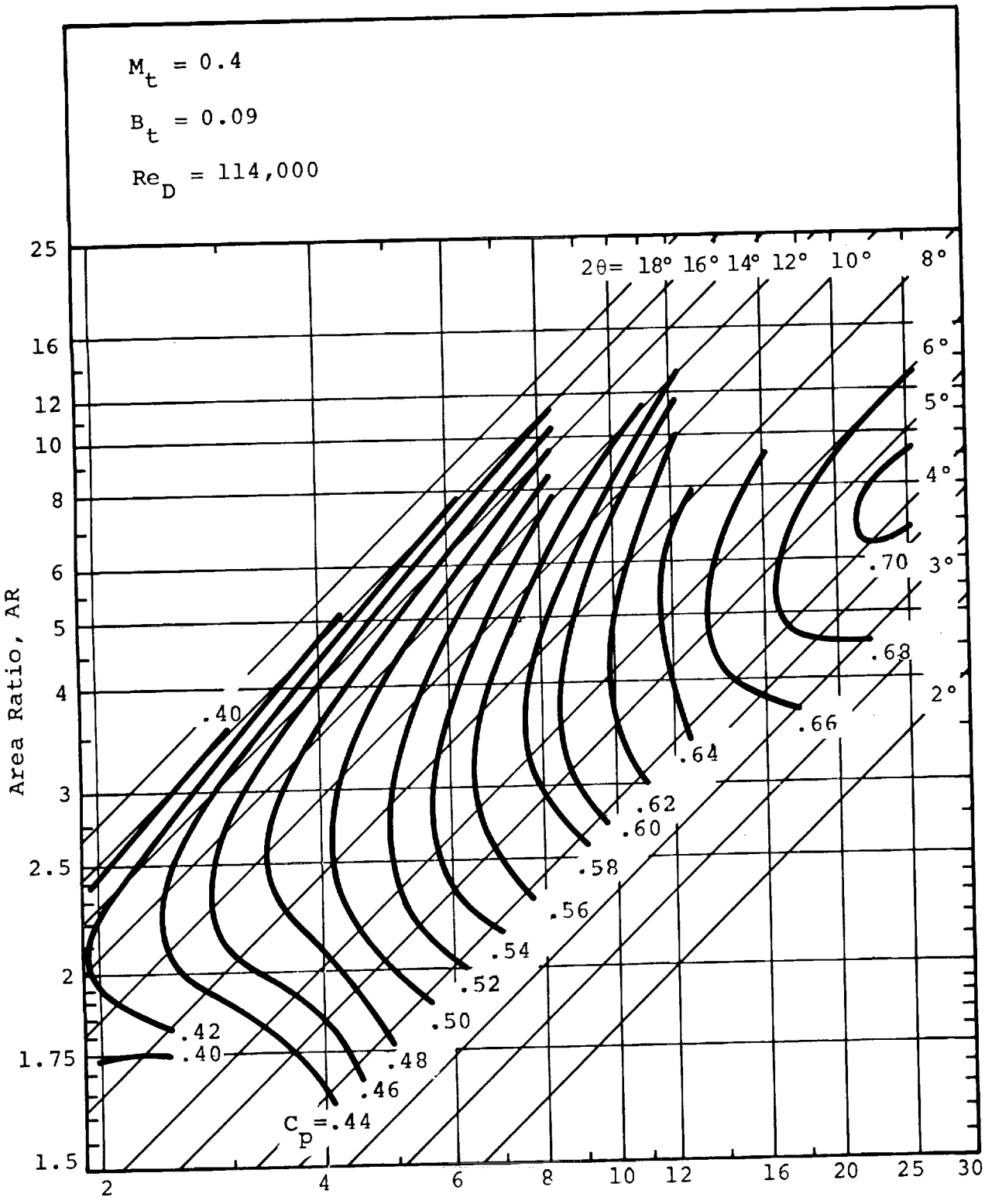


Figure 38 - Conical Diffuser Performance Map - $p_{ot}$ = 109 kN/m$^2$

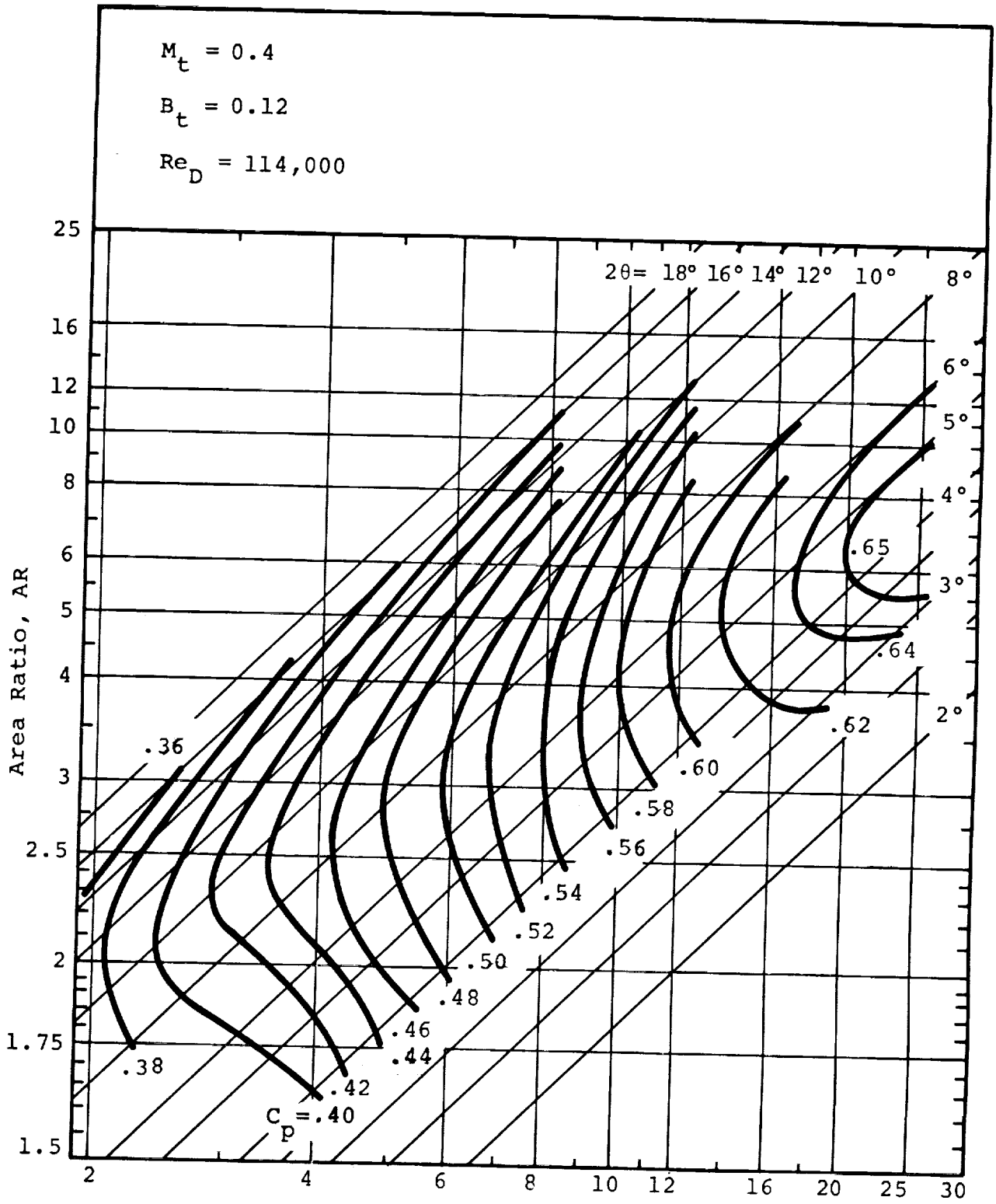


Figure 39 - Conical Diffuser Performance Map - $p_{ot}$ = 109 kN/m$^2$

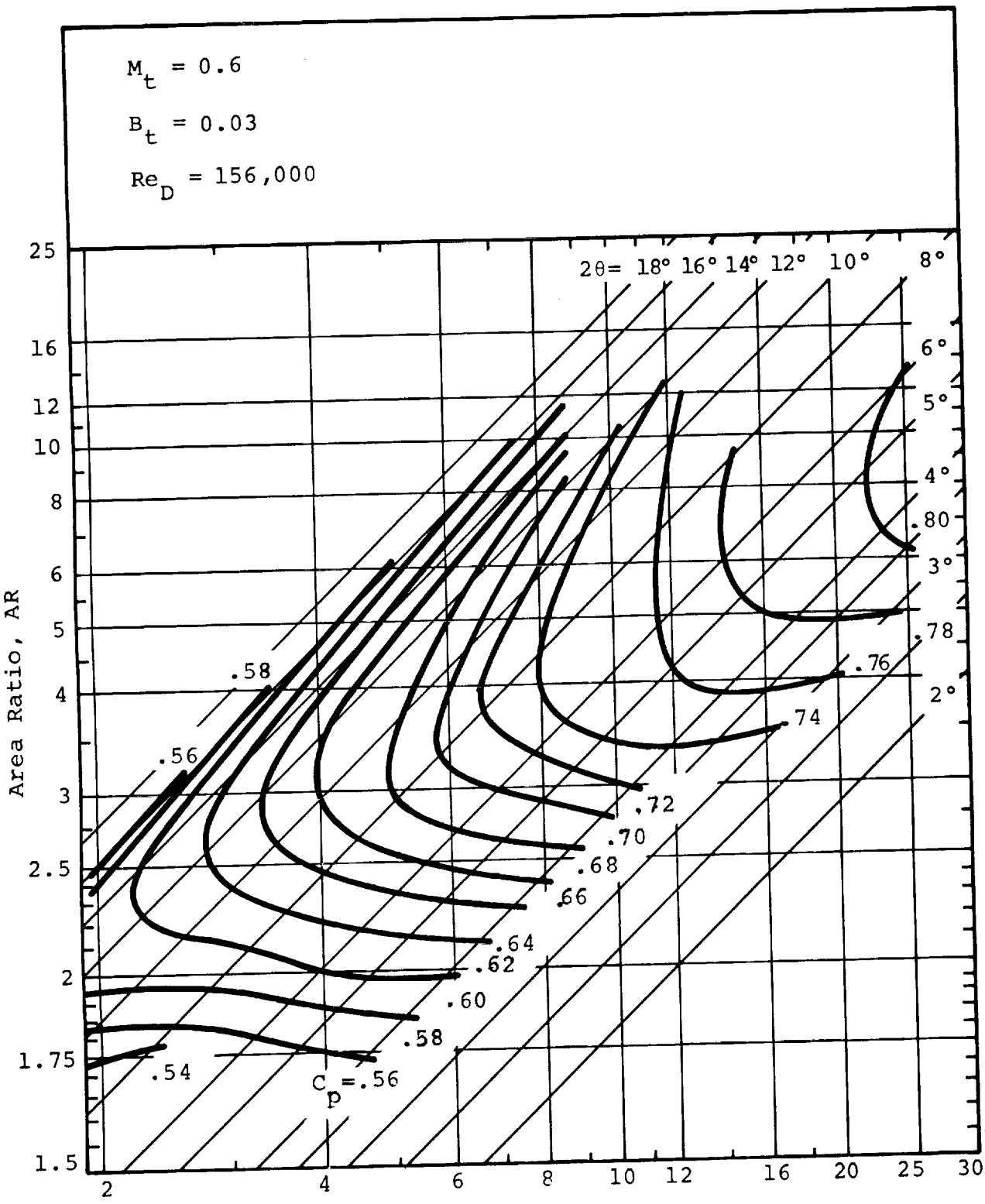


Figure 40 - Conical Diffuser Performance Map - $P_{ot}$ = 109 kN/m$^2$

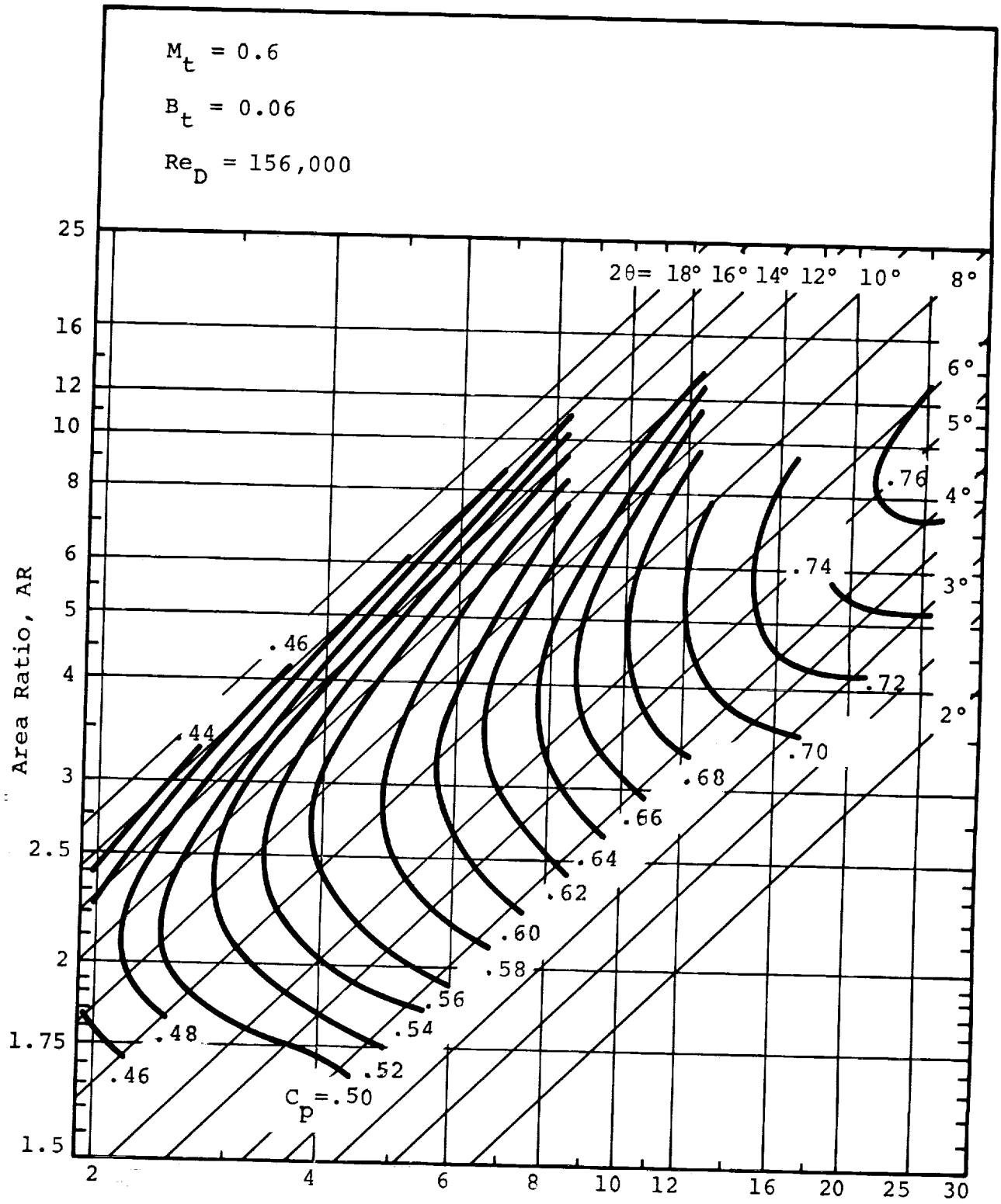


Figure 41 - Conical Diffuser Performance Map - $p_{ot}$ = 109 kN/m$^2$

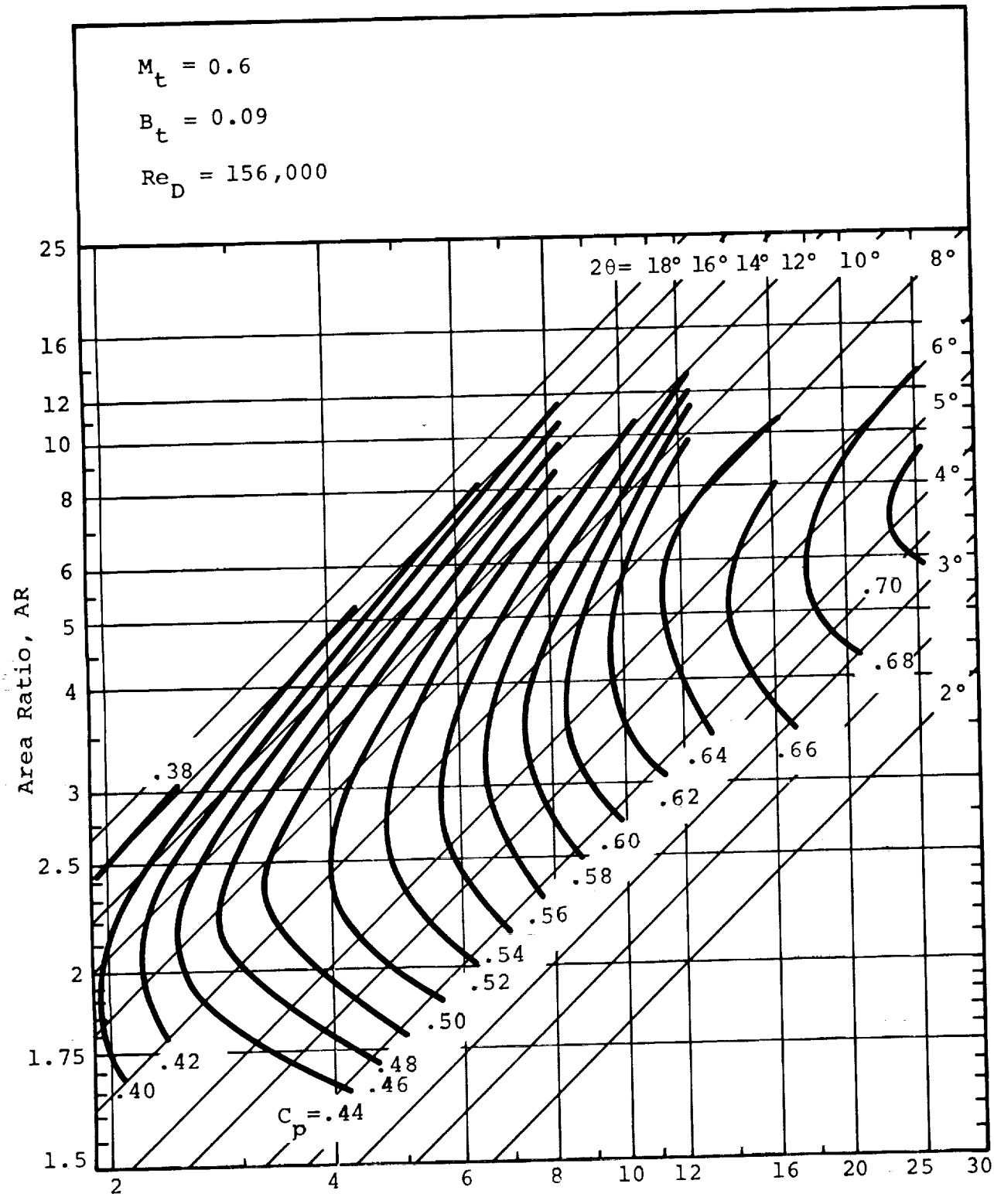


Figure 42 - Conical Diffuser Performance Map - $p_{ot}$ = 109 kN/m$^2$

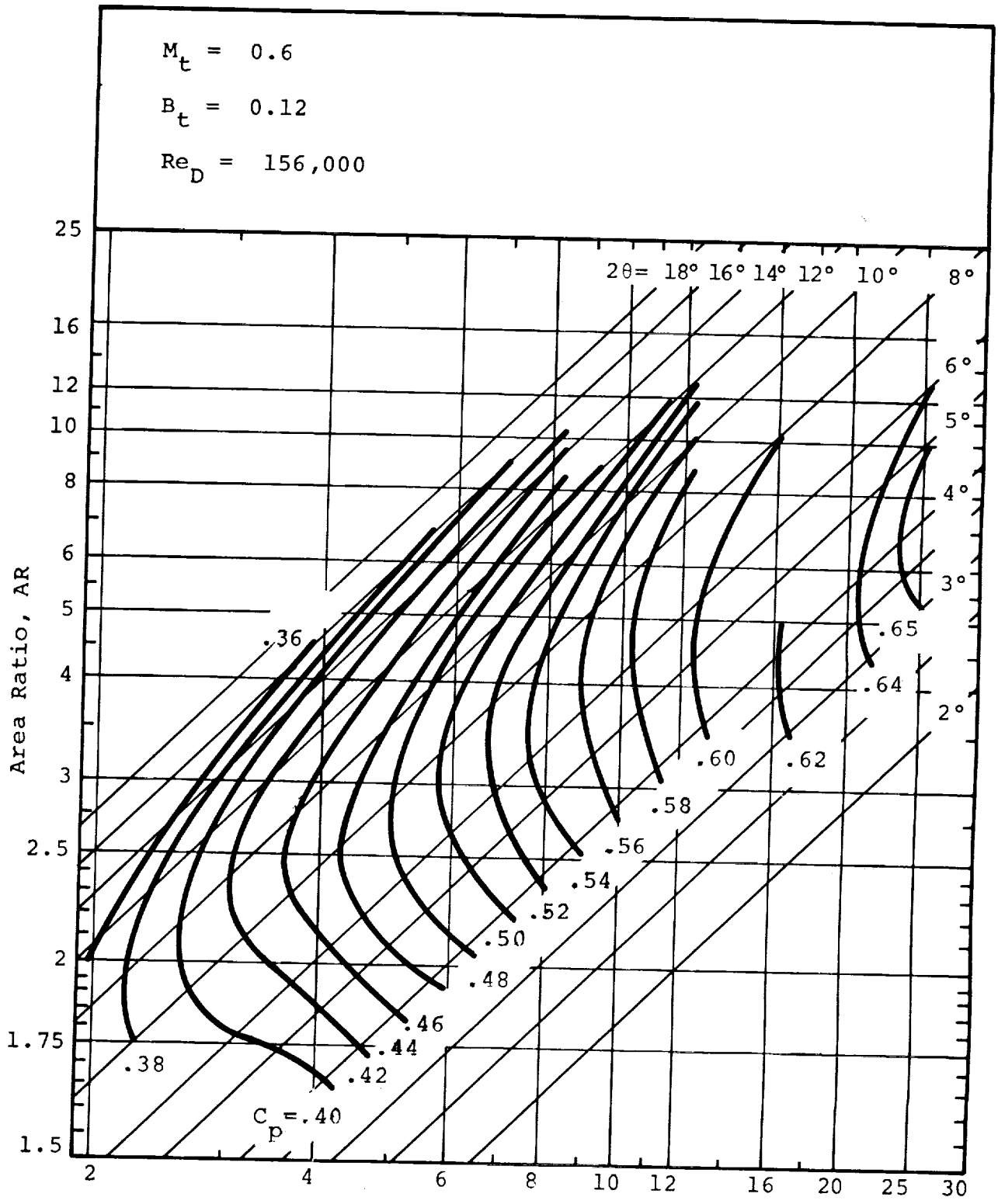


Figure 43 - Conical Diffuser Performance Map - $p_{ot}$ = 109 kN/m$^2$

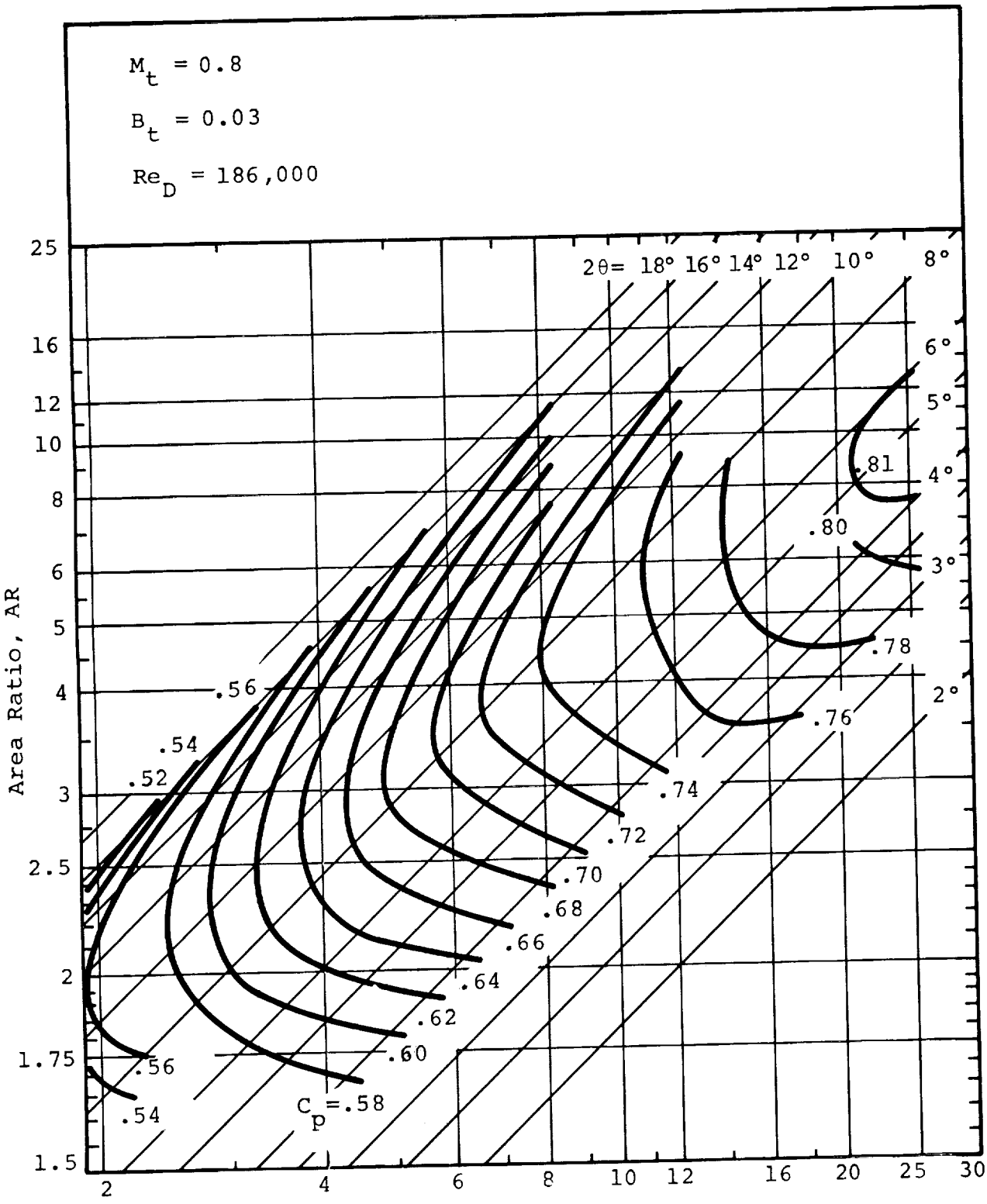


Figure 44 - Conical Diffuser Performance Map - $p_{ot}$ = 109 kN/m$^2$

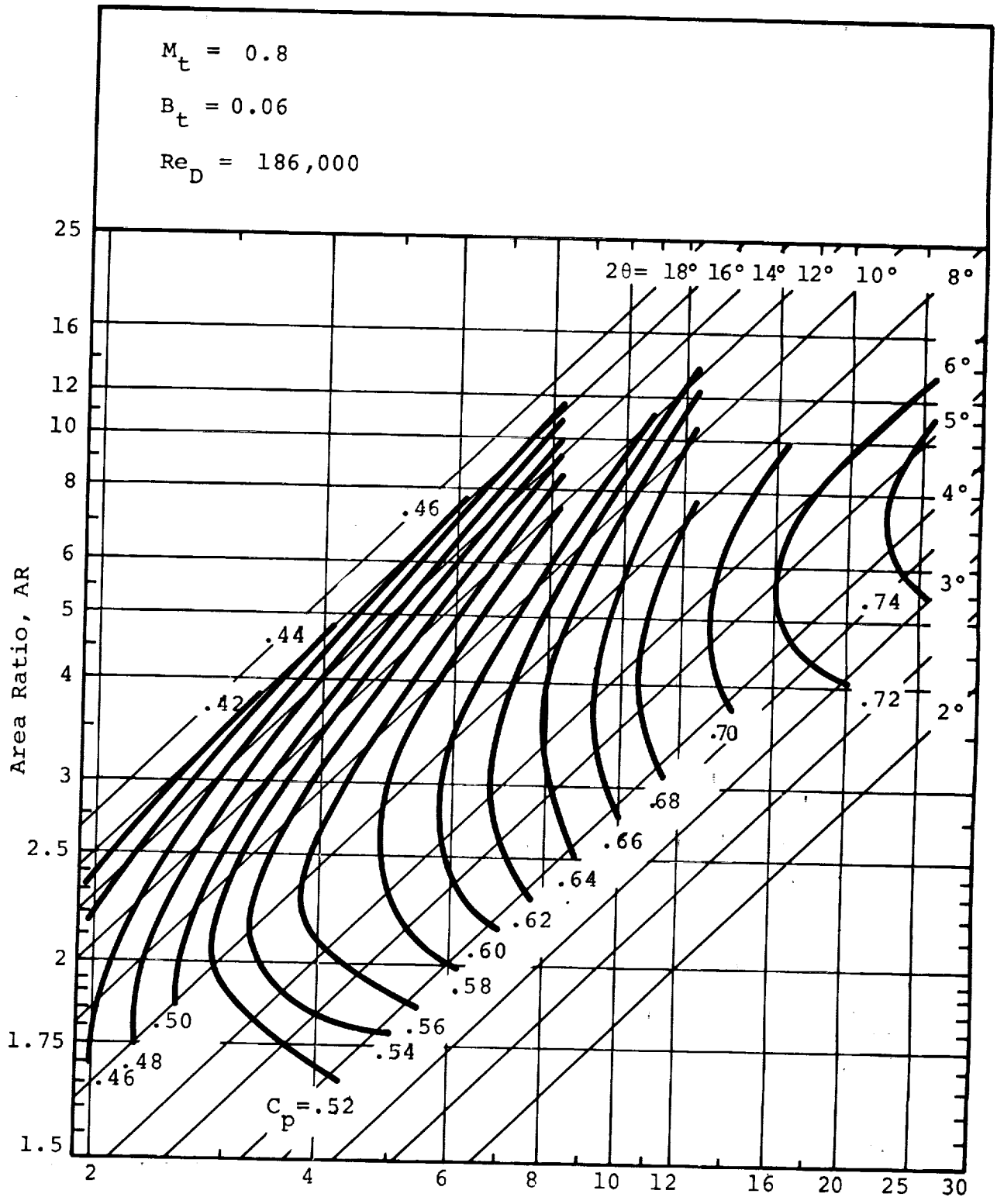


Figure 45 - Conical Diffuser Performance Map - $p_{ot}$ = 109 kN/m$^2$

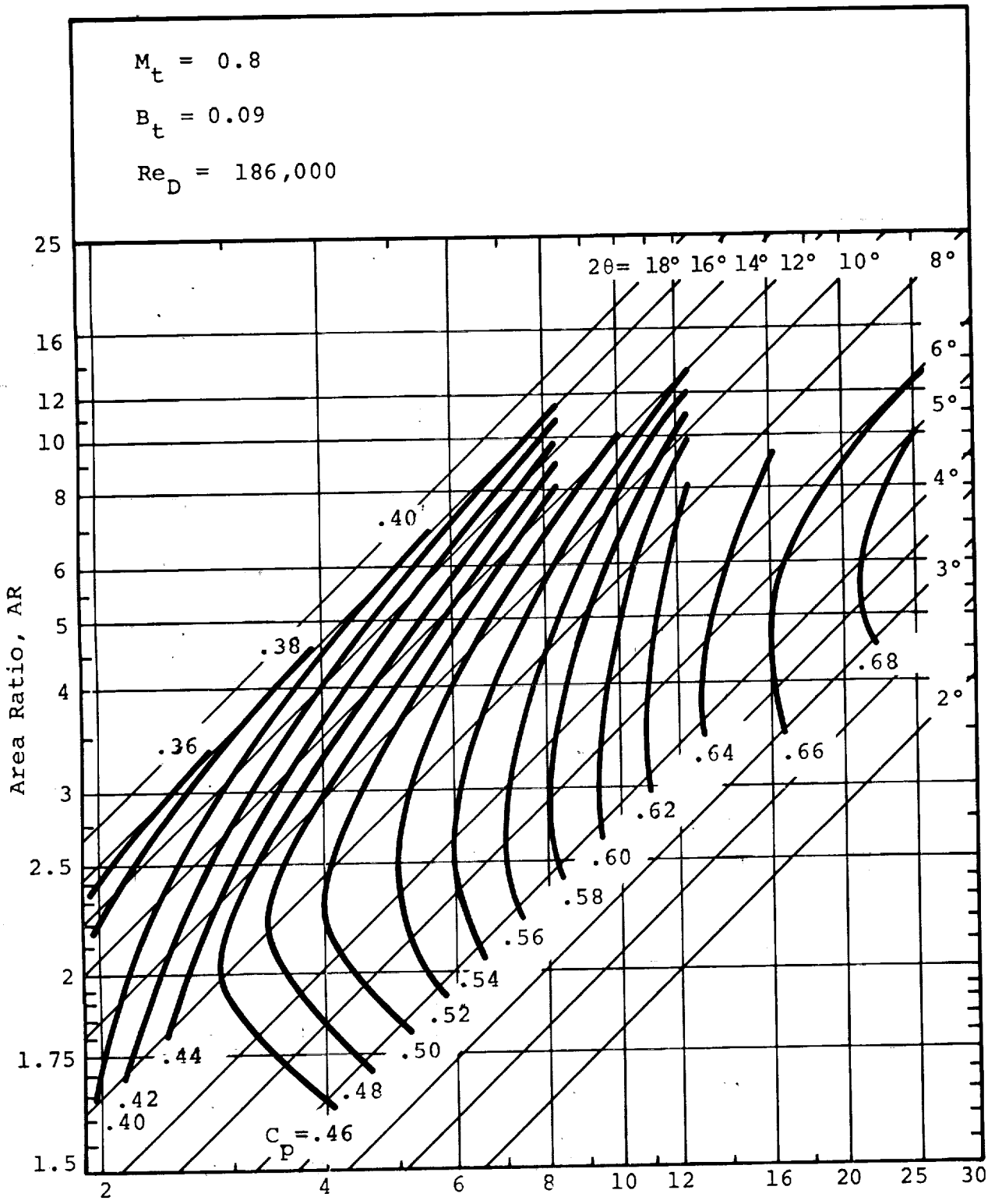


Figure 46 - Conical Diffuser Performance Map - $p_{ot}$ = 109 kN/m$^2$

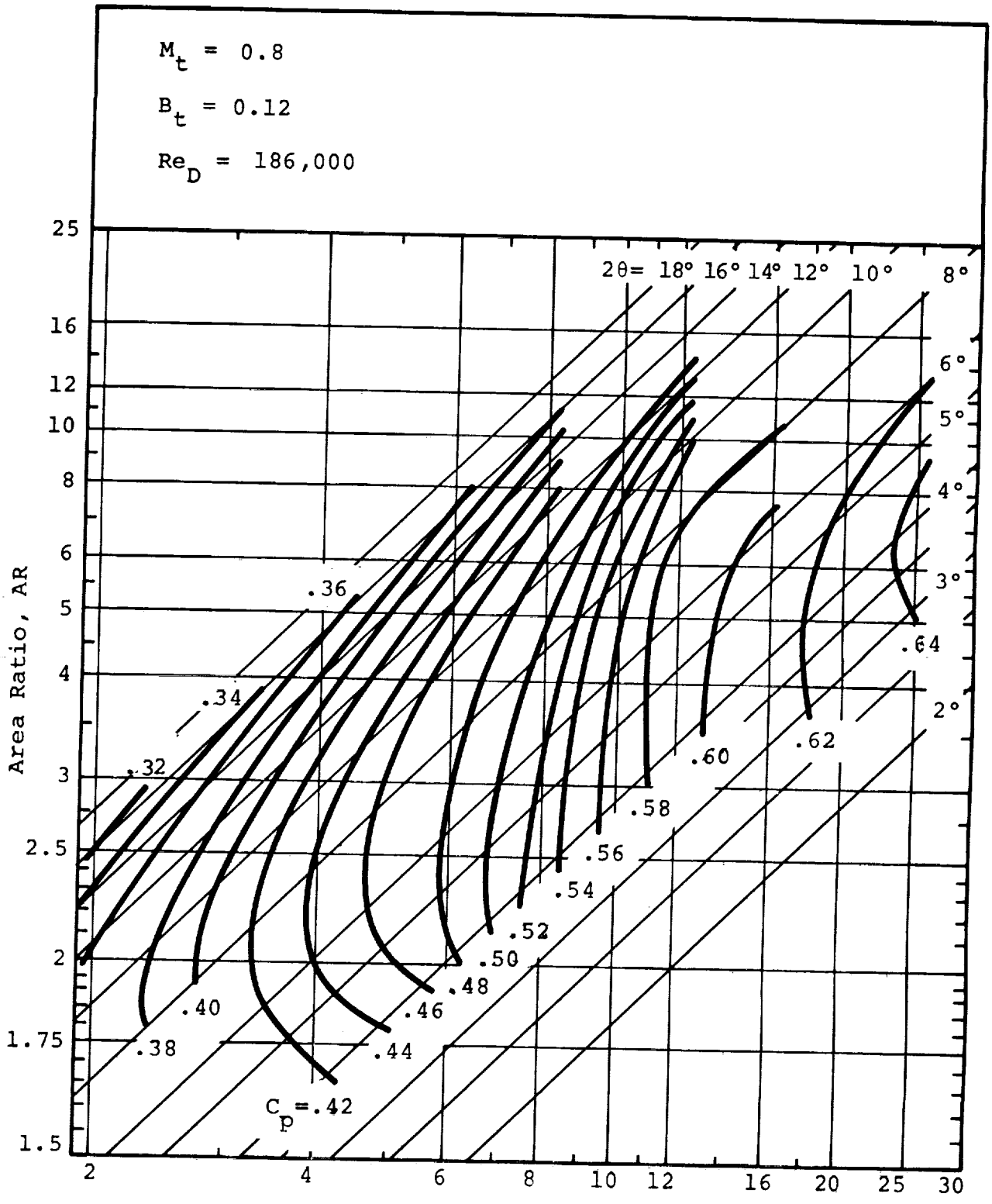


Figure 47 - Conical Diffuser Performance Map - $p_{ot}$ = 109 kN/m$^2$

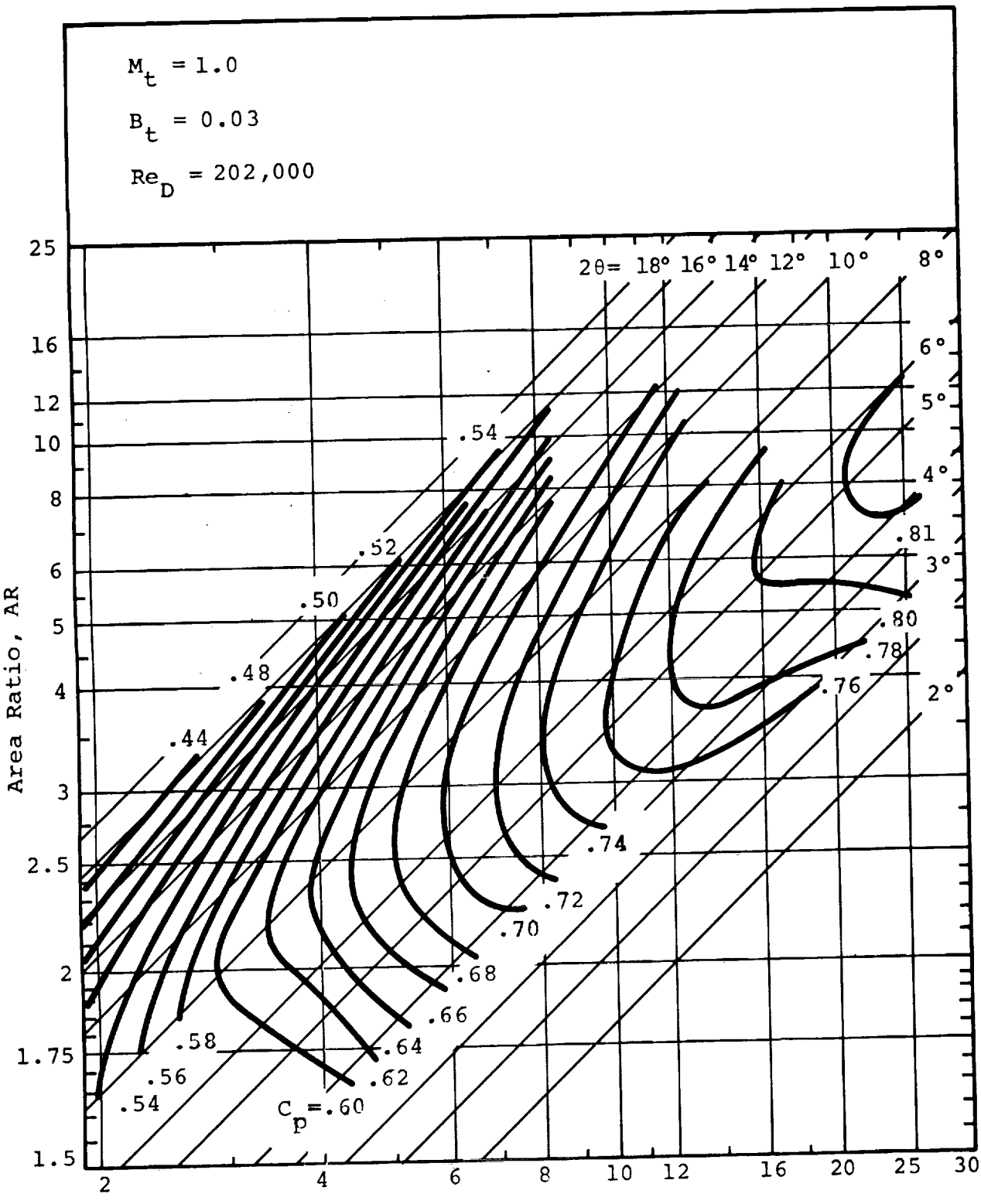


Figure 48 - Conical Diffuser Performance Map - $p_{ot}$ = 109 kN/m$^2$

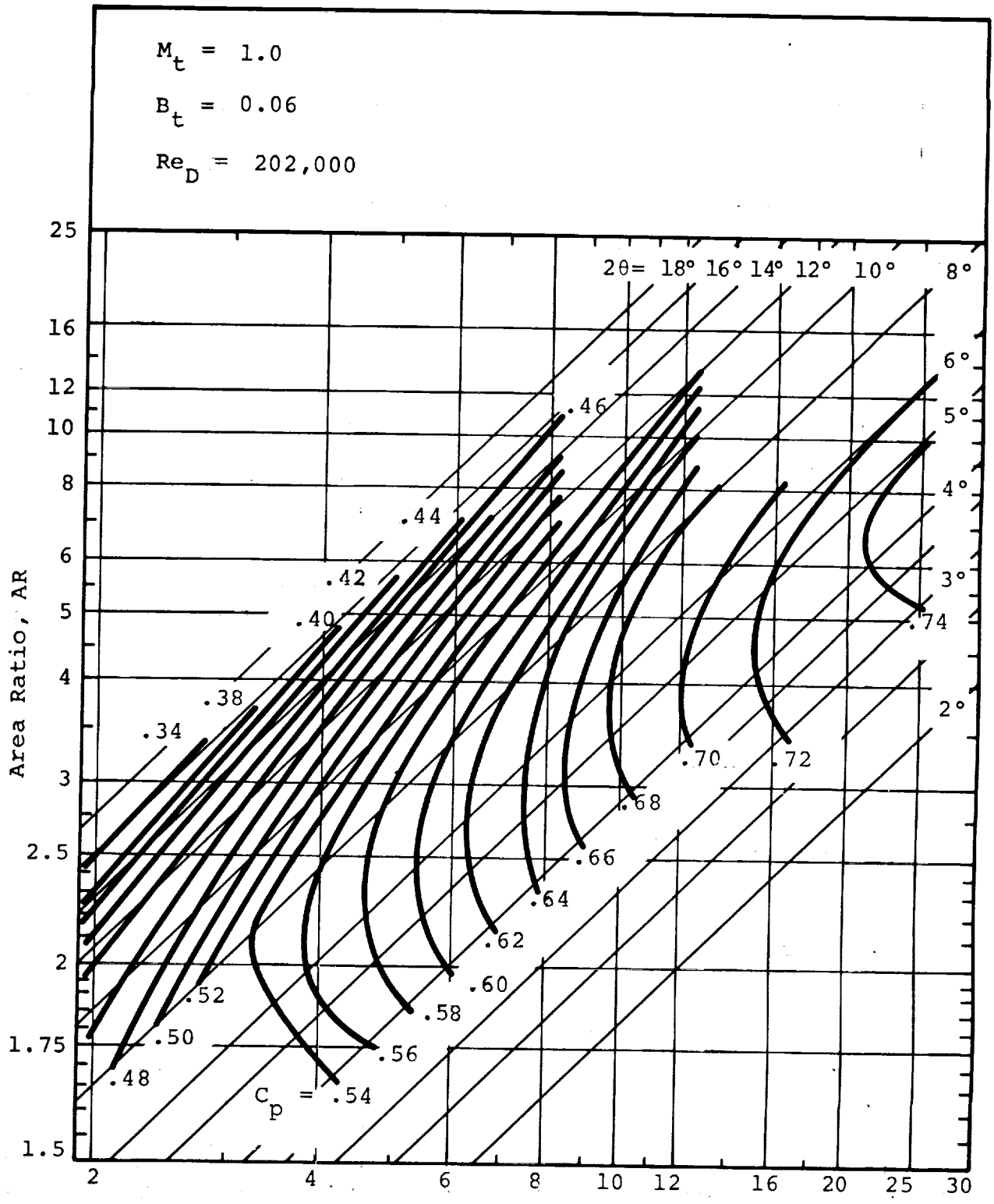


Figure 49 - Conical Diffuser Performance Map - $p_{ot}$ = 109 kN/m$^2$

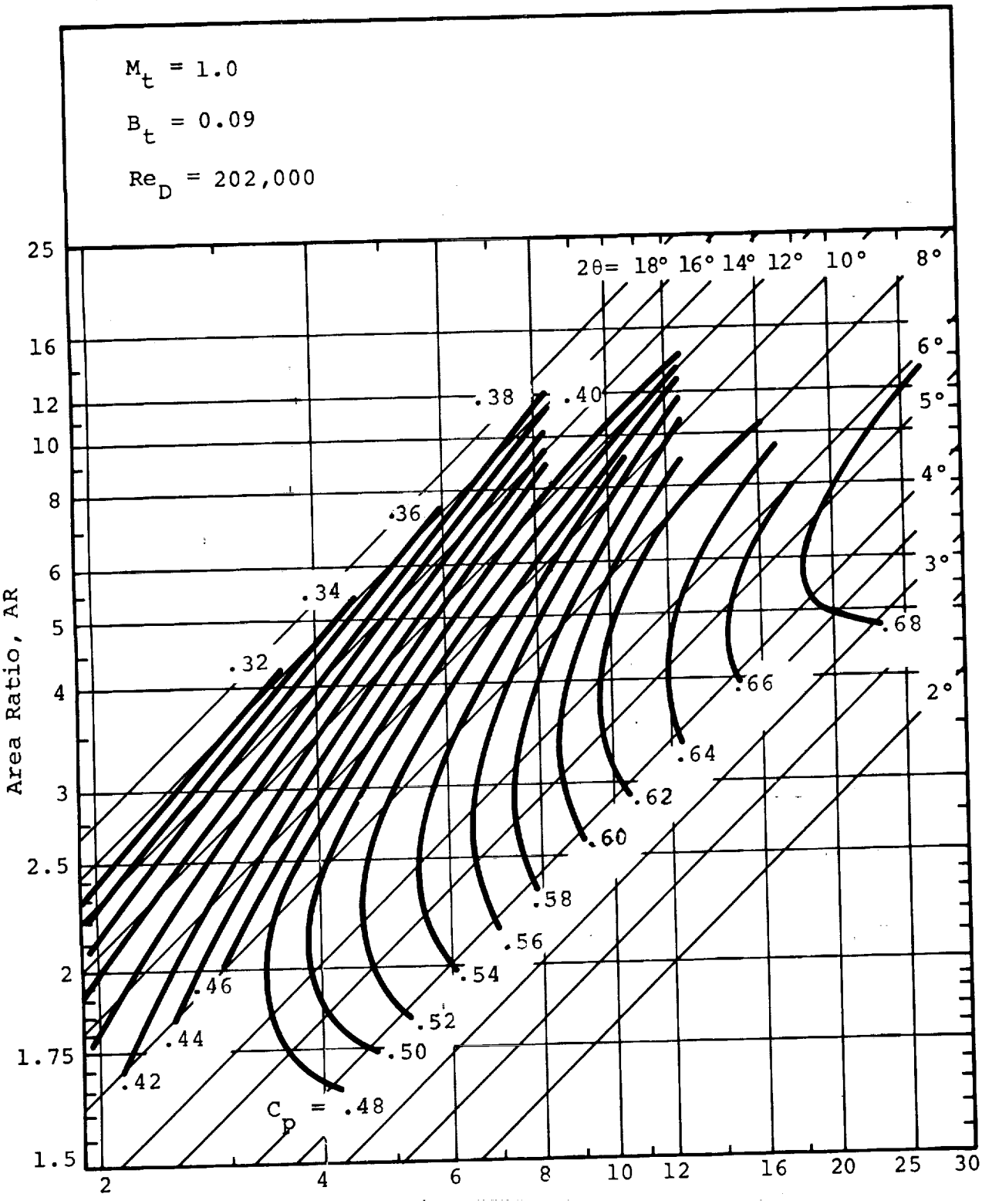


Figure 50 - Conical Diffuser Performance Map - $p_{ot}$ = 109 kN/m$^2$

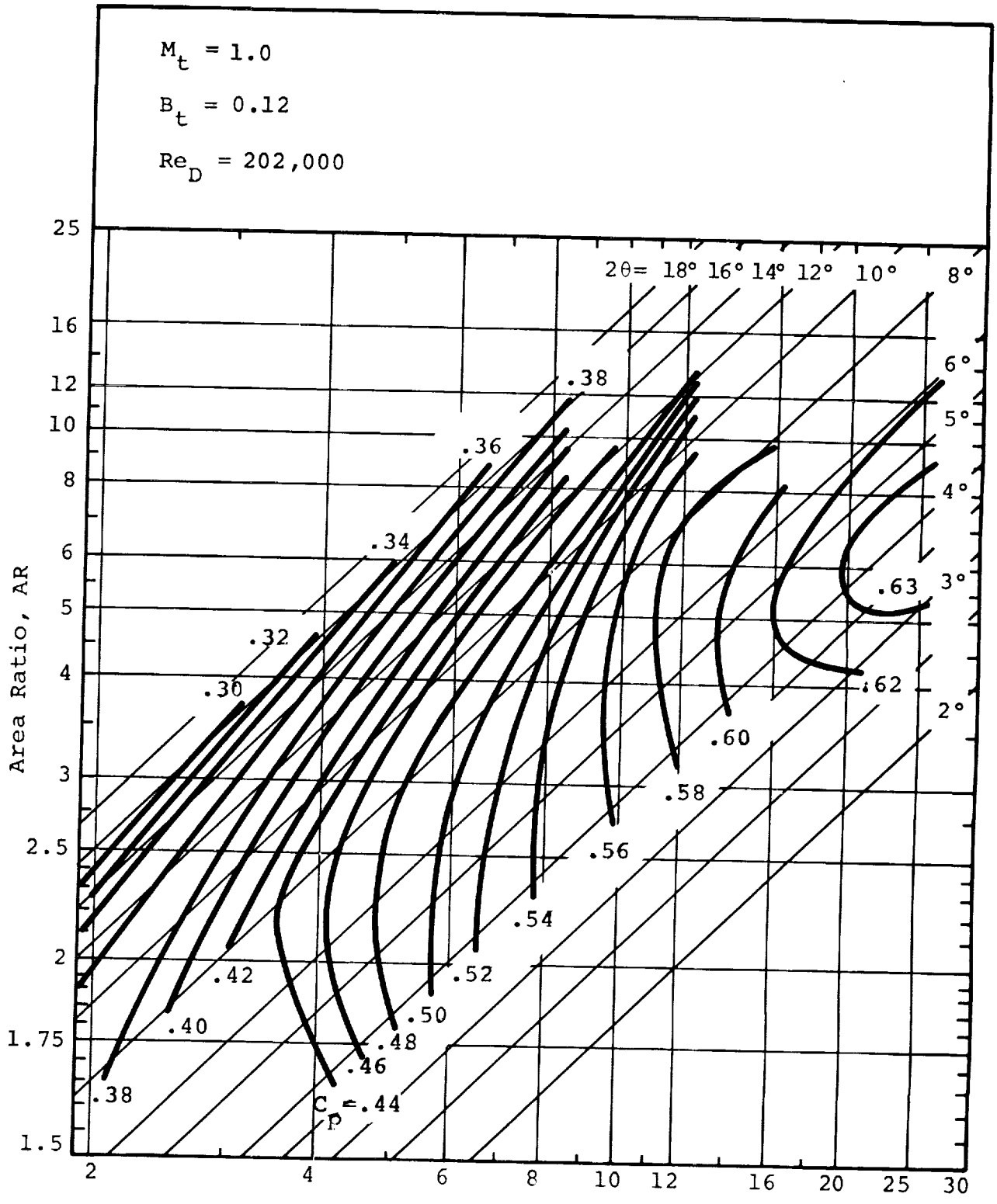


Figure 51 - Conical Diffuser Performance Map - $P_{ot}$ = 109 kN/m$^2$

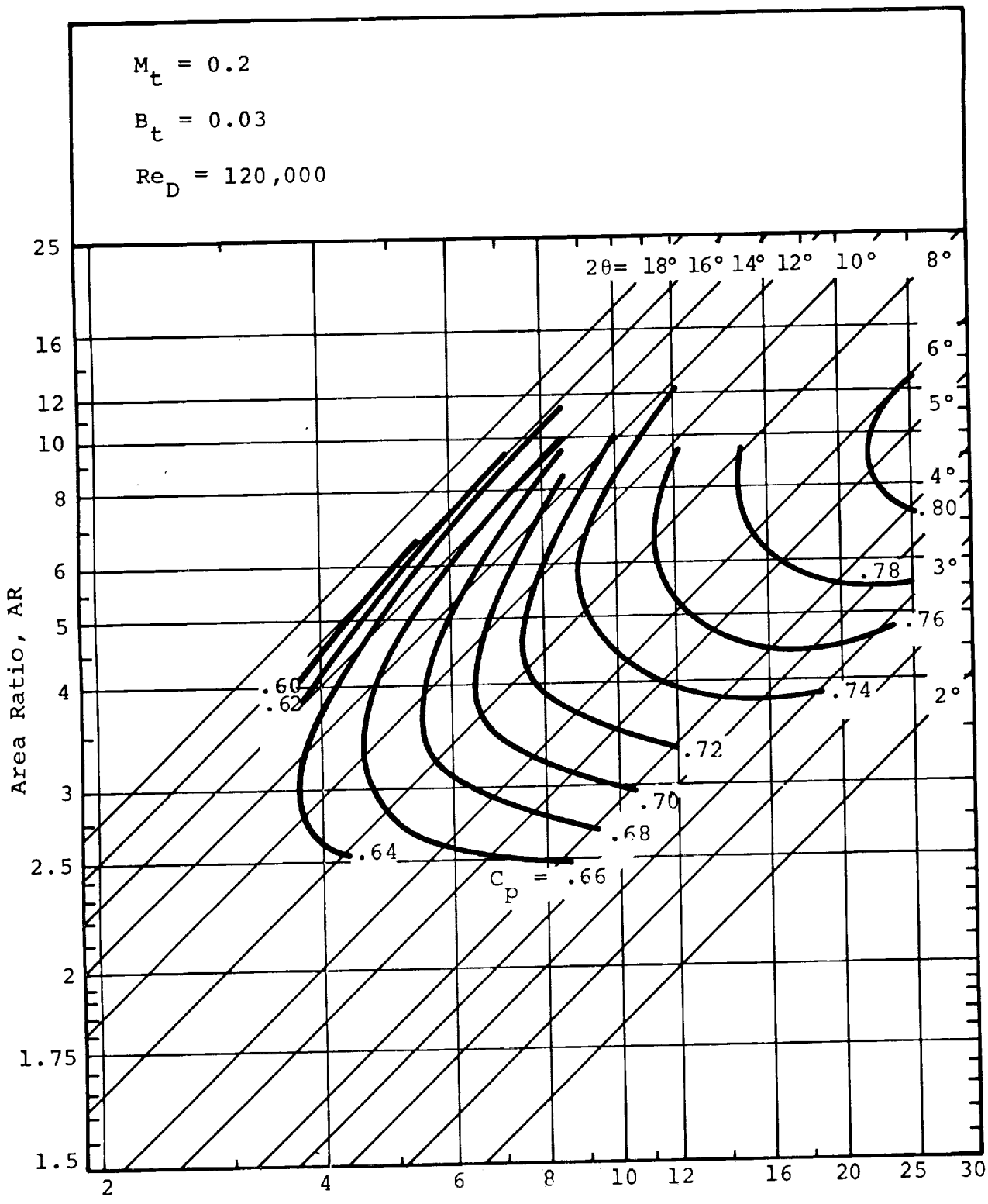


Figure 52 - Conical Diffuser Performance Map - $p_{ot}$ = 218 kN/m$^2$

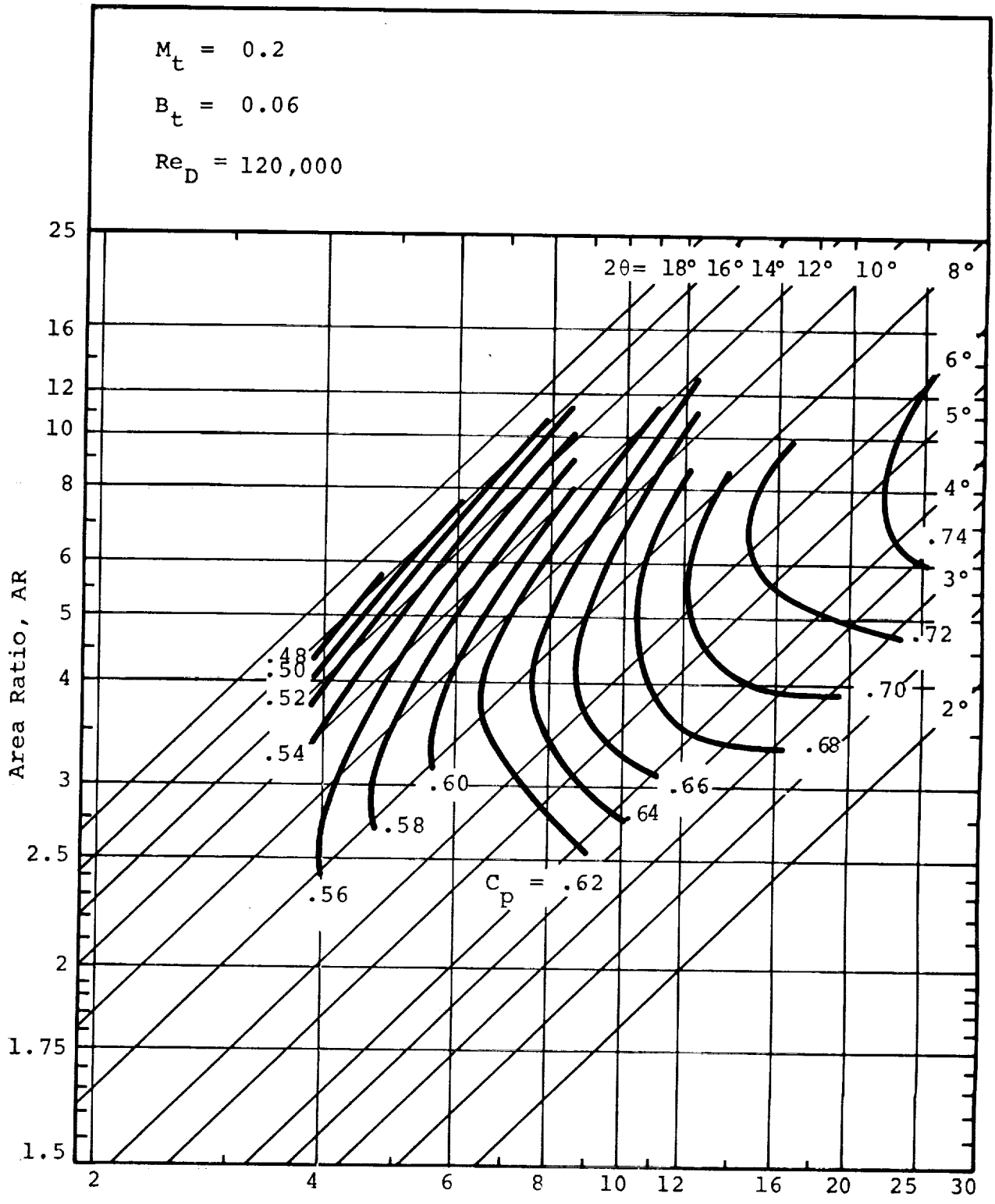


Figure 53 - Conical Diffuser Performance Map - $p_{ot}$ = 218 kN/m$^2$

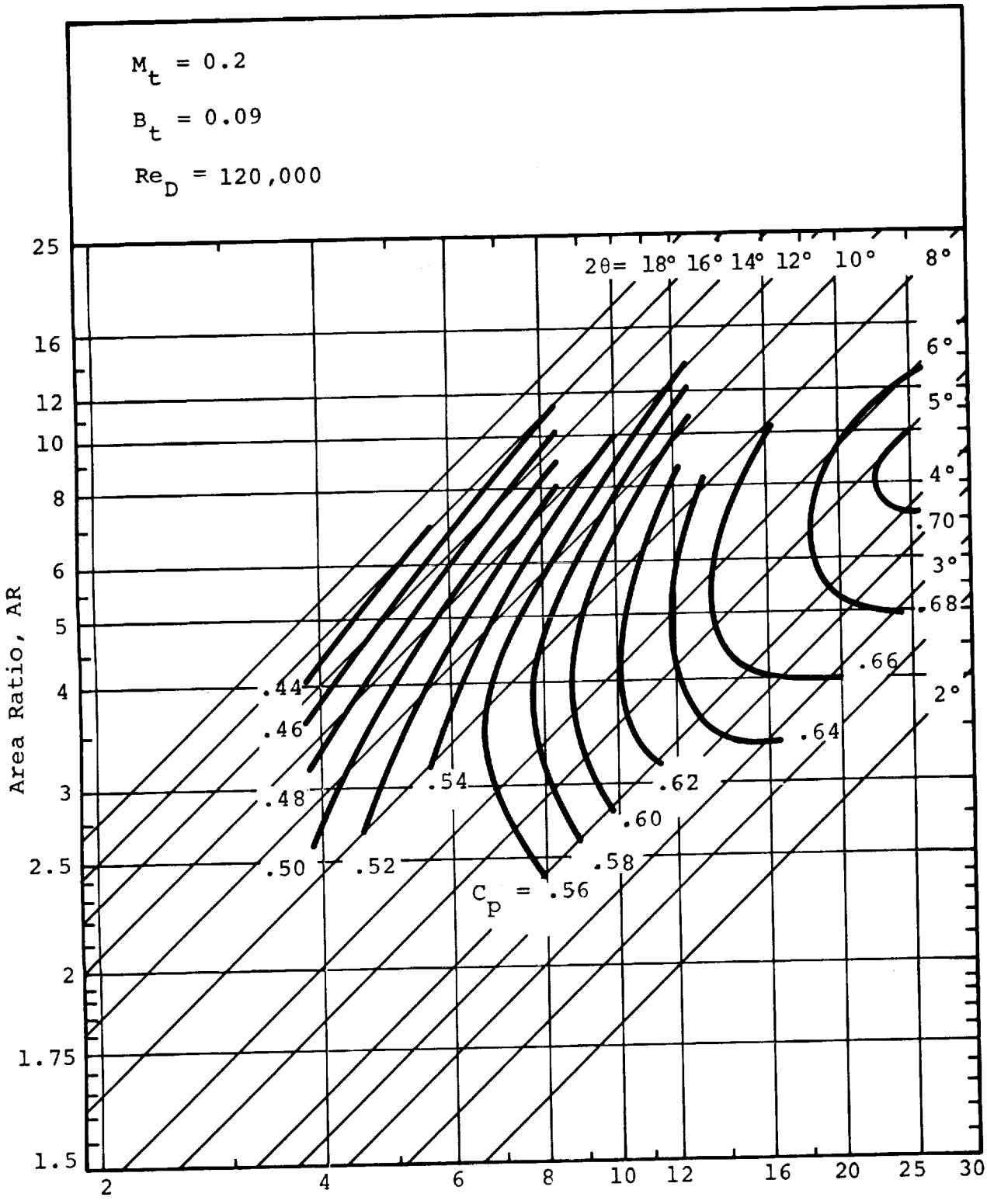


Figure 54 - Conical Diffuser Performance Map - $p_{ot}$ = 218 kN/m$^2$

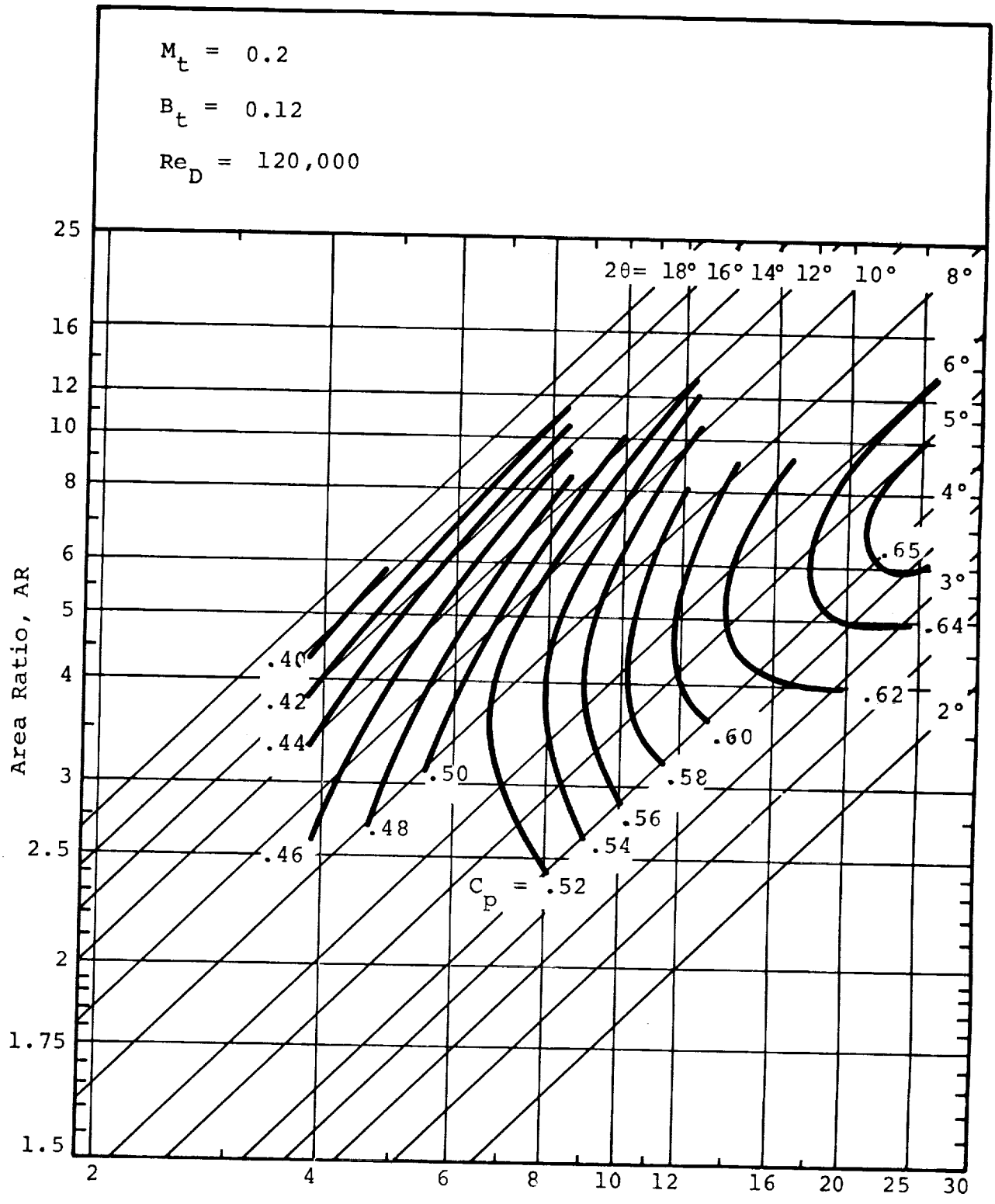


Figure 55 - Conical Diffuser Performance Map - $p_{ot}$ = 218 kN/m$^2$

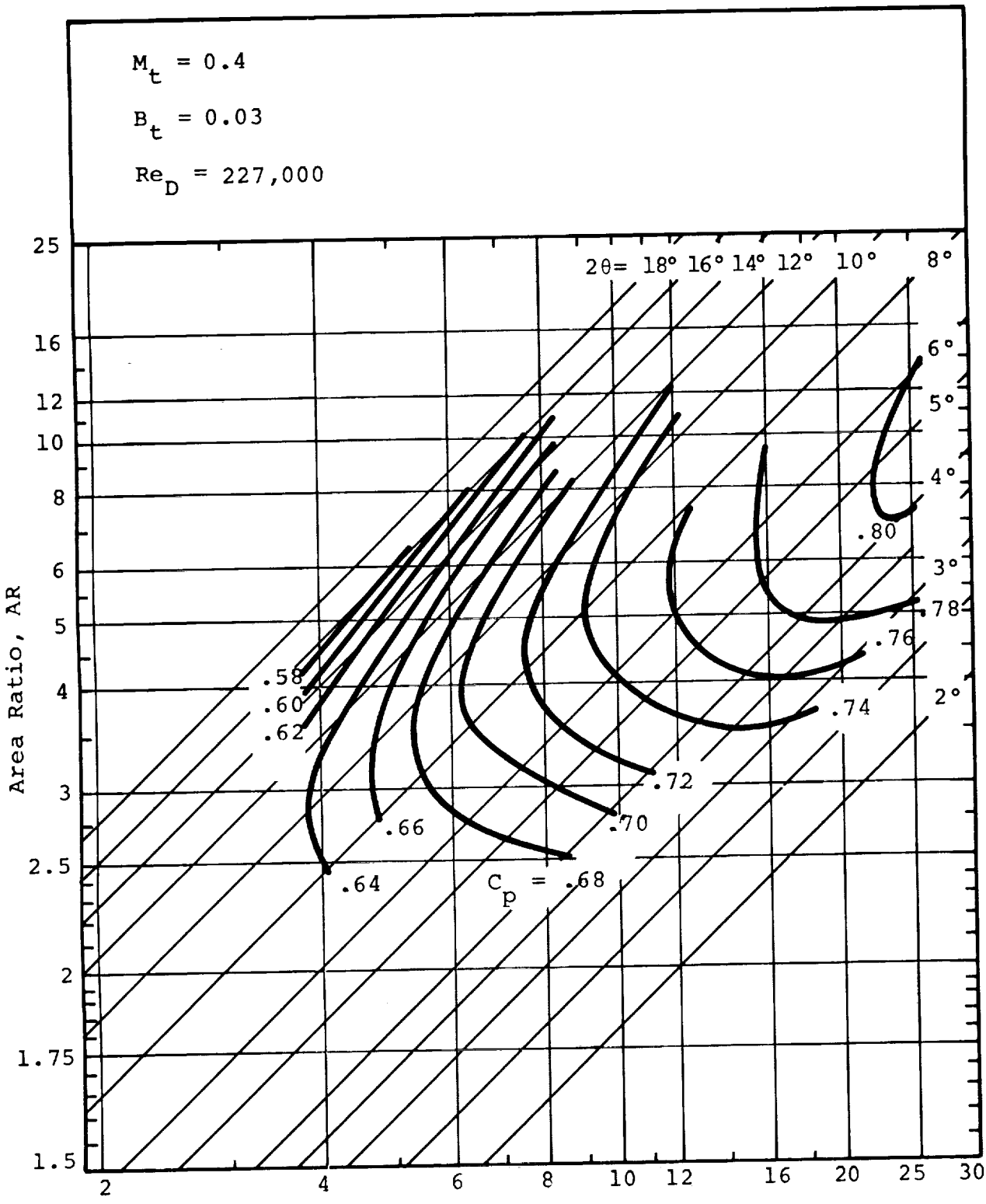


Figure 56 - Conical Diffuser Performance Map - $p_{ot}$ = 218 kN/m$^2$

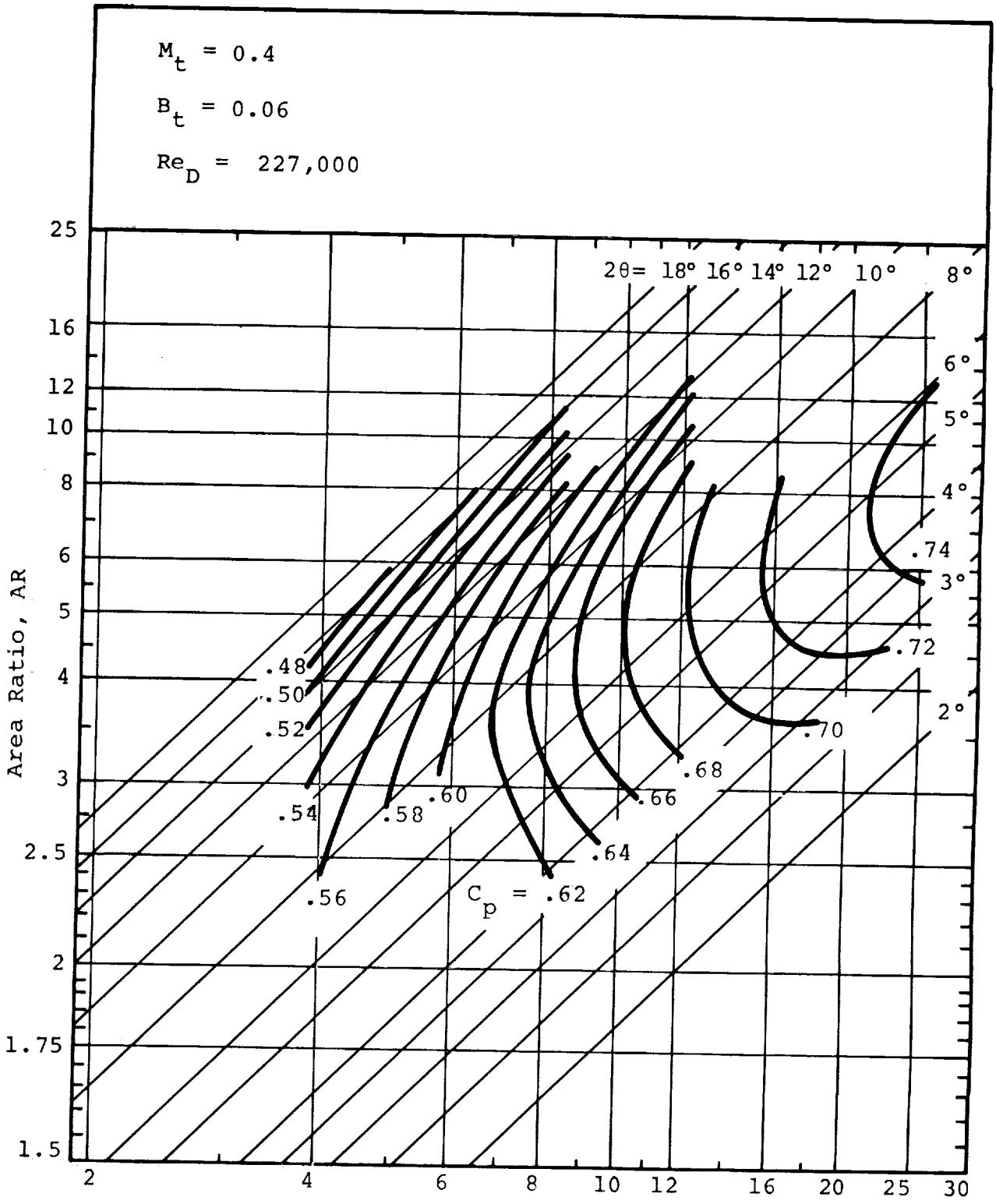


Figure 57 - Conical Diffuser Performance Map - $p_{ot}$ = 218 kN/m$^2$

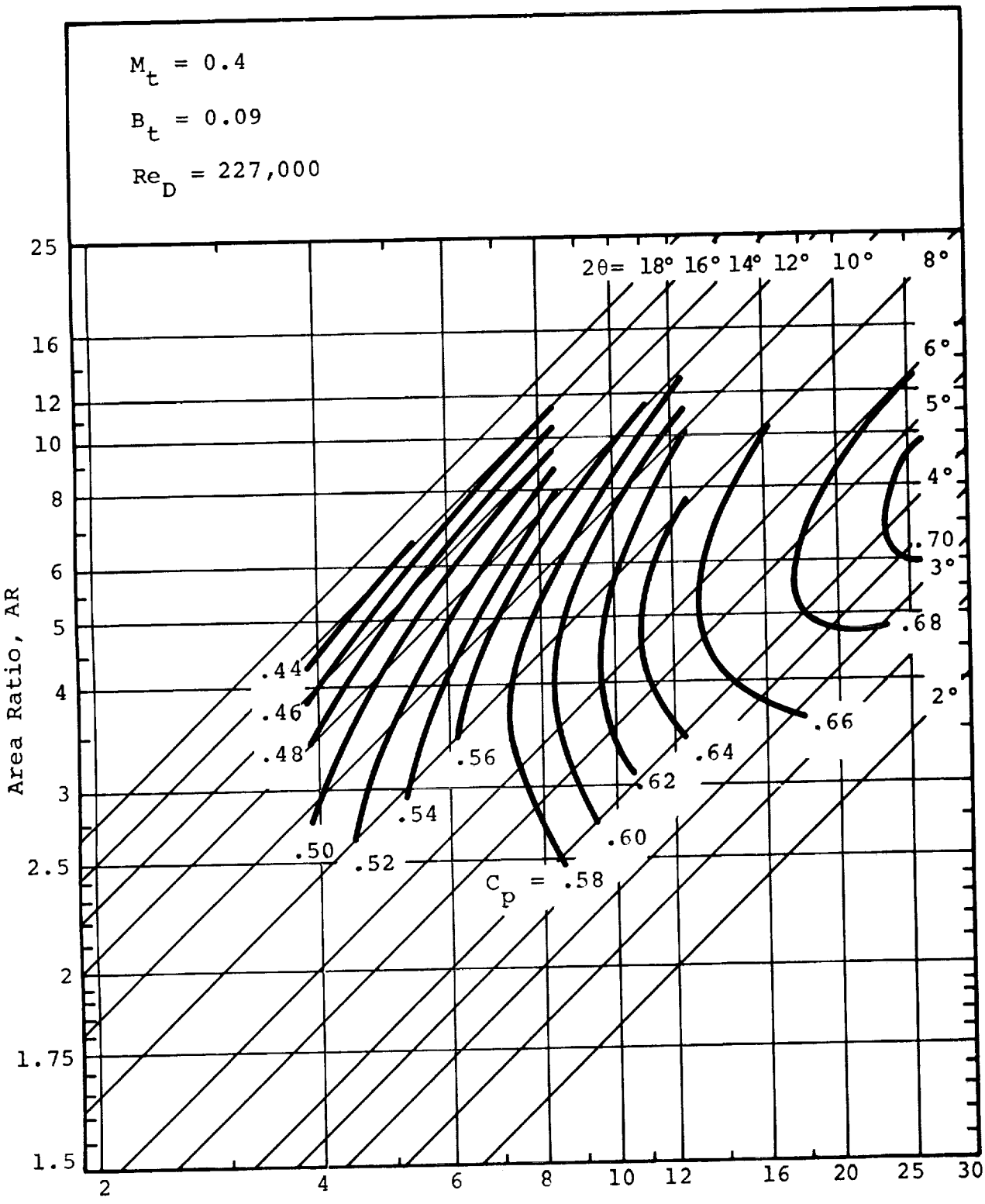


Figure 58 - Conical Diffuser Performance Map - $p_{ot}$ = 218 kN/m$^2$

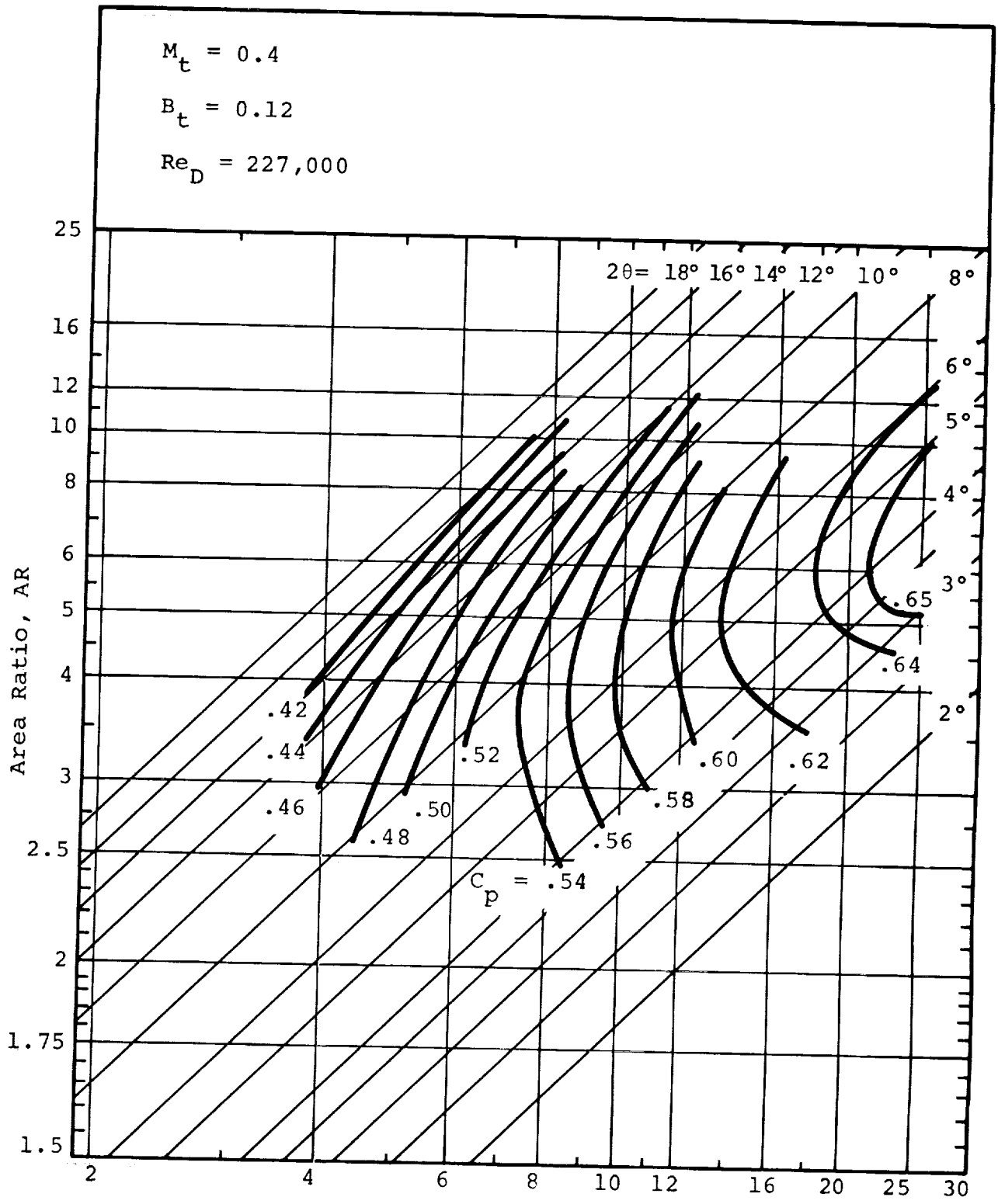


Figure 59 - Conical Diffuser Performance Map - $p_{ot}$ = 218 kN/m$^2$

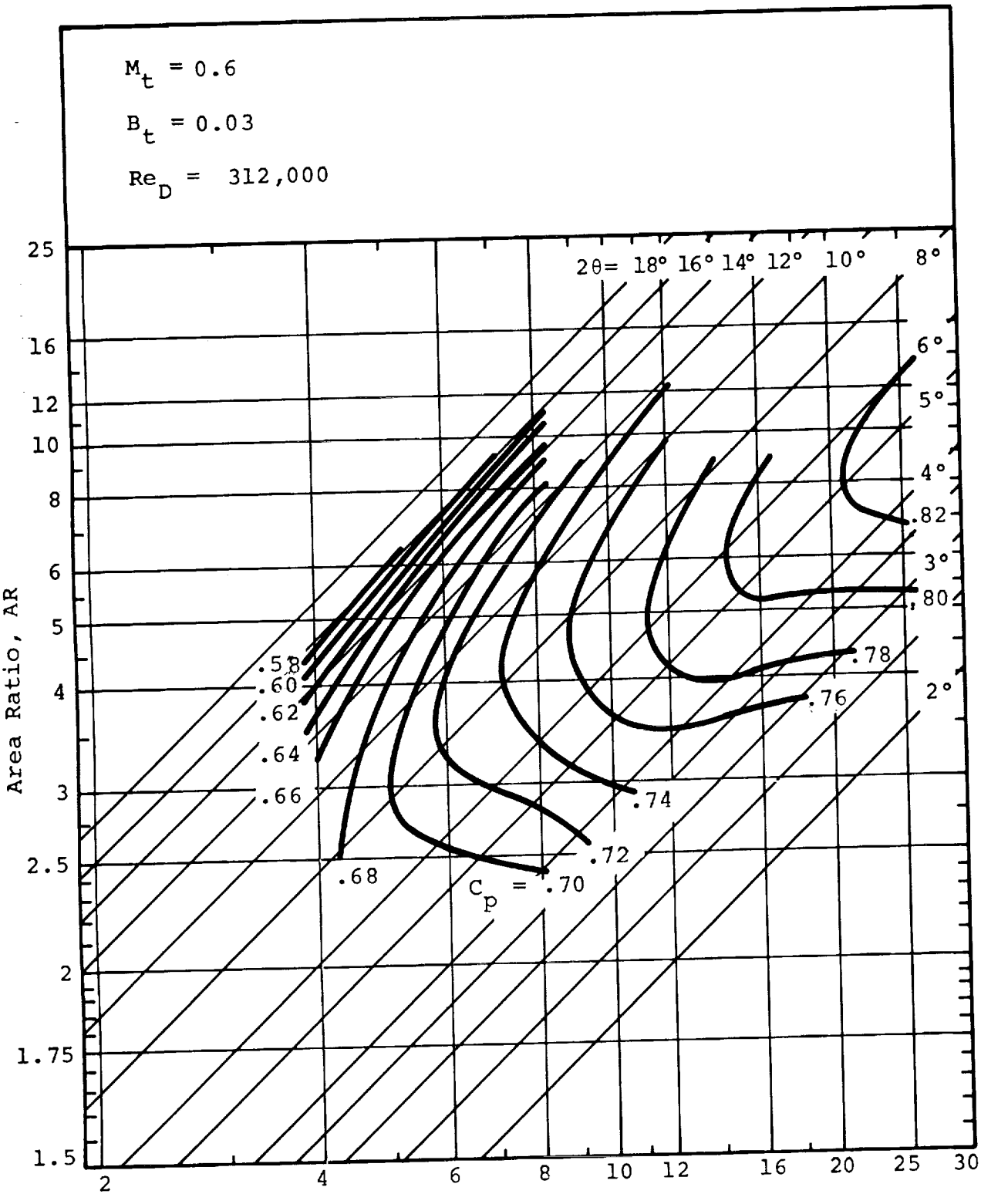


Figure 60 - Conical Diffuser Performance Map - $p_{ot}$ = 218 kN/m$^2$

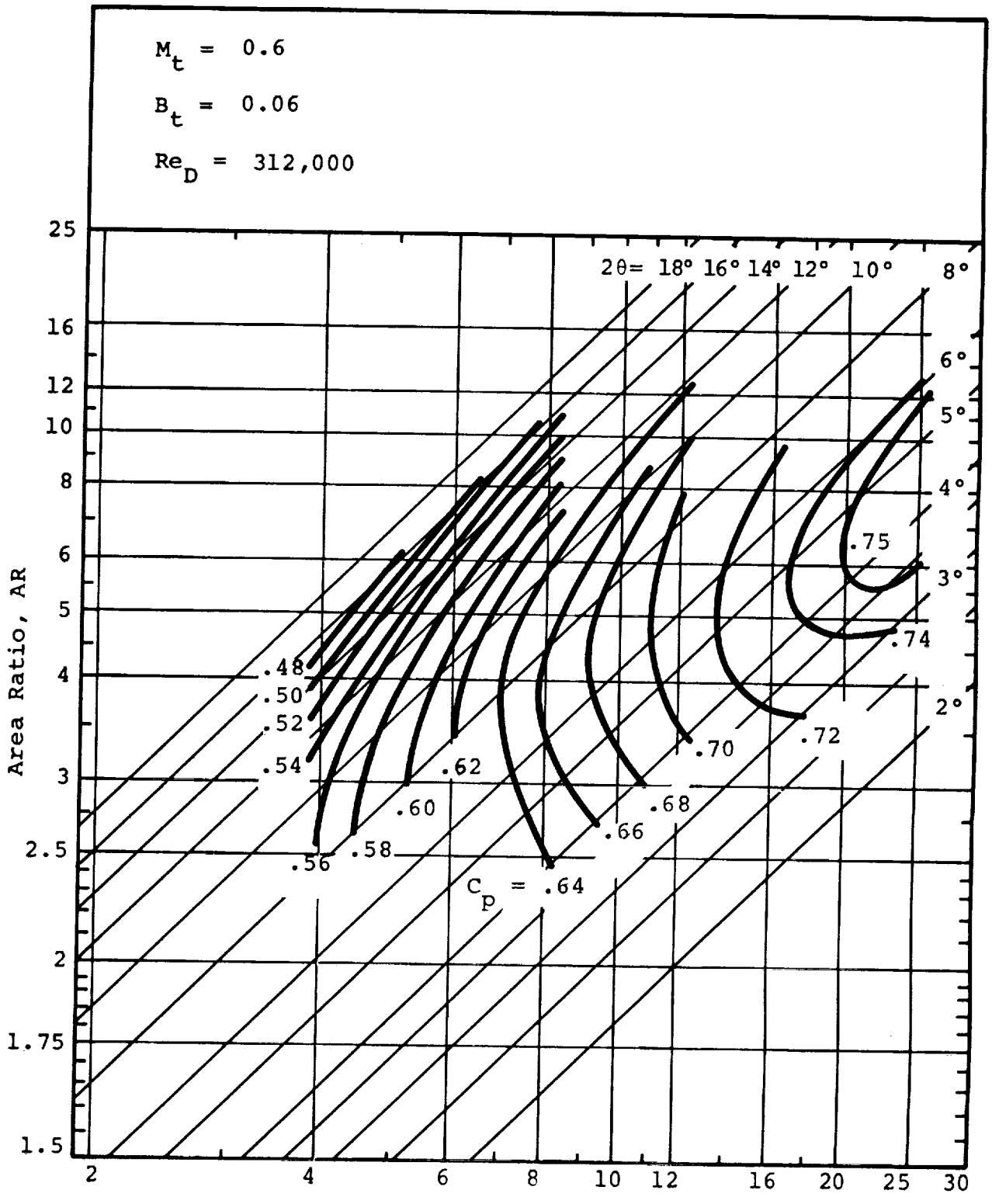


Figure 61 - Conical Diffuser Performance Map - $p_{ot}$ = 218 kN/m$^2$

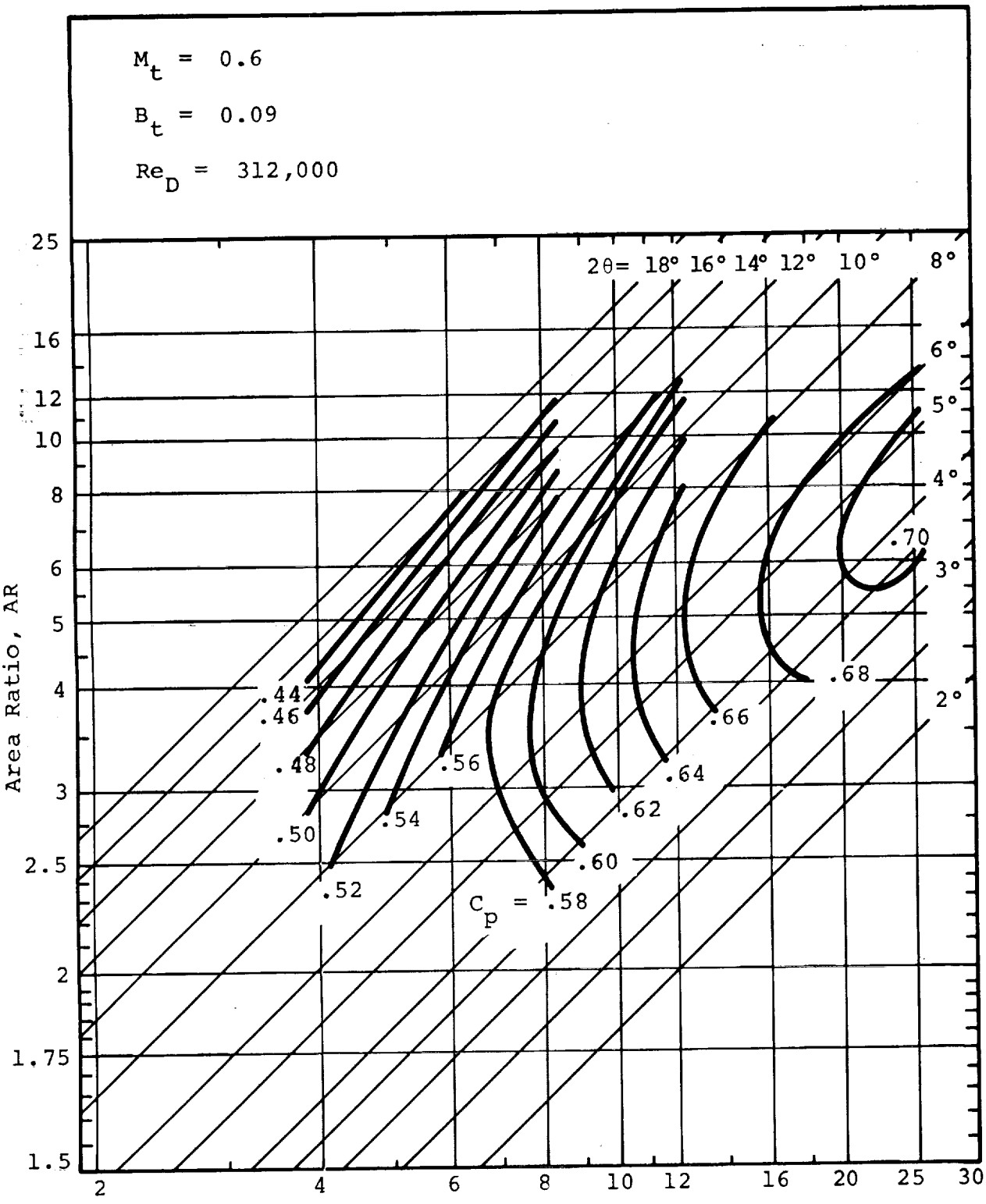


Figure 62 - Conical Diffuser Performance Map - $p_{ot}$ = 218 kN/m$^2$

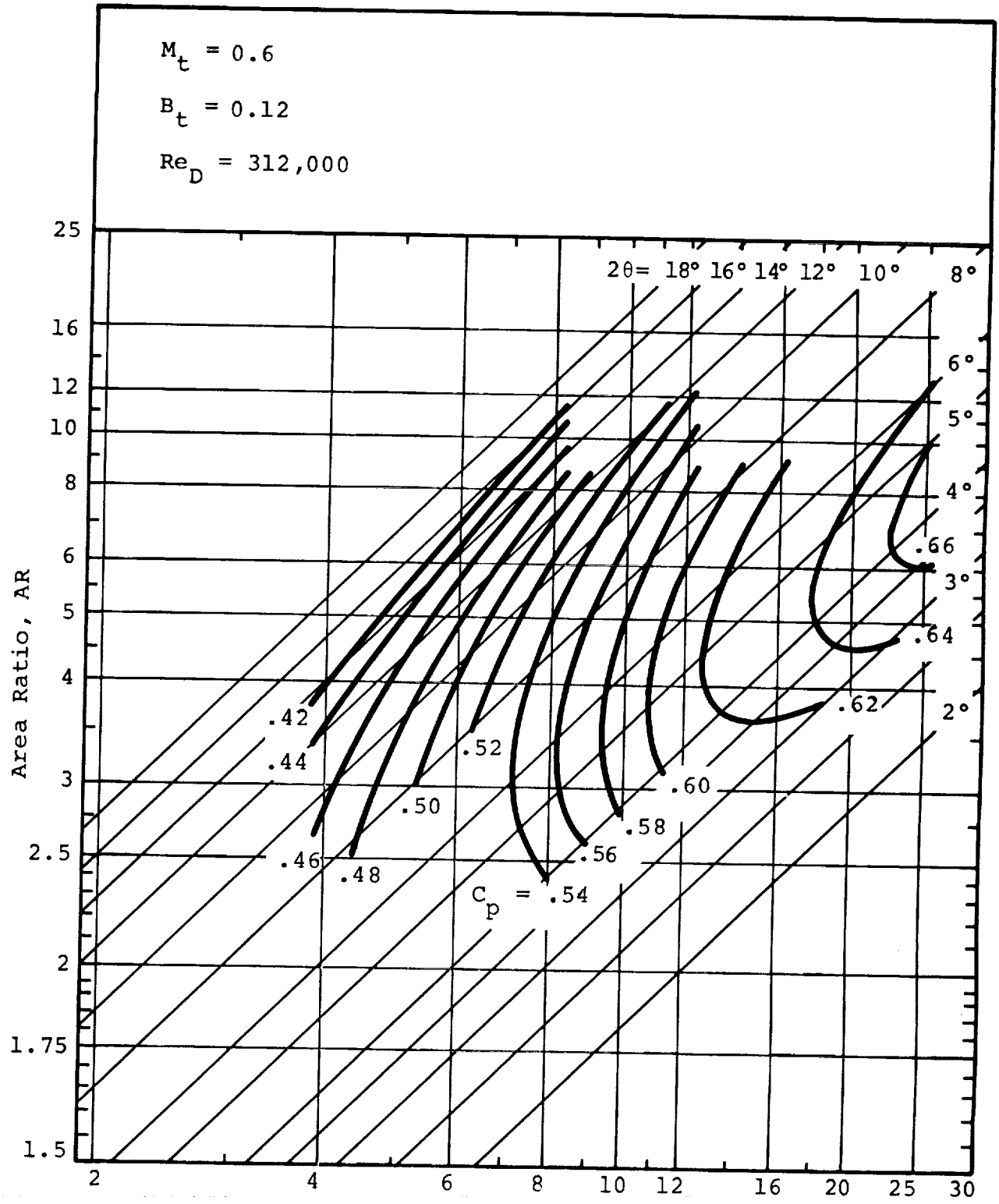


Figure 63 - Conical Diffuser Performance Map - $p_{ot}$ = 218 kN/m$^2$

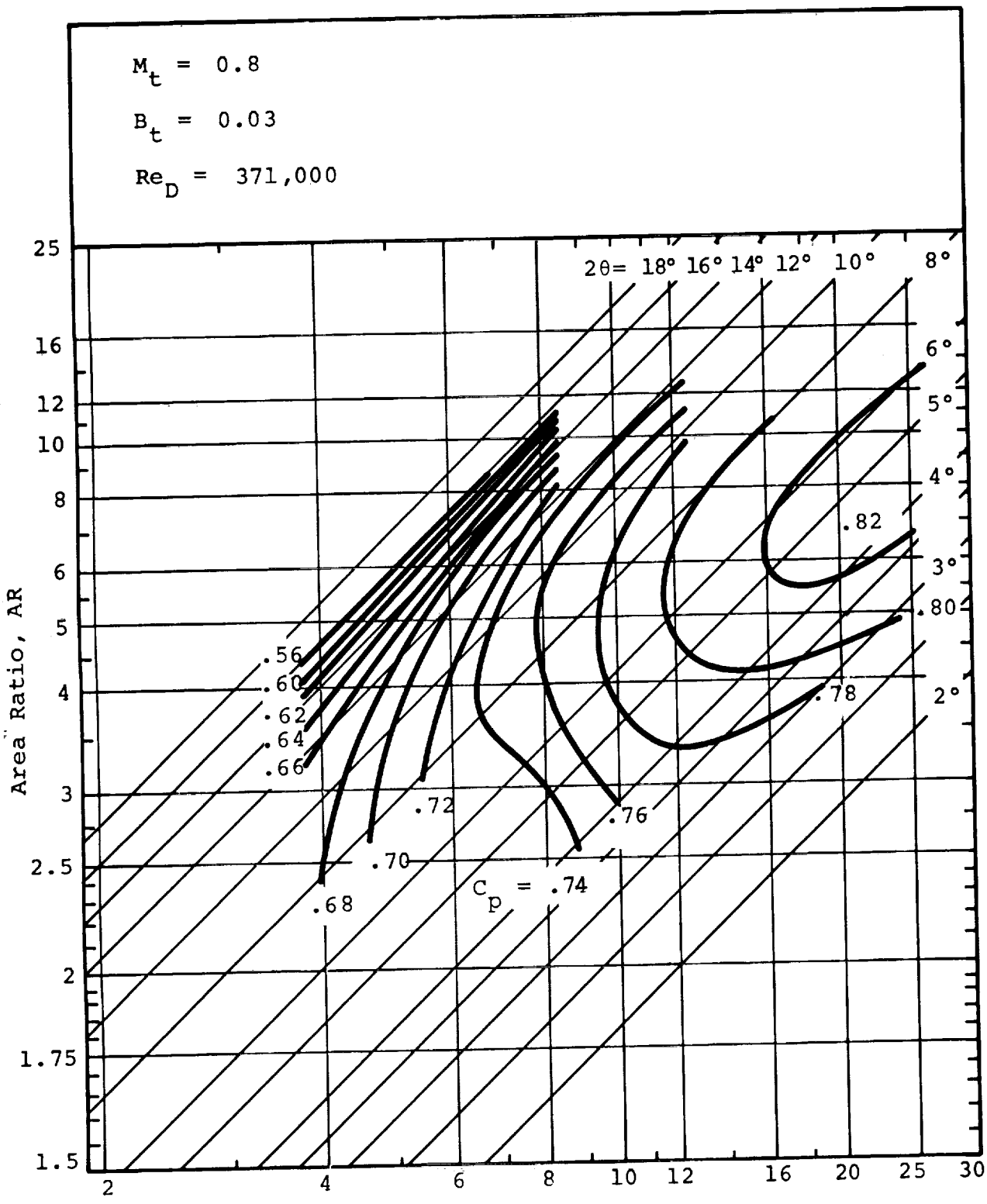


Figure 64 - Conical Diffuser Performance Map - $p_{ot}$ = 218 kN/m$^2$

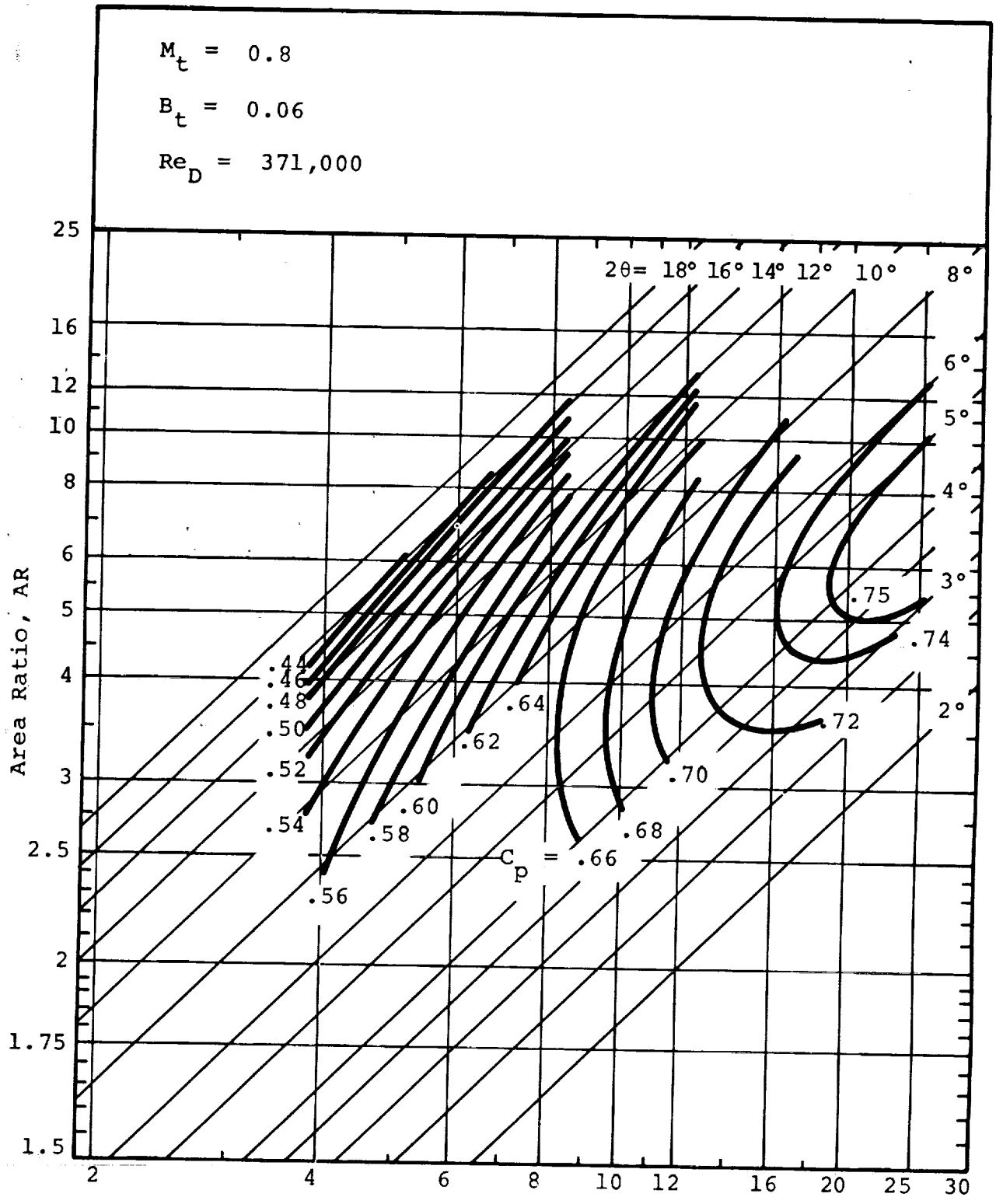


Figure 65 - Conical Diffuser Performance Map - $p_{ot}$ = 218 kN/m$^2$

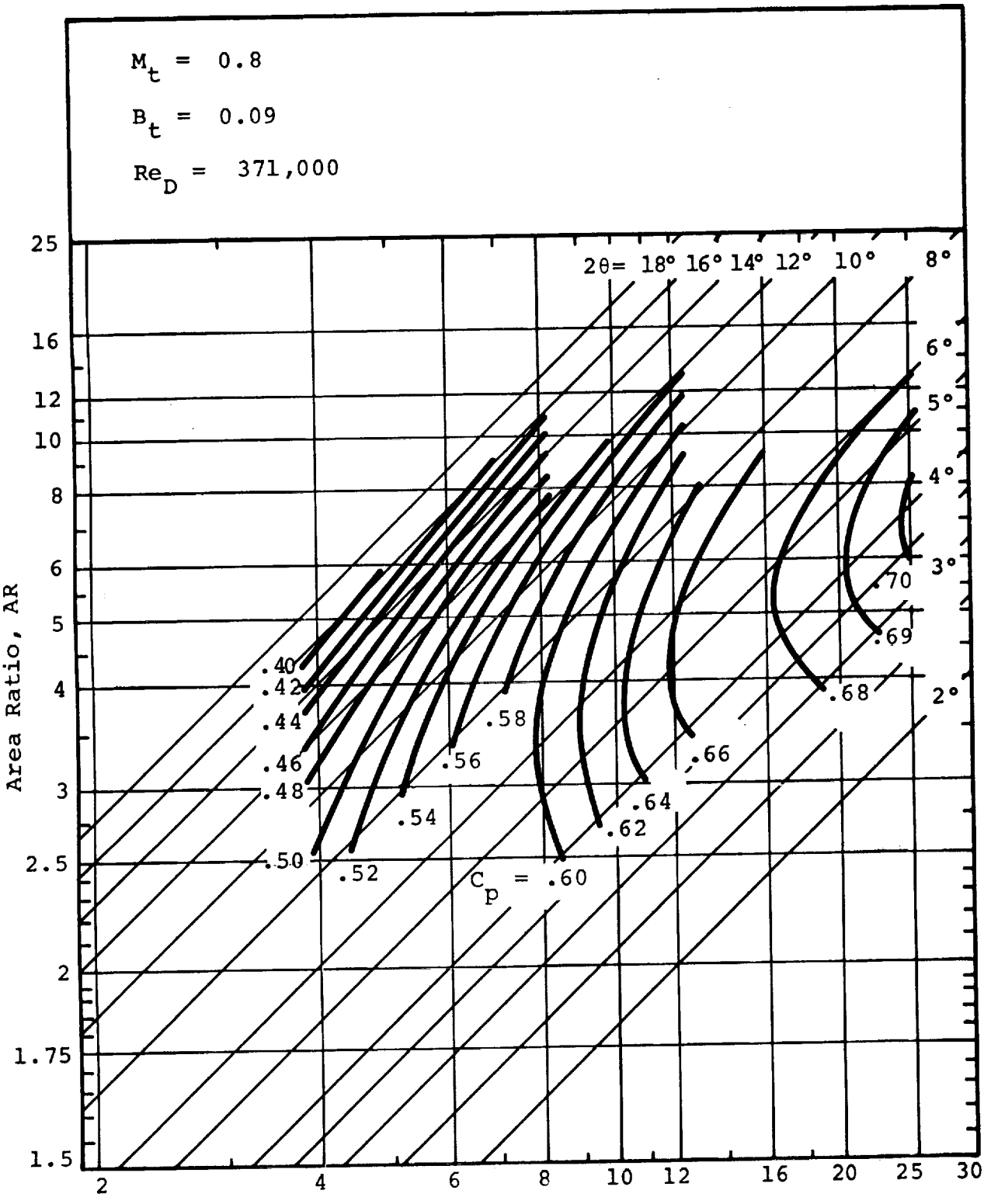


Figure 66 - Conical Diffuser Performance Map - $p_{ot}$ = 218 kN/m$^2$

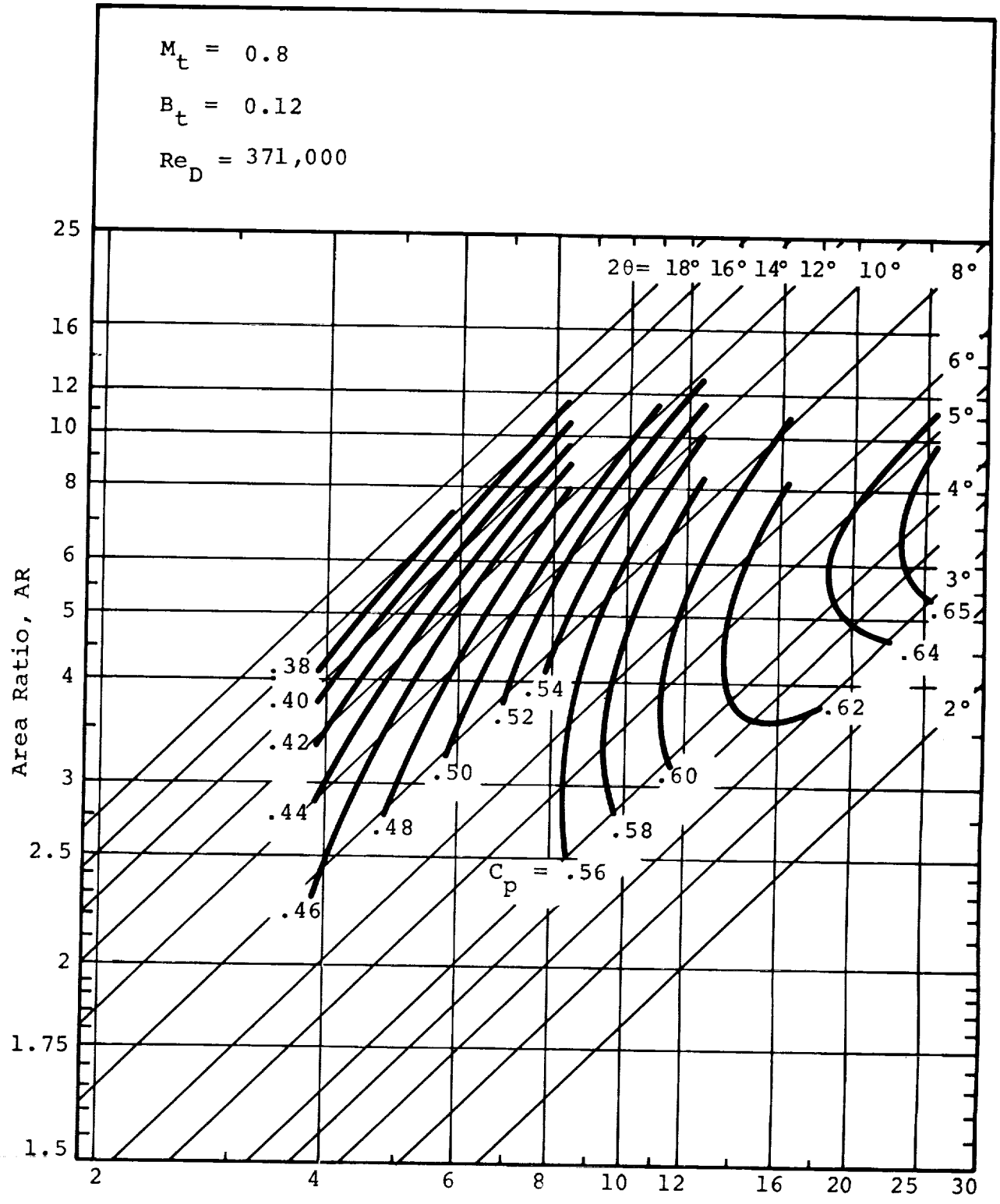


Figure 67 - Conical Diffuser Performance Map - $p_{ot}$ = 218 kN/m$^2$

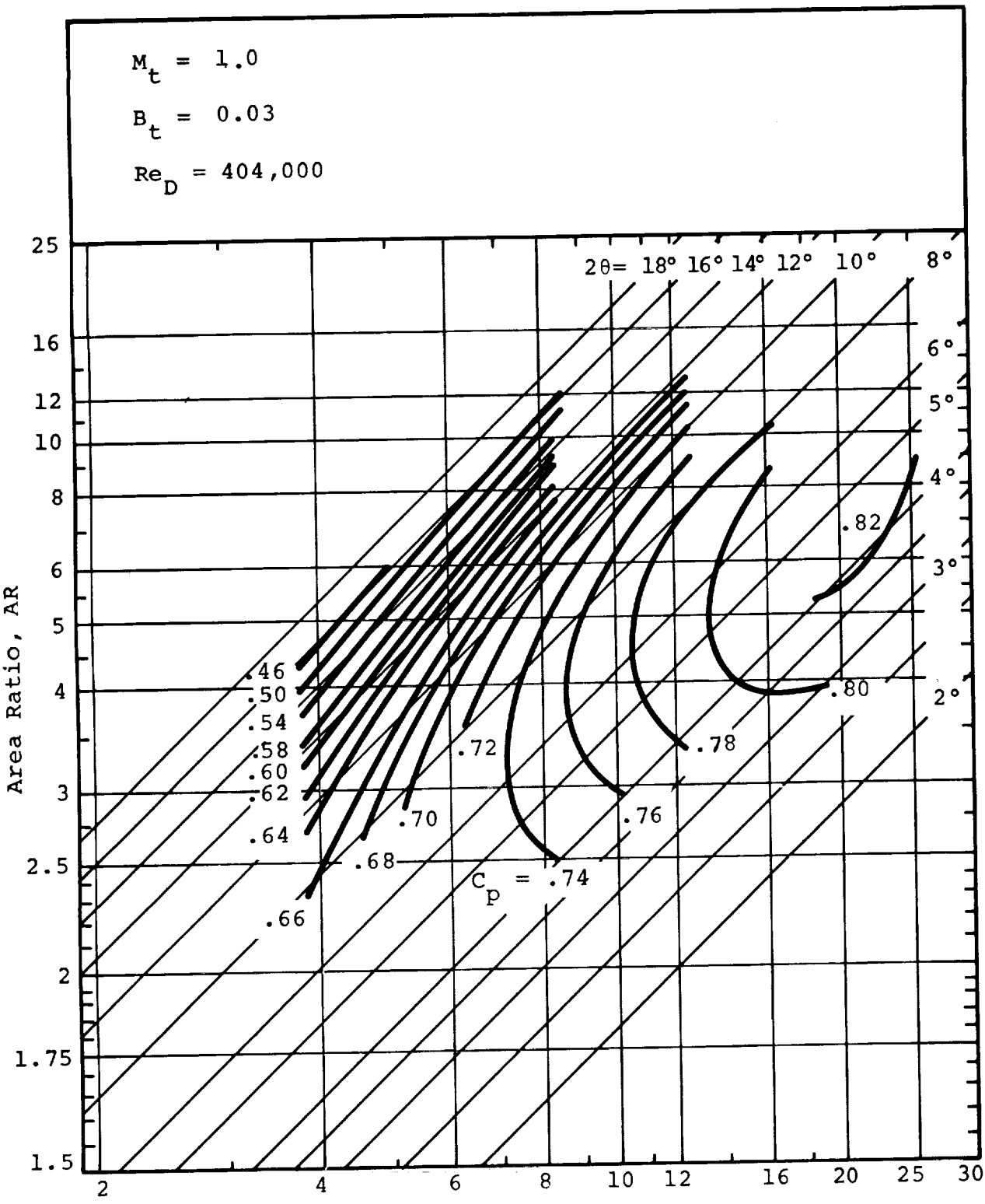


Figure 68 - Conical Diffuser Performance Map - $p_{ot}$ = 218 kN/m$^2$

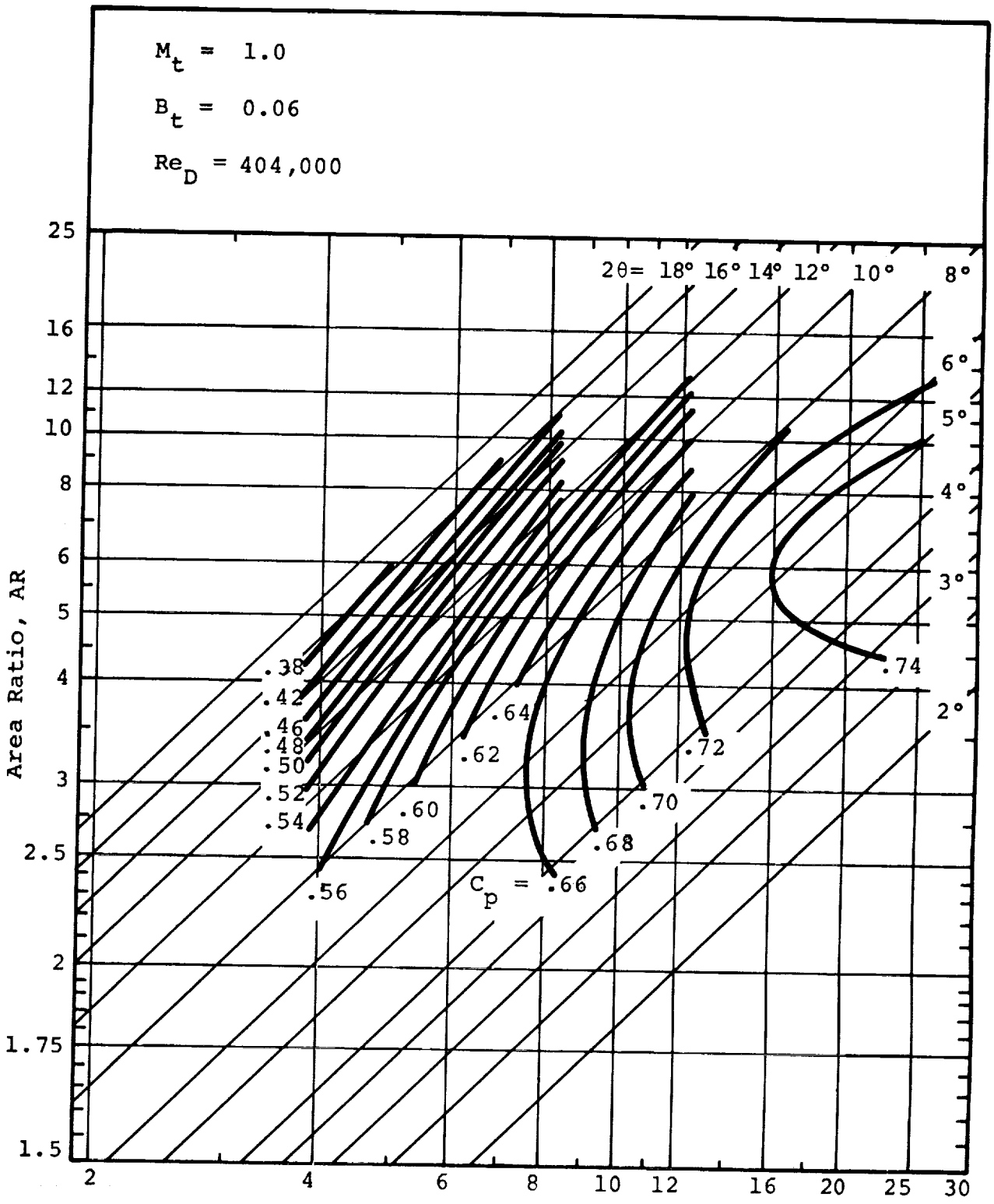


Figure 69 - Conical Diffuser Performance Map - $p_{ot}$ = 218 kN/m$^2$

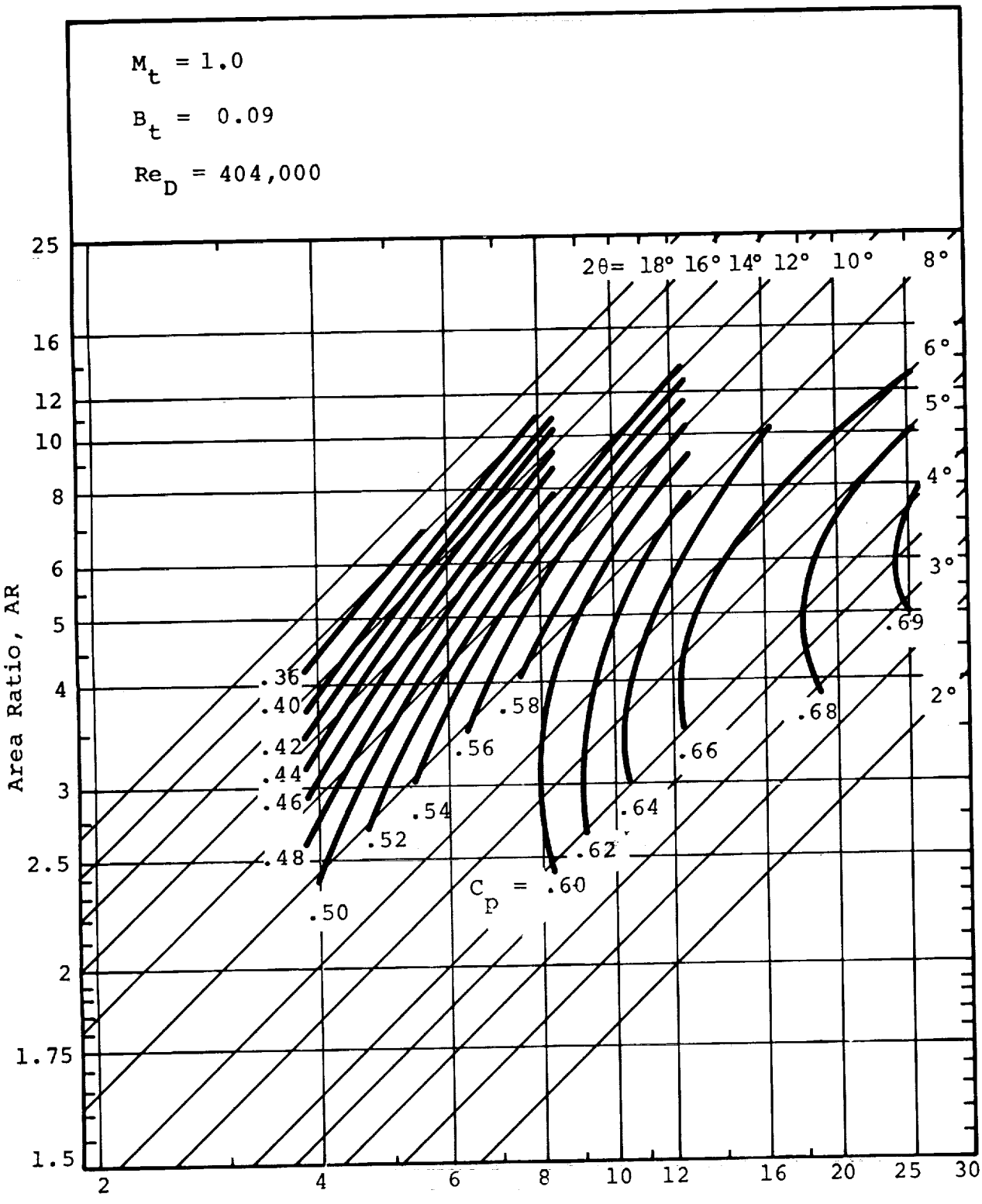


Figure 70 - Conical Diffuser Performance Map - $p_{ot}$ = 218 kN/m$^2$

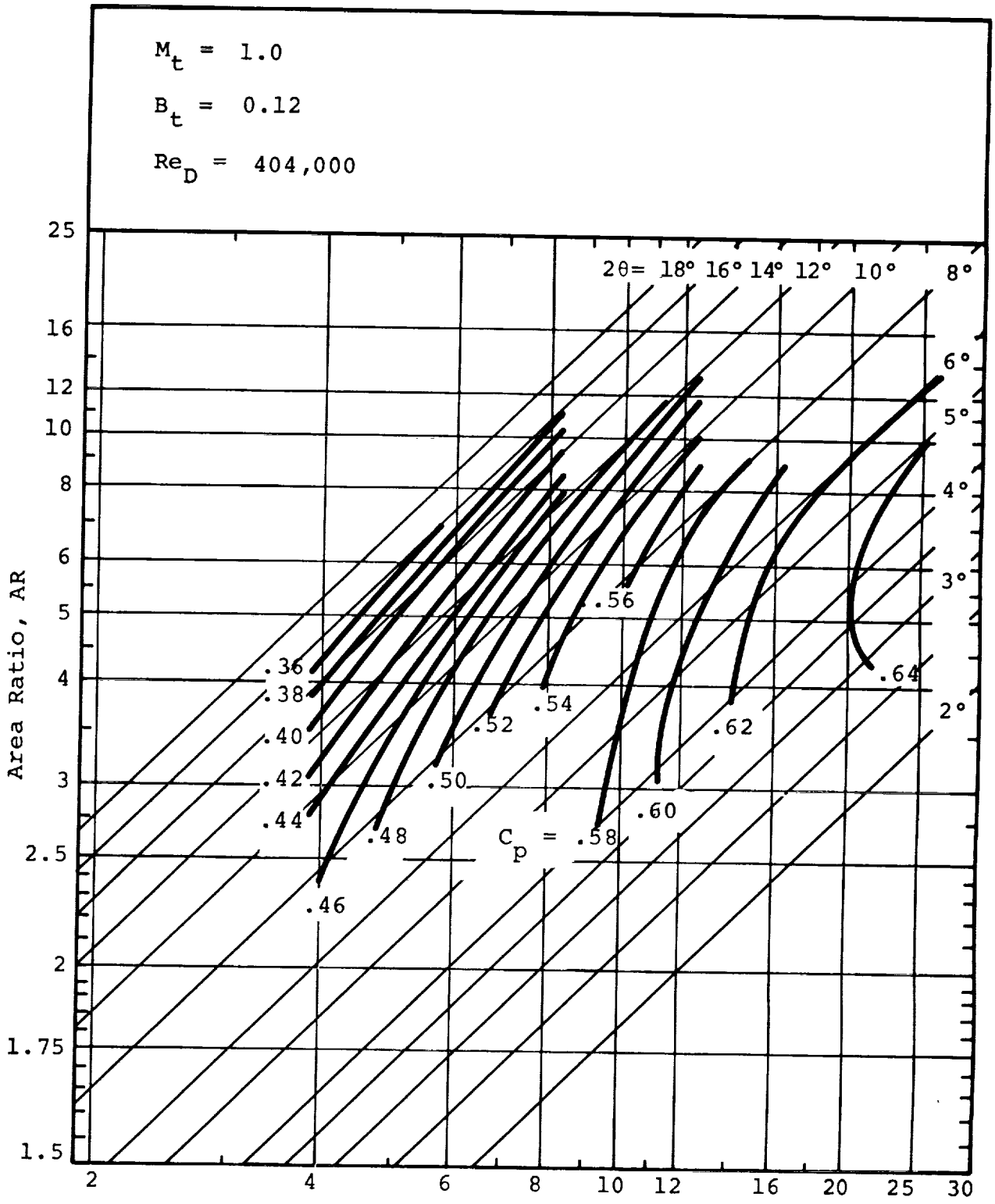


Figure 71 - Conical Diffuser Performance Map - $p_{ot}$ = 218 kN/m$^2$

In at least one case ($M_t$ = 0.4, $B_t$ = 0.12, $Re_D$ = 57,000, Figure 19) the actual maximum recovery (i.e. the highest value of pressure recovery that will be found anywhere in the AR - L/D domain) has been found. Since all maps are very similar, we suspect that the highest values of $C_p$ shown on each map are very close to the maximum recovery that will be found for each set of inlet conditions.

Along the ridge of optimum recovery (see Reference 8 for definition of optimum recovery ridge) the increase in $C_p$ above L/D = 16 is small, being no more than 2 to 3 points in recovery (0.02 to 0.03) from L/D = 16 to L/D = 25. Above the ridge, the slope of the recovery hill is precipitous. A small increase in AR (2θ) produces a rapid reduction in $C_p$. A typical "cut" through the pressure recovery map displaying this behavior is shown in Figure 72 for $M_t$ = 0.6, $B_t$ = 0.12, L/D = 6.

Above the ridge of optimum recovery the $C_p$ contours tend to be parallel to lines of constant 2θ. Therefore, in this region diffusers of constant divergence angle 2θ have almost constant performance over a wide range of diffuser geometries (i.e. combinations of AR and L/D corresponding to constant 2θ).

## Effect of Inlet Parameters on Performance

Throat blockage. Of the three inlet parameters investigated in this program, throat blockage $B_t$ has by far the largest effect on the level of performance in conical diffusers. For fixed $M_t$ and $Re_D$, diffuser performance can decrease by as much as 20 points at an off optimum geometry over the range of blockage values 0.03 to 0.12. This effect can be seen in the cross-plot of Figure 9, or by comparing any group of four performance maps having the same $M_t$ and $Re_D$.

For the same $M_t$ and $Re_D$ the decrease in maximum $C_p$ may not be as great, being 15 to 18 points over the range of $B_t$ = 0.03 to 0.12.

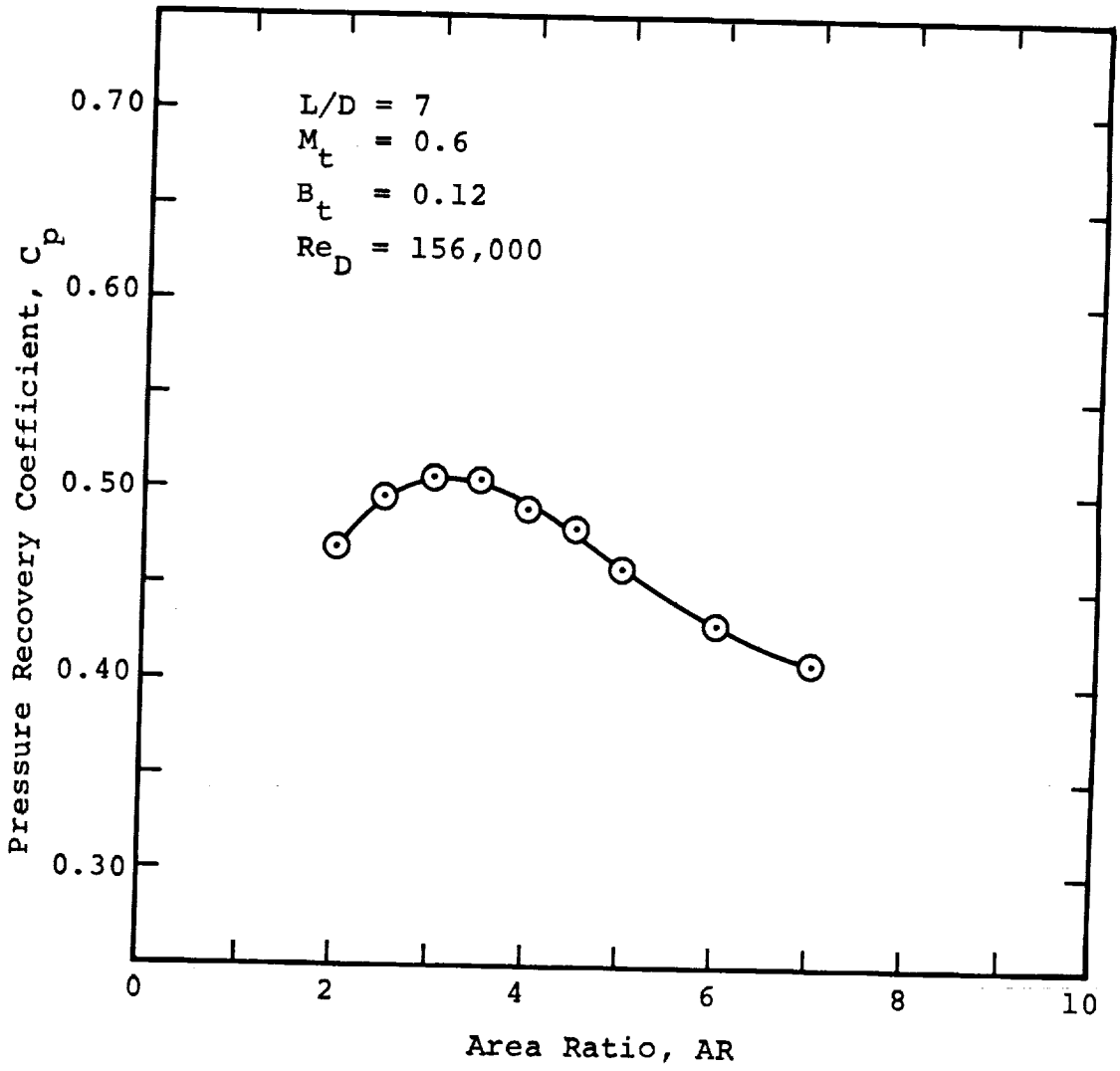


Figure 72 - Conical Diffuser Performance Versus Area Ratio

A more subtle effect of blockage than the decrease in recovery at fixed geometry is the change in the general shape of the $C_p$ contours as blockage is changed. When blockage is increased, the ridge of optimum recovery tends to move to smaller divergence angles $2\theta$ at constant L/D. Thus, in all of the maps presented, the maximum $C_p$ geometry moves to smaller values of $2\theta$ at $L/D \simeq 25$.

Throat Mach number and Reynolds number. For the conical diffusers, the effects of inlet Mach number $M_t$ and Reynolds number $Re_D$ are much less pronounced than the influence of blockage.

Figure 73 shows the variation in peak recovery as a function of $M_t$ and $Re_D$. The cross hatched curves in this figure cover the full range of Reynolds numbers for the data of this study. The maximum $C_p$ changes only slightly, on the order of 1 to 2 points in most cases, with Reynolds number at constant $M_t$. The variation with Mach number at constant $Re_D$ is of the same order of magnitude.

For a fixed diffuser geometry, a variation with Mach number may be more pronounced than shown in Figure 73, depending upon the geometry and blockage chosen. Figure 74 displays the pressure recovery as a function of $Re_D$ for a fixed geometry near the maximum pressure recovery ($L/D = 25$, $2\theta = 5°$) for constant values of $B_t = 0.03$ and 0.12 with $M_t$ as a variable. At low Reynolds number, the variation in $C_p$ may approach 6 to 7 points, although the variation is less with Mach number at higher Reynolds numbers.

## Effect of Inlet Boundary Layer Condition on Pressure Recovery Performance

A "best estimate" of the inlet boundary layer condition (laminar or turbulent) at the throat of the diffuser has been made using the experimental blockage data and calculations of boundary layer growth in Appendix B. This is important

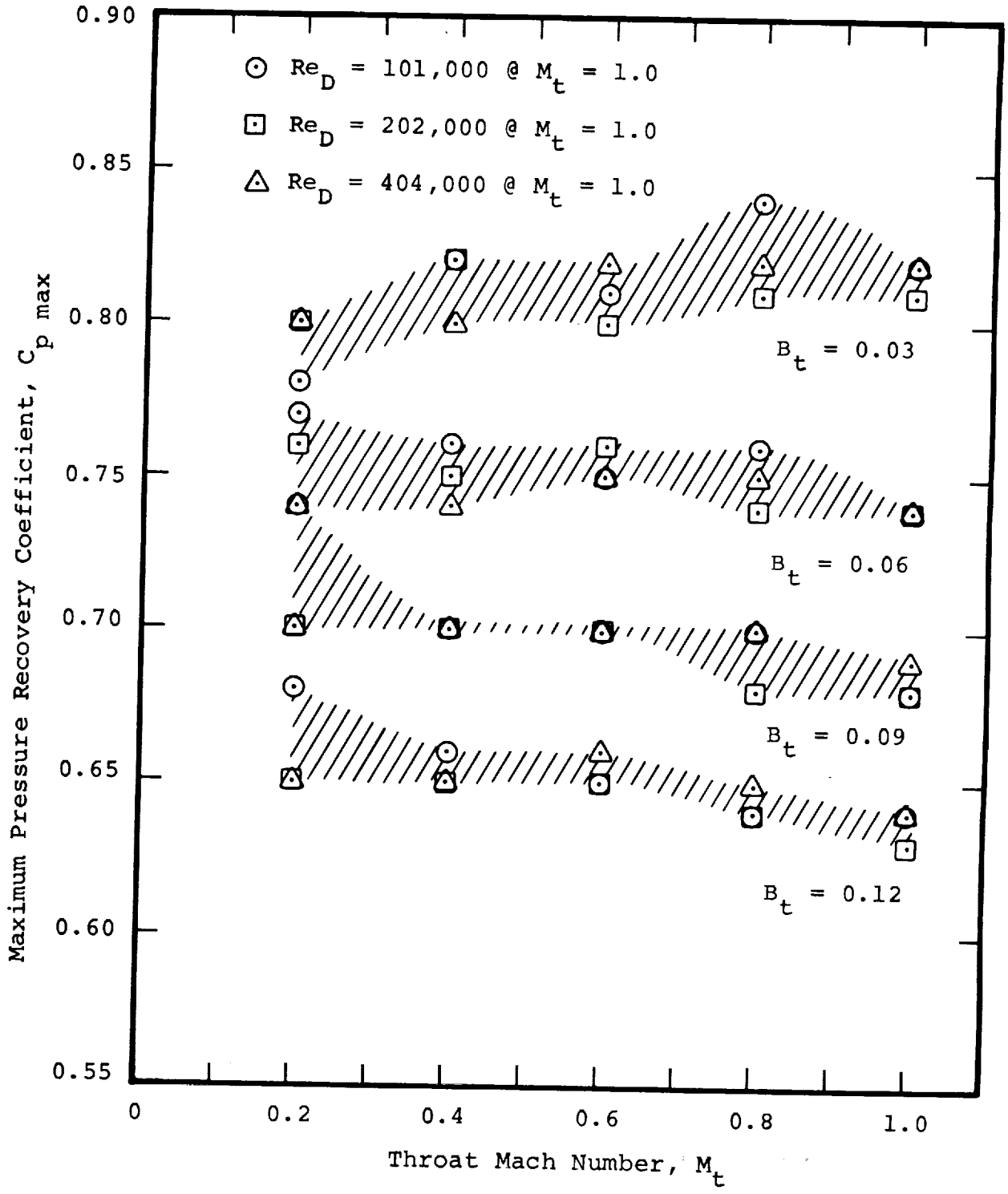


Figure 73 - Maximum Pressure Recovery Versus Mach Number

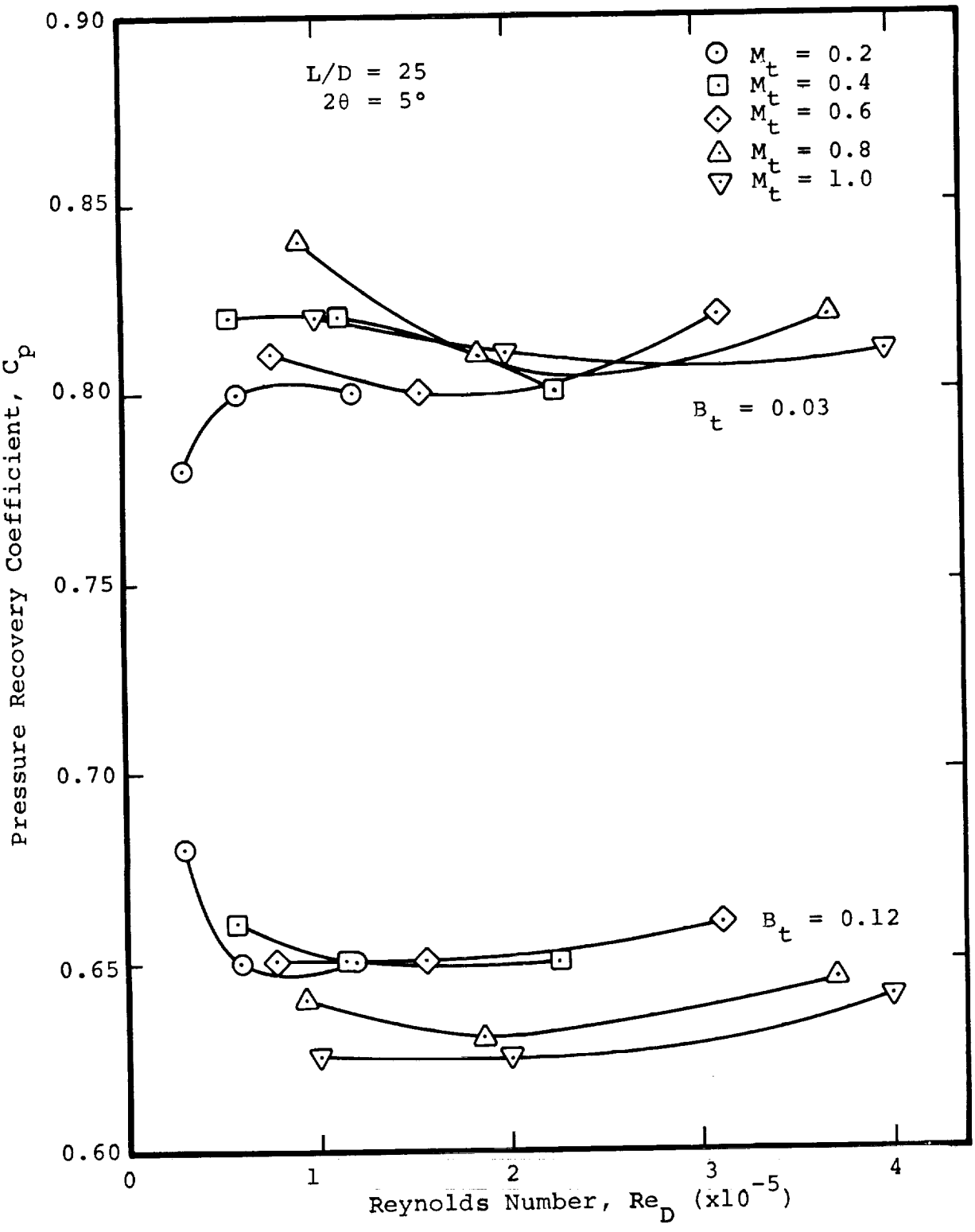


Figure 74 - Pressure Recovery Versus Reynolds Number

since a laminar boundary layer at the diffuser inlet may produce a different pressure recovery performance in a given diffuser than would be obtained with a turbulent boundary layer at the same values of Reynolds number, blockage and Mach number.

Due to the large velocity gradients in the inlet nozzle, the boundary layers at the beginning of the constant diameter (1.27 cm) boundary layer growth section are laminar (see Reference 9 for a discussion of this laminarizing process). For a fixed inlet flow condition ($p_{ot}$, $M_t$, $T_{ot}$) the transition of the boundary layer is primarily dependent upon the flow channel length, i.e. transition is assumed to occur where some critical length Reynolds number $Re_{crit}$ is reached:

$$Re_{crit} = \frac{x_{crit} V}{\nu} \tag{23}$$

Now, since throat blockage $B_t$ was varied by using different lengths of inlet channel, it is conceivable that for long inlet channels, the boundary layer would undergo a transition from laminar to turbulent flow. But for shorter channel lengths the boundary layer at the throat would still be laminar, given the same $p_{ot}$, $T_{ot}$ and $M_t$ conditions.

Diffuser throat blockage can be expressed as a function of the displacement thickness $\delta^*$ (Equation 4) which in turn is a function of boundary layer development length x and length Reynolds number (Equation 5).

$$B_t \propto \frac{\delta^*}{D} \propto \frac{x/D}{Re_x^{\,n}} \propto \frac{x/D}{(Re_D \frac{x}{D})^n} \tag{24}$$

In the present case, $Re_D$ is a function only of the throat pressure level and throat Mach number (Table IV). Thus, we can generate a correlation among $p_{ot}$, $B_t$ and $M_t$ that shows for which combinations of these parameters the boundary layer is expected to be turbulent at the diffuser throat.

Using a compressible, laminar and turbulent boundary layer calculation program with a transition criterion suggested in

Reference 10, the correlation shown in Figure 75 was generated. In this correlation, inlet flows having $B_t$ vs $M_t$ values lying below a given $p_{ot}$ line are assumed to have a laminar boundary layer. These $p_{ot}$ lines thus define a transition region. The correlation shown is unique to this program since the transition is in part determined by the apparatus, i.e. the presence of the trip slot, the shape of the inlet nozzle and the level of turbulence in the inlet flow.

We are not certain what the implications are, relative to diffuser performance, to have a laminar as opposed to turbulent boundary layer at the throat. However, we can see from Figure 75 and Table IV that for the Reynolds numbers and blockages of greatest interest in centrifugal compressor design, the data presented are for fully developed turbulent boundary layers at the throat.

## Design Applications

The performance maps provided by this program offer the designer a unique tool for optimizing centrifugal compressor performance. Performance maps such as these for the conical diffuser (and similar maps for the straight-wall, single-plane-divergence diffuser reported in Reference 3) are needed to optimize diffuser design. Because the fundamental aerodynamics of the flow in the diffuser is such a strong function of the geometry as well as inlet conditions, maps covering the important range of these conditions are required to select the best among a particular family of diffusers, as well as between different types of diffusers (e.g. conical vs single-plane-divergence diffusers). Unless such maps are available, the arbitrary choice of a diffuser geometry appears at best a "hit and miss" affair. While boundary layer/potential flow calculations can predict performance of some diffuser configurations, as pointed out in Reference 2, without empirical data the present techniques cannot now calculate optimum diffusers.

Faced with this situation, the designers' most logical approach is to work with a family of diffusers for which performance maps are available. In this way an optimum design, to meet specified design constraints, can be adopted with some assurance. Today, only two diffuser families have sufficient data to make this approach possible. These are the

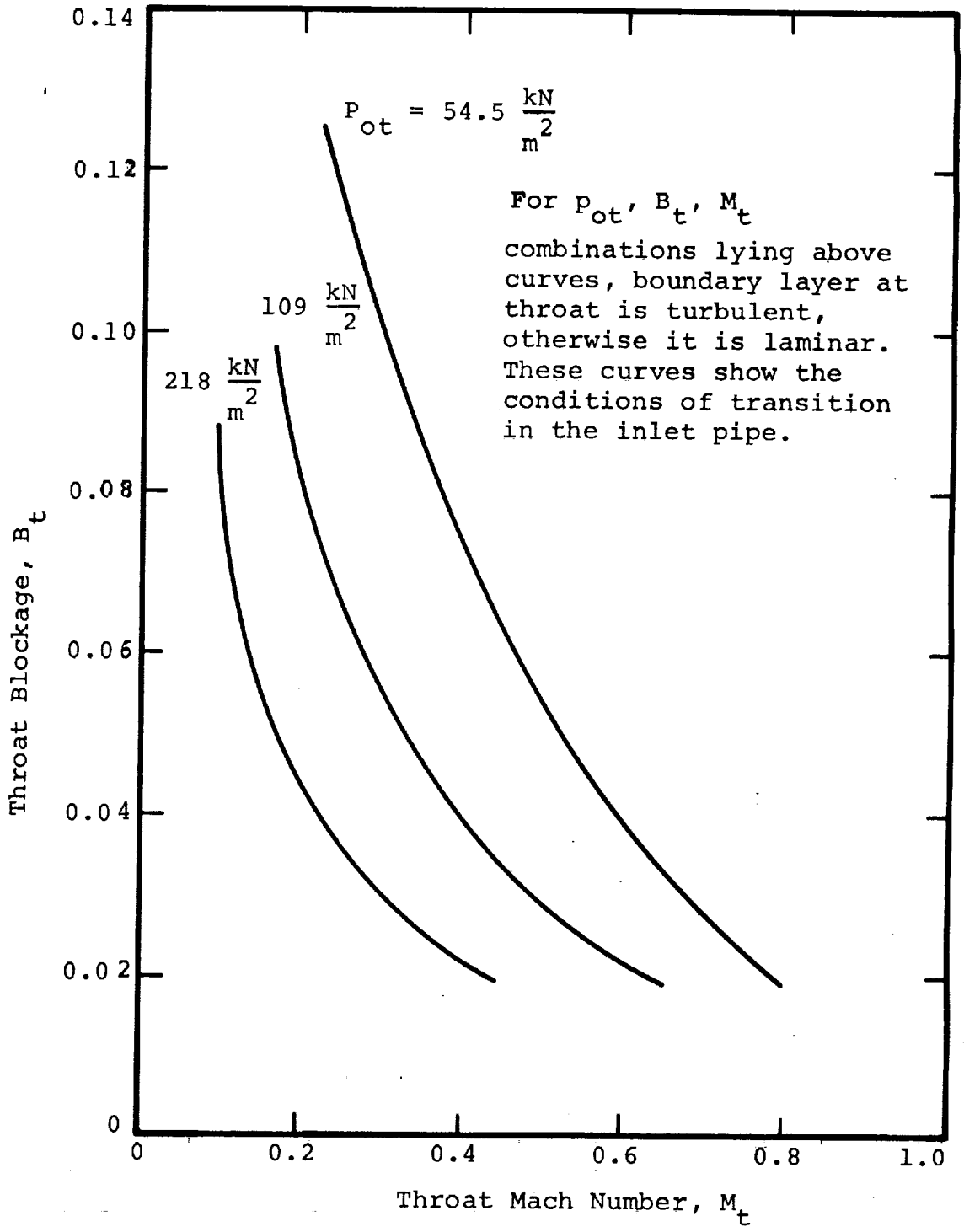


Figure 75 - Boundary Layer Transition Correlation

conical diffusers studied in this program and the straight-wall, single-plane-divergence diffusers for which the performance map data are presented in Reference 3.

The conical performance maps can be compared on a maximum recovery basis with the data for single-plane-divergence straight-wall diffusers. The results are shown in Figures 76 through 80. Here maximum $C_p$ is shown vs blockage $B_t$ over the range of Mach numbers $M_t$ from 0.2 to 1.0. In these figures conical and square diffuser data have been compared, using data where the inlet Reynolds numbers are as close as possible for the two families of diffusers. (The Reynolds number values for the square data are approximately twice the values for the conical maps.)

In comparing these data, the highest values of $C_p$ available on each set of performance maps has been taken to be approximately the value of maximum $C_p$. Interestingly, this comparison shows that over the complete subsonic Mach number range and blockage values from 0.03 to 0.12, the maximum pressure recovery for conical and square diffusers is approximately the same.

However, this does not imply that an optimum geometry of one type of diffuser can necessarily be replaced by an optimum diffuser of the other type; the second type of diffuser may not fit the design constraints imposed by the application.

Figure 81 displays the situation typical of the design constraints for a high pressure ratio centrifugal compressor diffuser. If the channel diffuser centerline is designed to lie in the radial plane shown, the governing non-dimensional parameter specifying diffuser performance is L/D. If a conical diffuser is used, this is the L/D for the conical geometry as defined in this report. If a single plane divergence diffuser is employed, L/D corresponds to L/W. Reference 3 shows that the aspect ratio AS = 1.0 (i.e. square) diffuser has the potential for the highest maximum recovery performance among the single-plane-divergence diffuser family. Assuming the optimum diffuser is being sought, L/D ≈ L/W for either radial plane or meridional plane divergence. For the square diffuser the L/W for maximum recovery is about

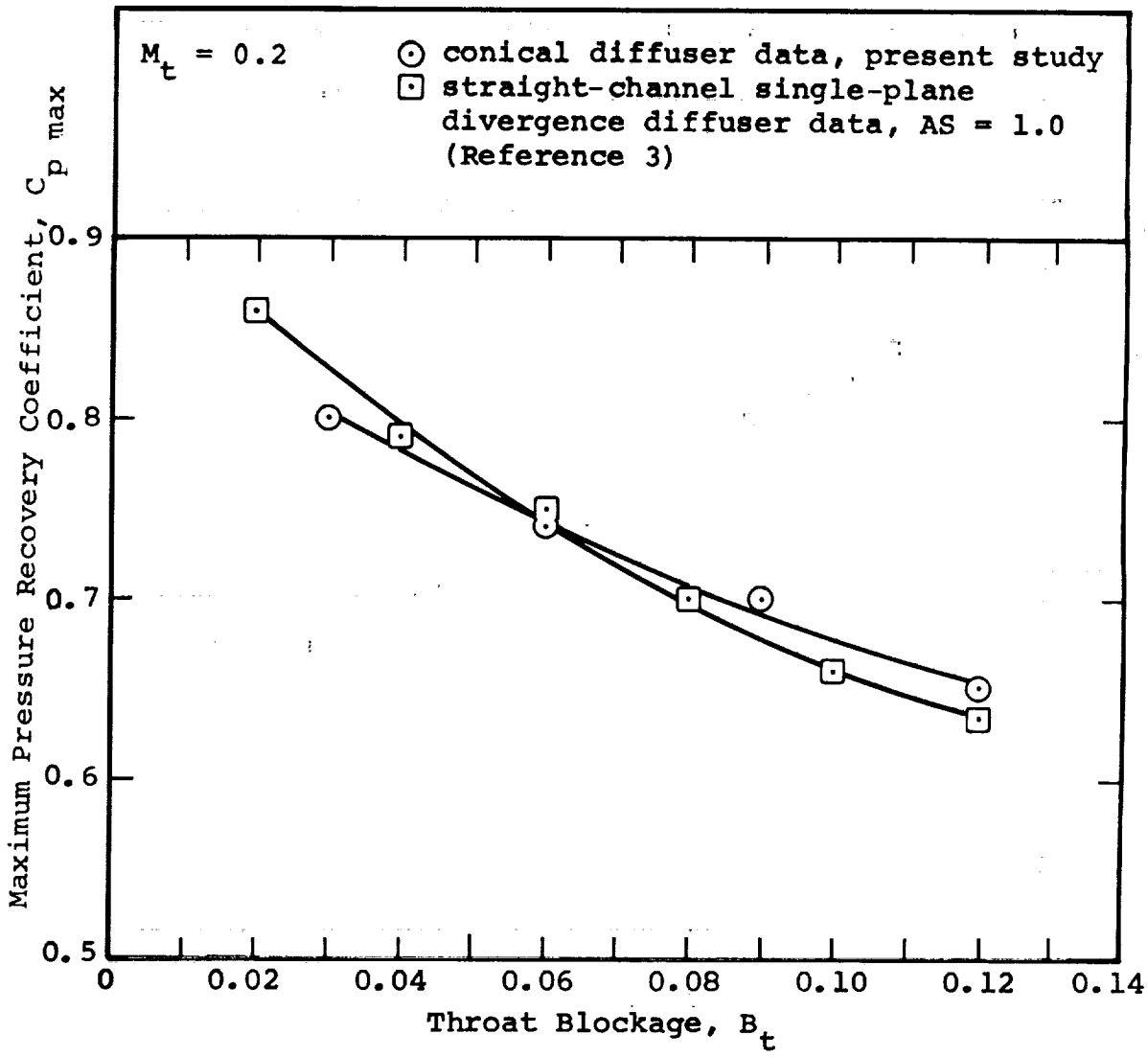


Figure 76 - Maximum Pressure Recovery of Conical and Square Diffusers - $M_t$ = 0.2

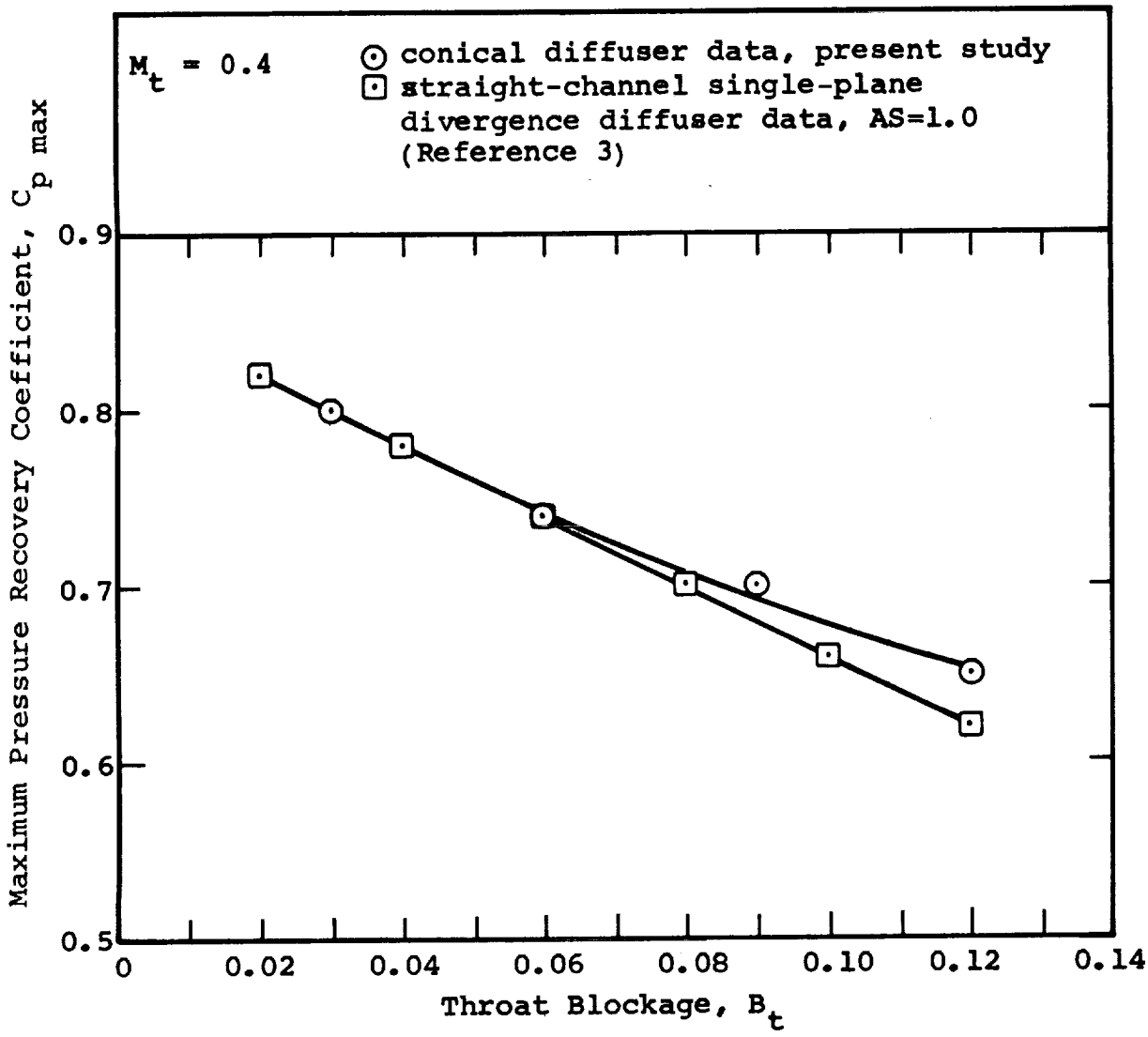


Figure 77 - Maximum Pressure Recovery of Conical and Square Diffusers - $M_t$ = 0.4

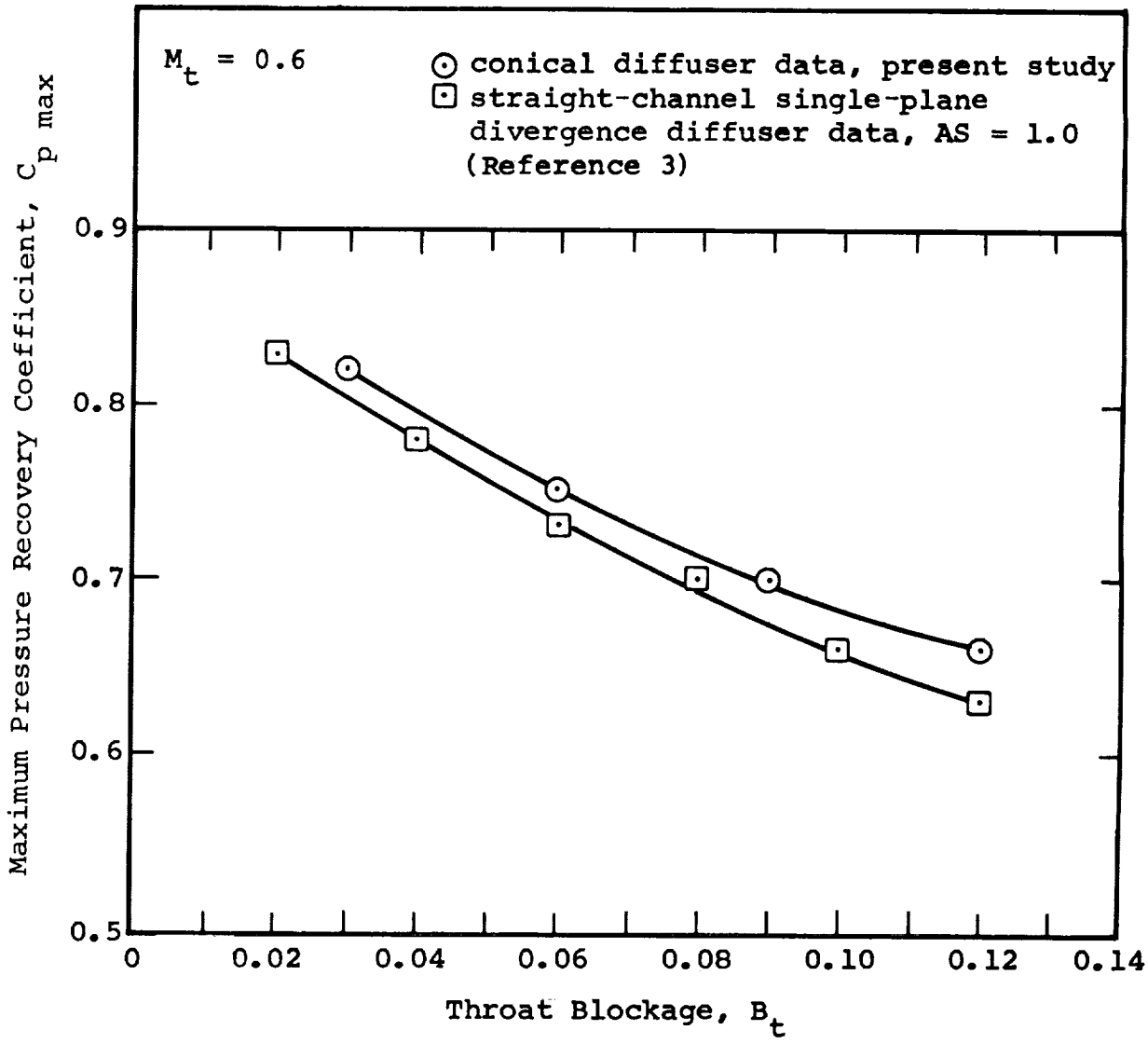


Figure 78 - Maximum Pressure Recovery of Conical and Square Diffusers - $M_t$ = 0.6

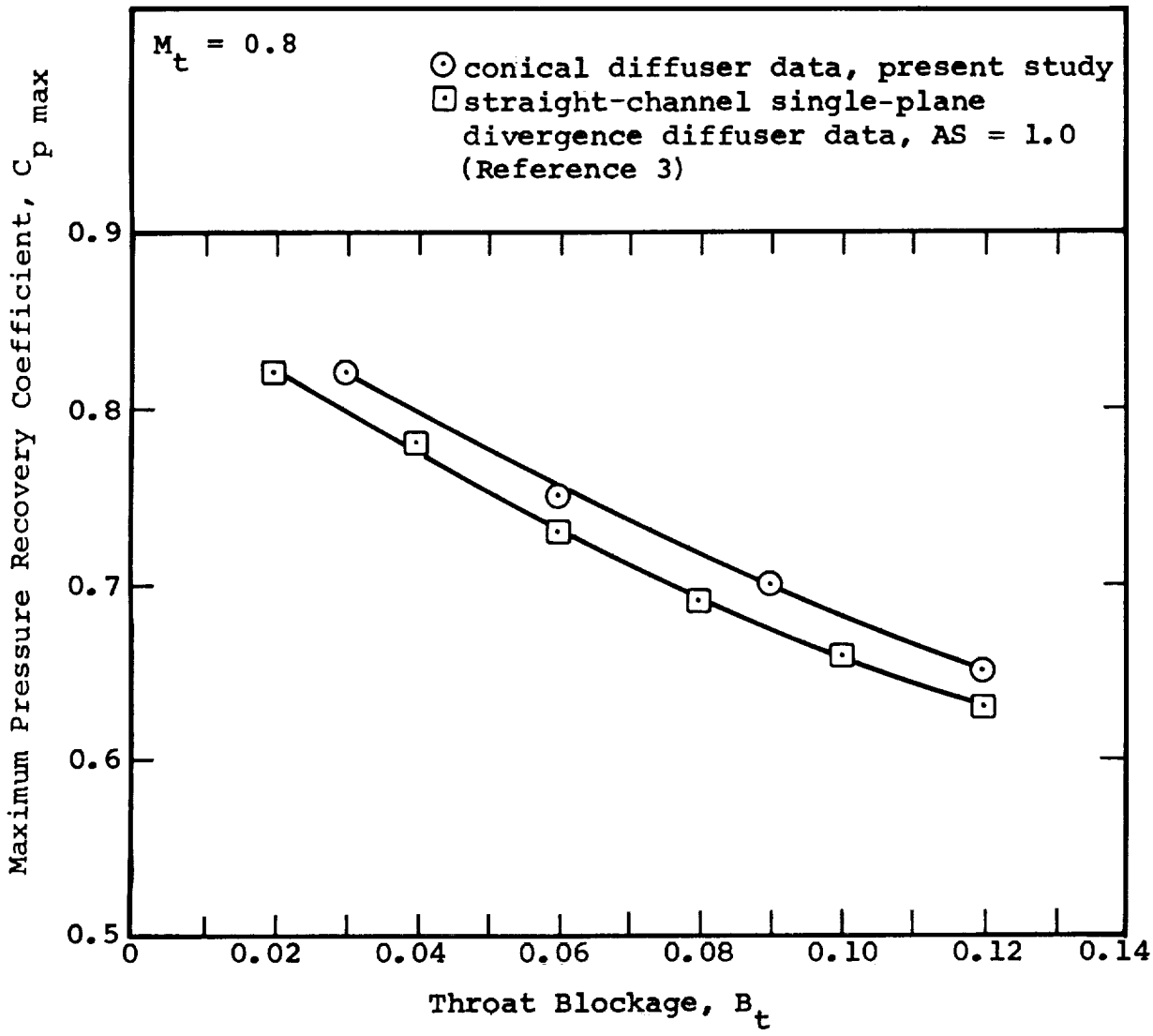


Figure 79 - Maximum Pressure Recovery of Conical and Square Diffusers - $M_t$ = 0.8

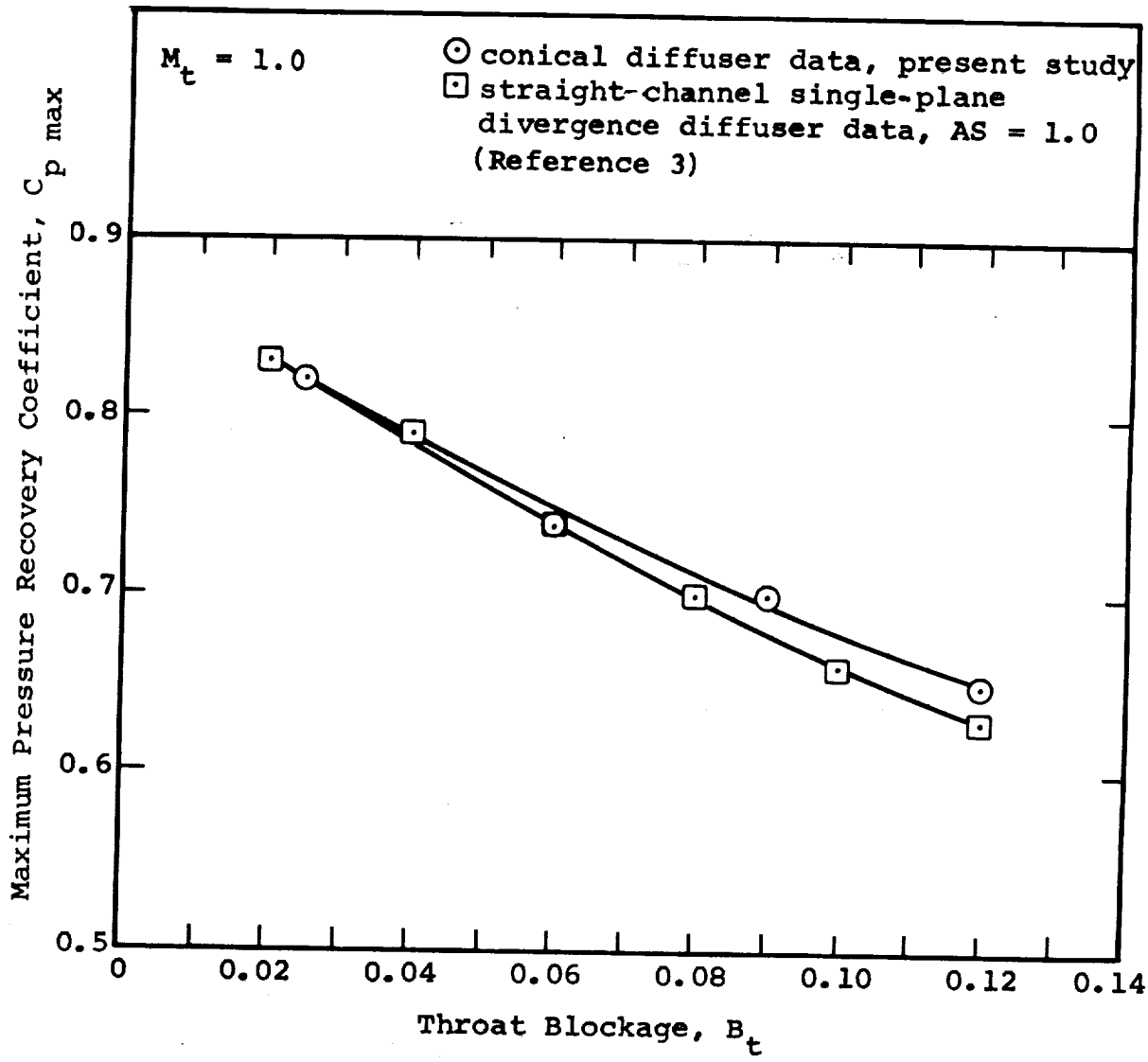


Figure 80 - Maximum Pressure Recovery of Conical and Square Diffusers - $M_t$ = 1.0

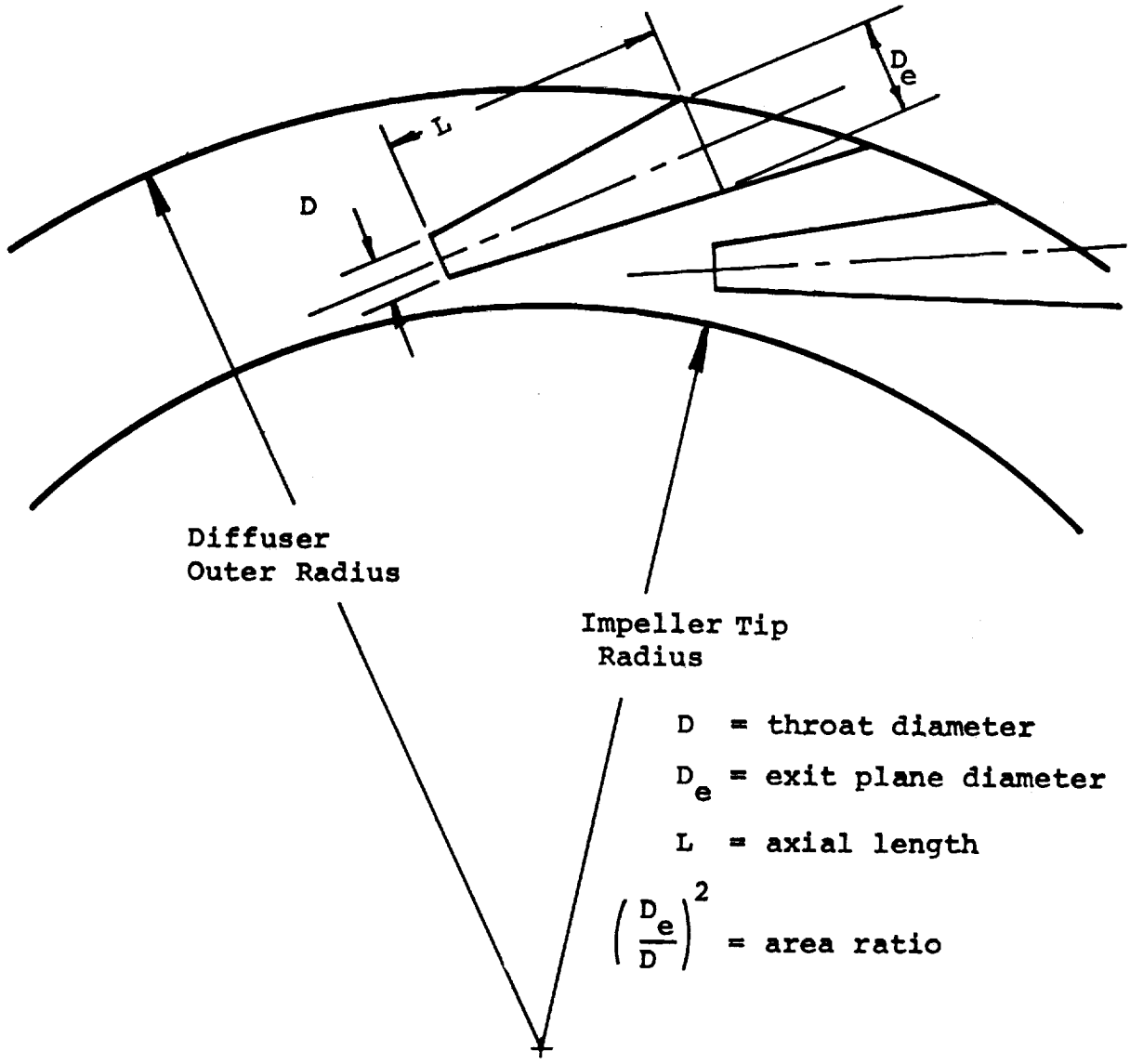


Figure 81 - Centrifugal Compressor Diffuser Geometry

18, and for the cone it is 25, although there is only a slight increase (order of 2 to 3 points) in the conical's recovery above L/D ≈ 18. The area ratios for which optimum performance is obtained for each type of diffuser is significantly different, however. The conical area ratios are much larger than those for the single-plane-divergence diffuser. However, in centrifugal compressor design, unless a very large number of channel diffusers is to be used (which is usually not the case) area ratio is not critical. Thus, there should be little reason for selecting one form of diffuser over the other.

Other considerations, however, may weigh in favor of a conical type design. Ease of manufacture and ability to hold close dimensional tolerances may make the conical more favorable than a single-plane-divergence diffuser.

For some compressor applications, the relatively small variation in pressure recovery contours with $B_t$ and $M_t$ on the performance map for conical diffusers, compared to rather significant changes for the single-plane-divergence diffusers, may make the conical a more suitable choice. For example, at design speed, a channel diffuser may operate with $B_t = 0.08$ and $M_t = 1.0$ at choke conditions, but change to $B_t \geq 0.12$ and $M_t \approx 0.6$ near surge. The sketch below displays the variation in performance for both a conical and a square entry, single-plane-divergence diffuser optimized near the $M_t = 1.0$ flow. The single-plane-divergence diffuser may lose as much as 7 points or more in recovery between choke and surge while the conical diffuser would lose only about 4 points. Thus, a significant difference in channel diffuser recovery, and hence compressor stage efficiency, would be obtained between the two types of diffusers.

Other design problems, such as designing for fixed area ratio, etc., are adequately discussed in the literature (e.g. References 8 and 11). The implications of other design constraints can be readily deduced from the set of diffuser maps provided from this work.

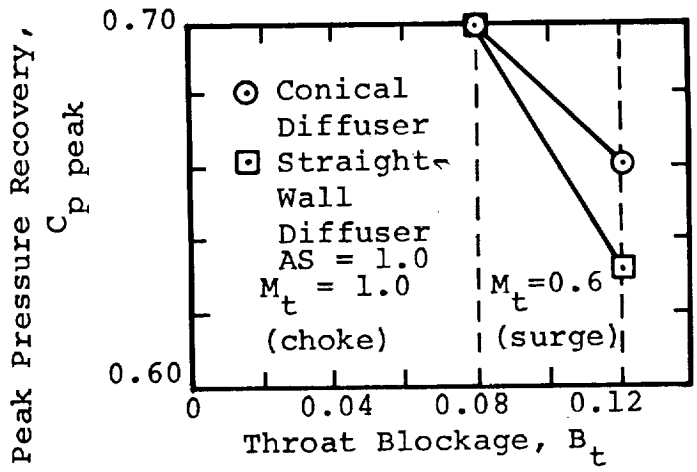


Non-Conical Study

Four diffusers having non-conical area schedules were also tested in this program. As discussed earlier, these non-conicals fall into the broad categories of trumpet-shapes and bell-shapes. Pressure recovery and blockage data were measured over the full range of subsonic inlet Mach numbers at a single throat total pressure, $P_{ot}$ = 109 kN/m$^2$. The results of these special tests are shown in Figures 82 through 89 as plots of $C_p$ vs $M_t$.

Figures 82 through 85 present the results for the diffusers with a length to throat diameter ratio L/D = 8 and area ratio AR = 3.4, while Figures 86 through 89 are for the longer L/D = 12 diffusers with area ratios of 5.1. In each case, the performance of the non-conicals is compared to the performance of conical diffusers having the same L/D and AR, and for the same inlet conditions, $M_t$, $B_t$ and $Re_D$.

For the shorter length, the bell-shaped diffuser shows better performance than either the cone or trumpet at the lower Mach numbers. As $M_t$ is increased, the performance of the bell decreases, until at $M_t$ = 1.0 it is below that of the other geometries. The trumpet and cone maintain nearly constant $C_p$ across the range of $M_t$ for fixed $B_t$, varying less than 4 points in recovery from minimum to maximum. The differences in $C_p$, at any $M_t$, among the three geometries decreases with in-increasing $B_t$, being less than about 4 points at $B_t$ = 0.12.

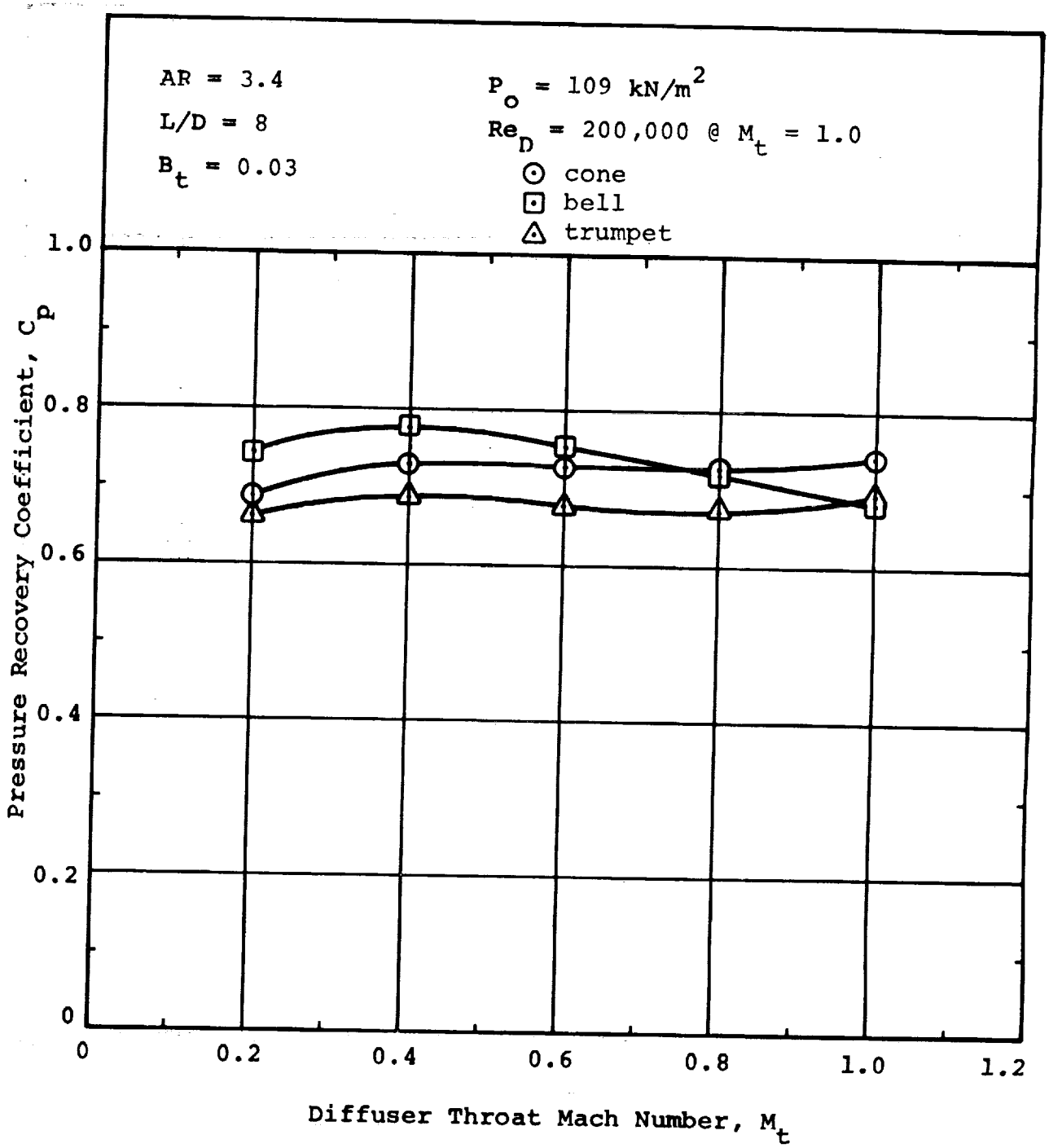


Figure 82 - Non-Conical Diffuser Performance
AR = 3.4, $B_t$ = 0.03

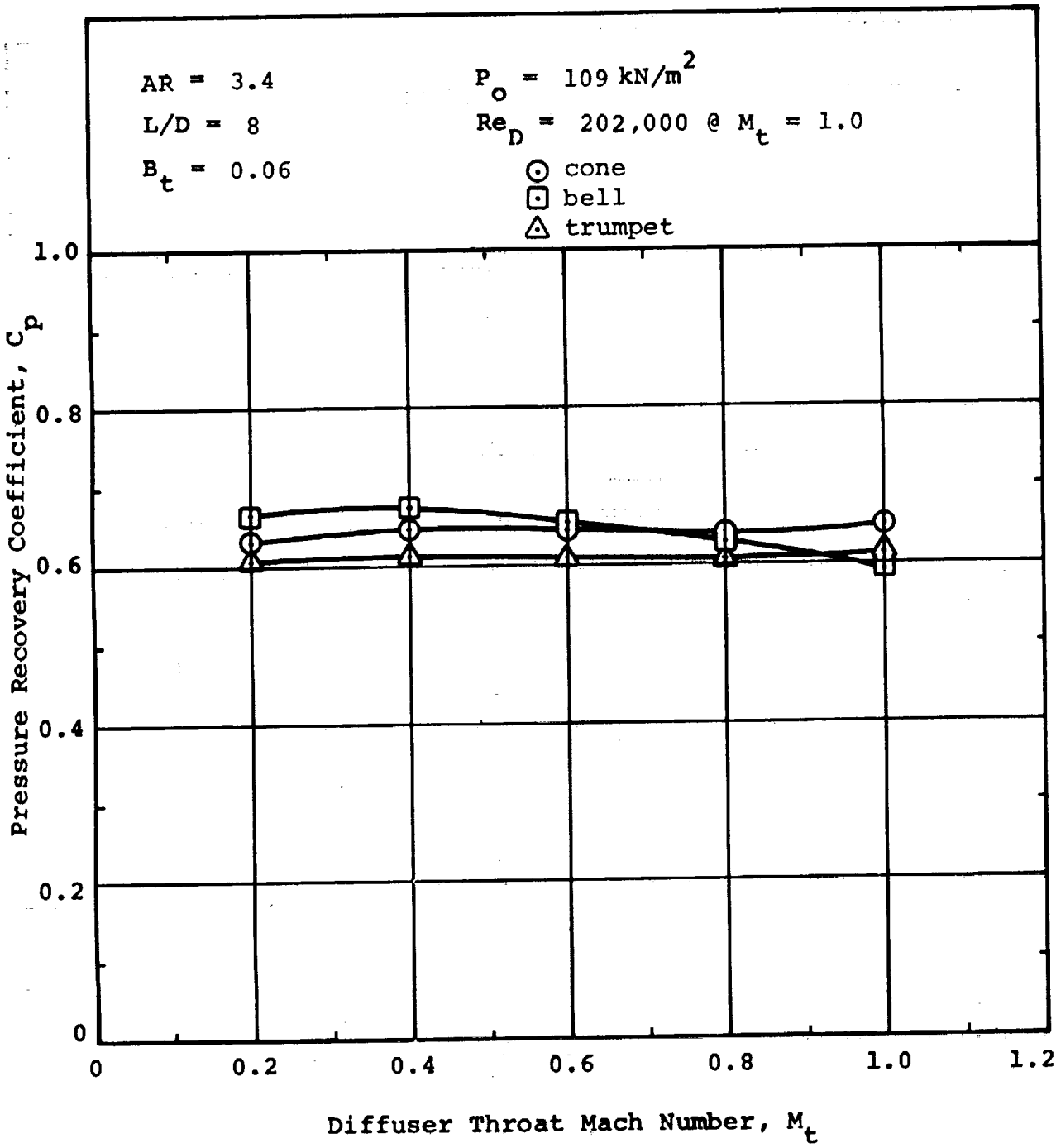


Figure 83 - Non-Conical Diffuser Performance
AR = 3.4, $B_t$ = 0.06

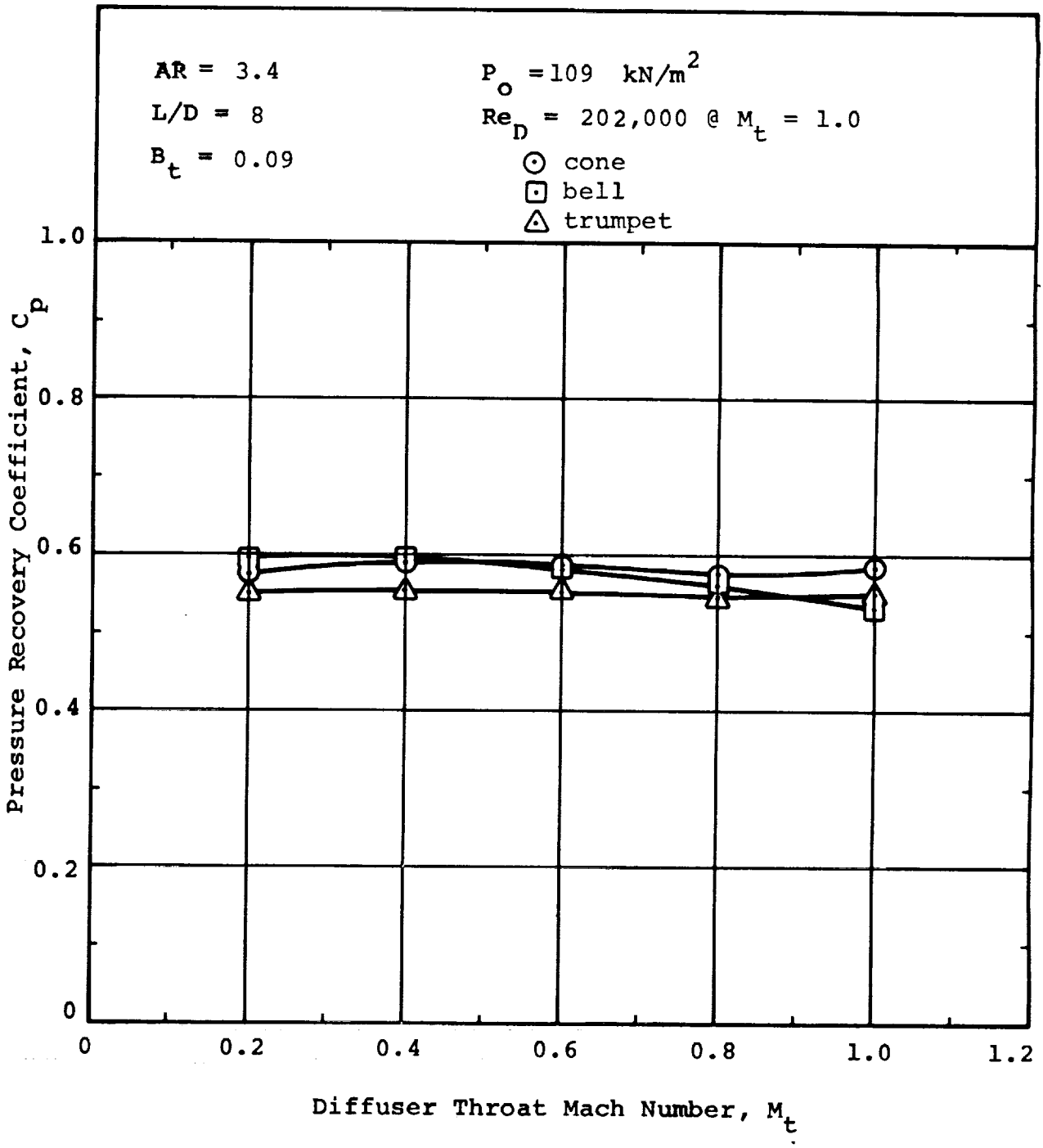


Figure 84 - Non-Conical Diffuser Performance
AR = 3.4, $B_t$ = 0.09

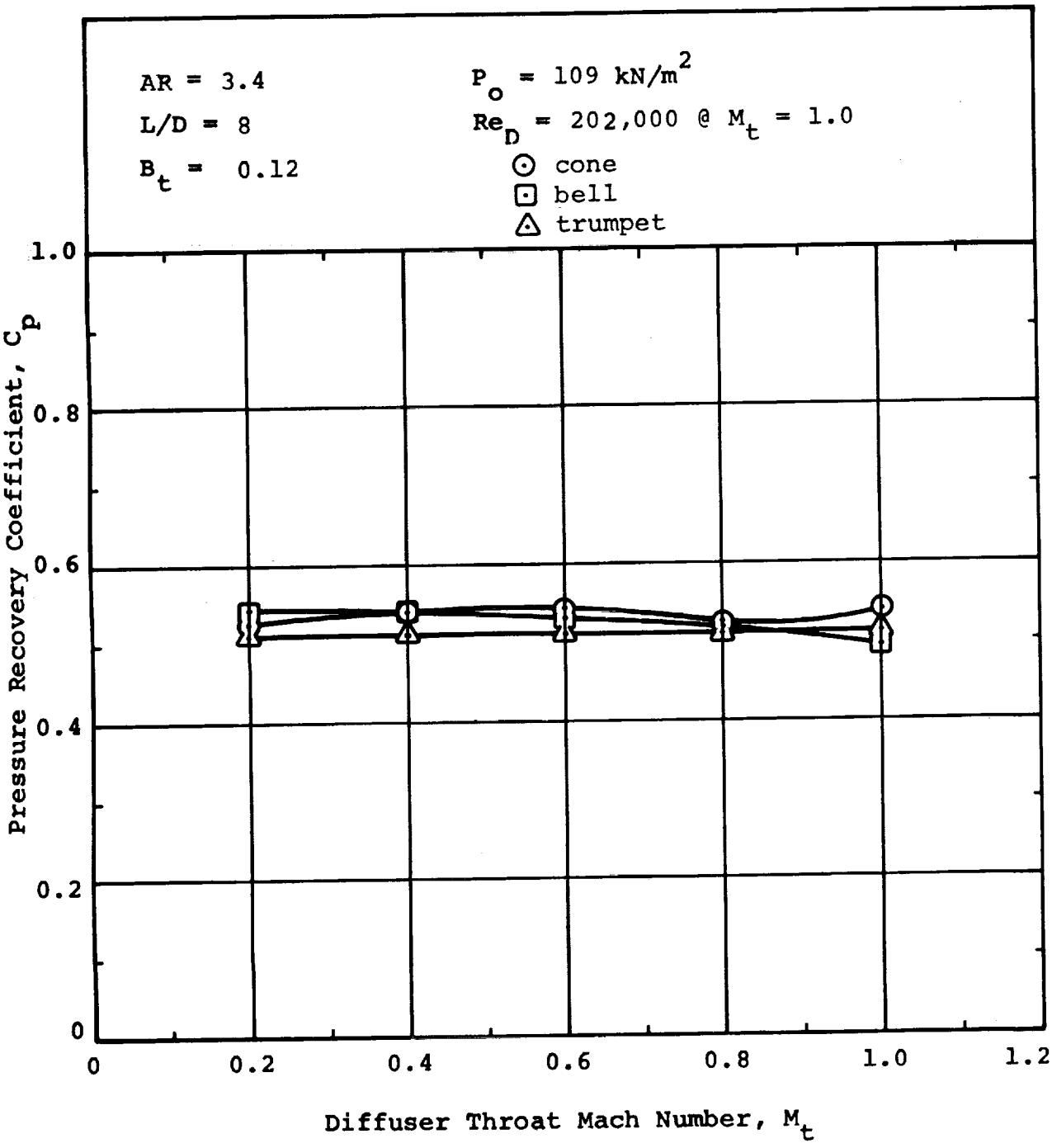


Figure 85 - Non-Conical Diffuser Performance
AR = 3.4, $B_t$ = 0.12

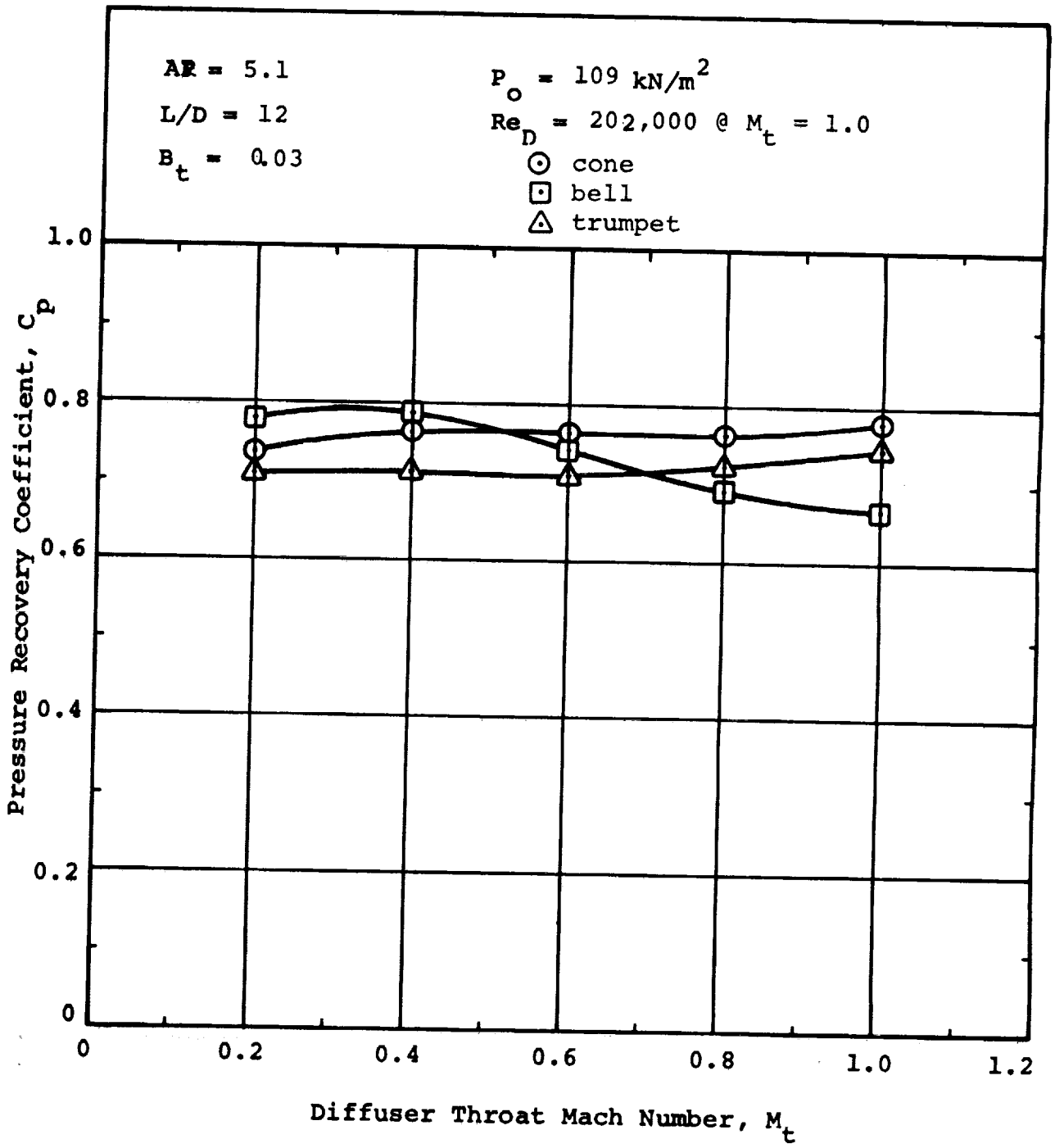


Figure 86 - Non-Conical Diffuser Performance
AR = 5.1, $B_t$ = 0.03

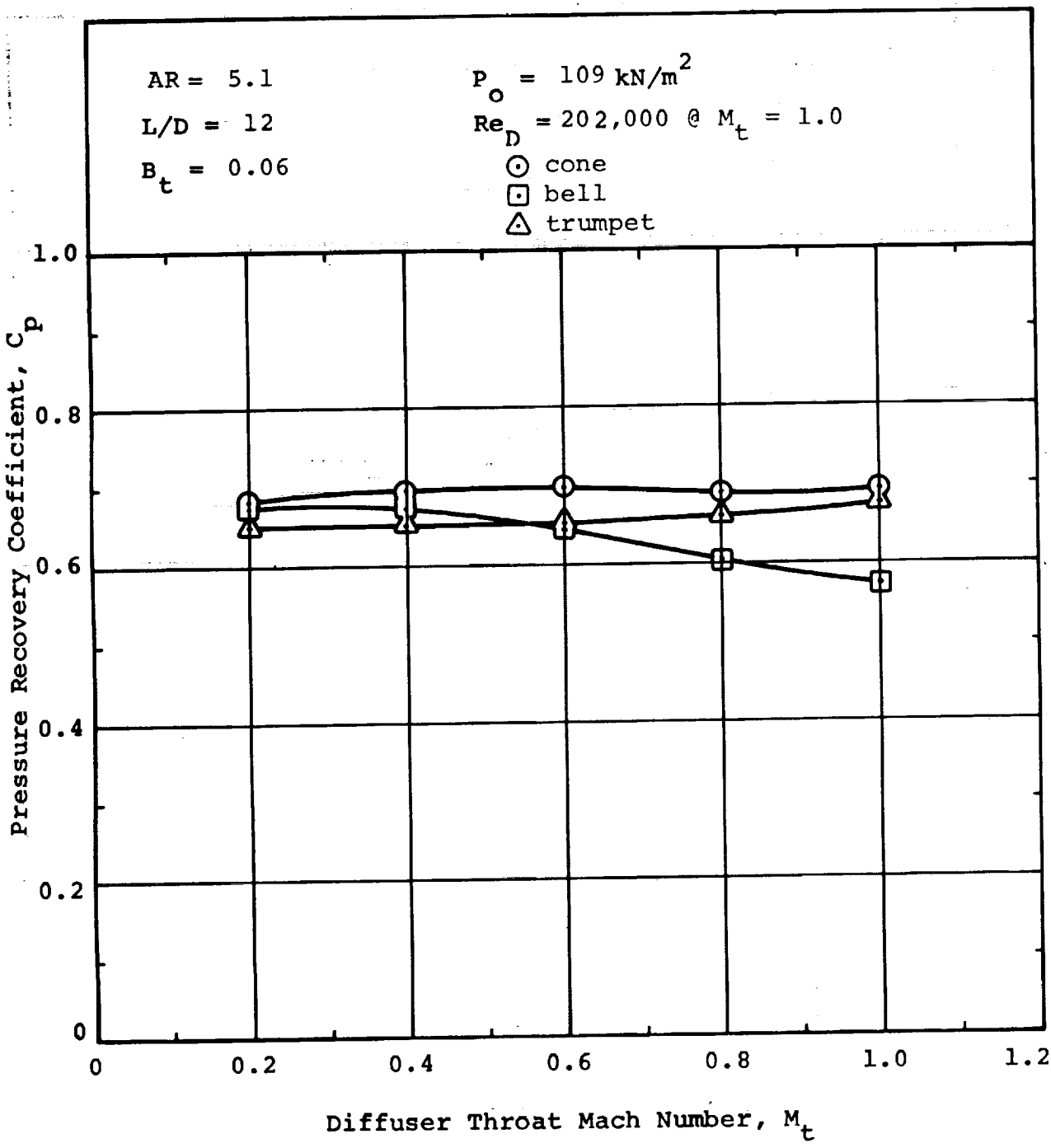


Figure 87 - Non-Conical Diffuser Performance
AR = 5.1, $B_t$ = 0.06

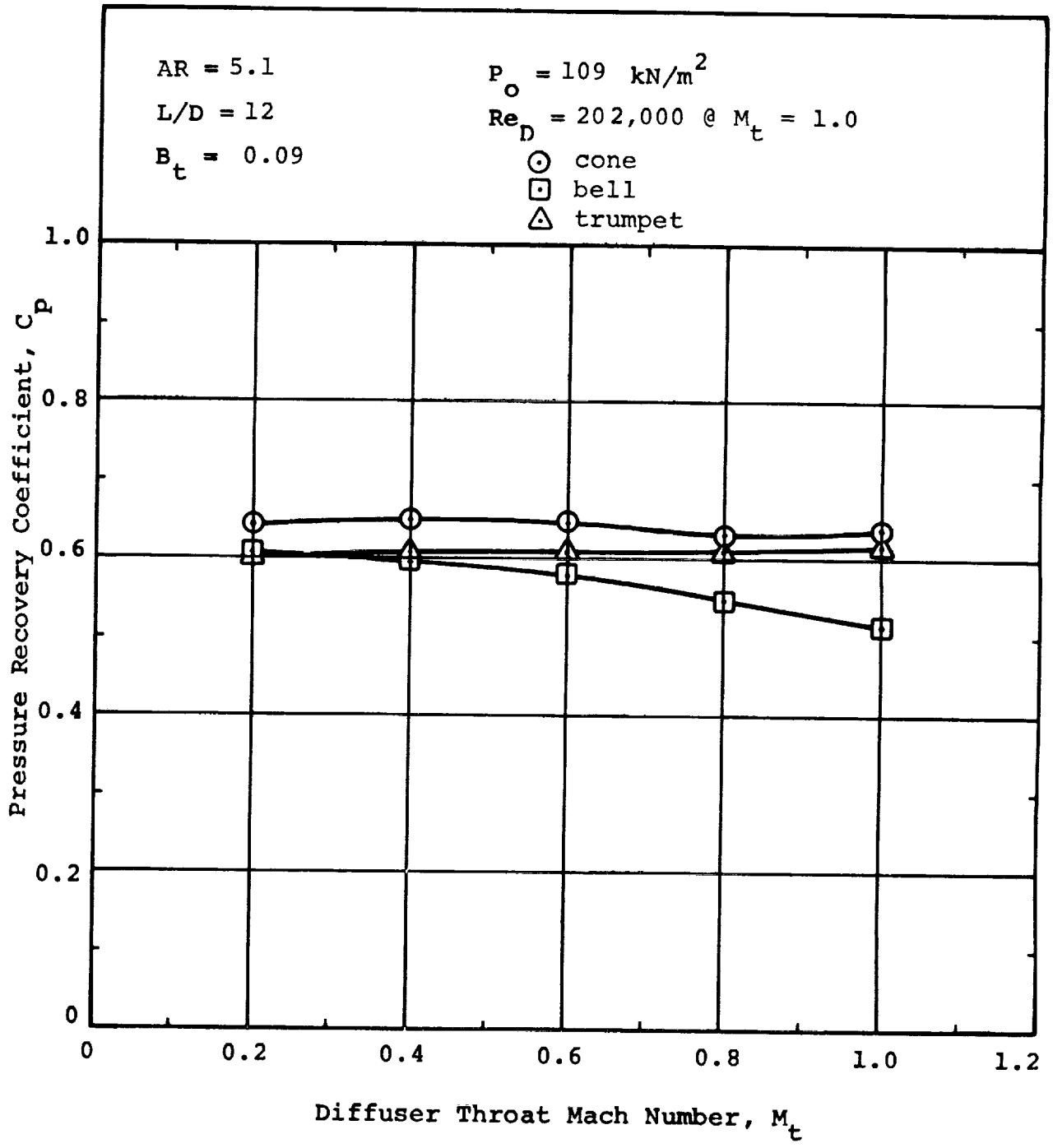


Figure 88 - Non-Conical Diffuser Performance
AR = 5.1, $B_t$ = 0.09

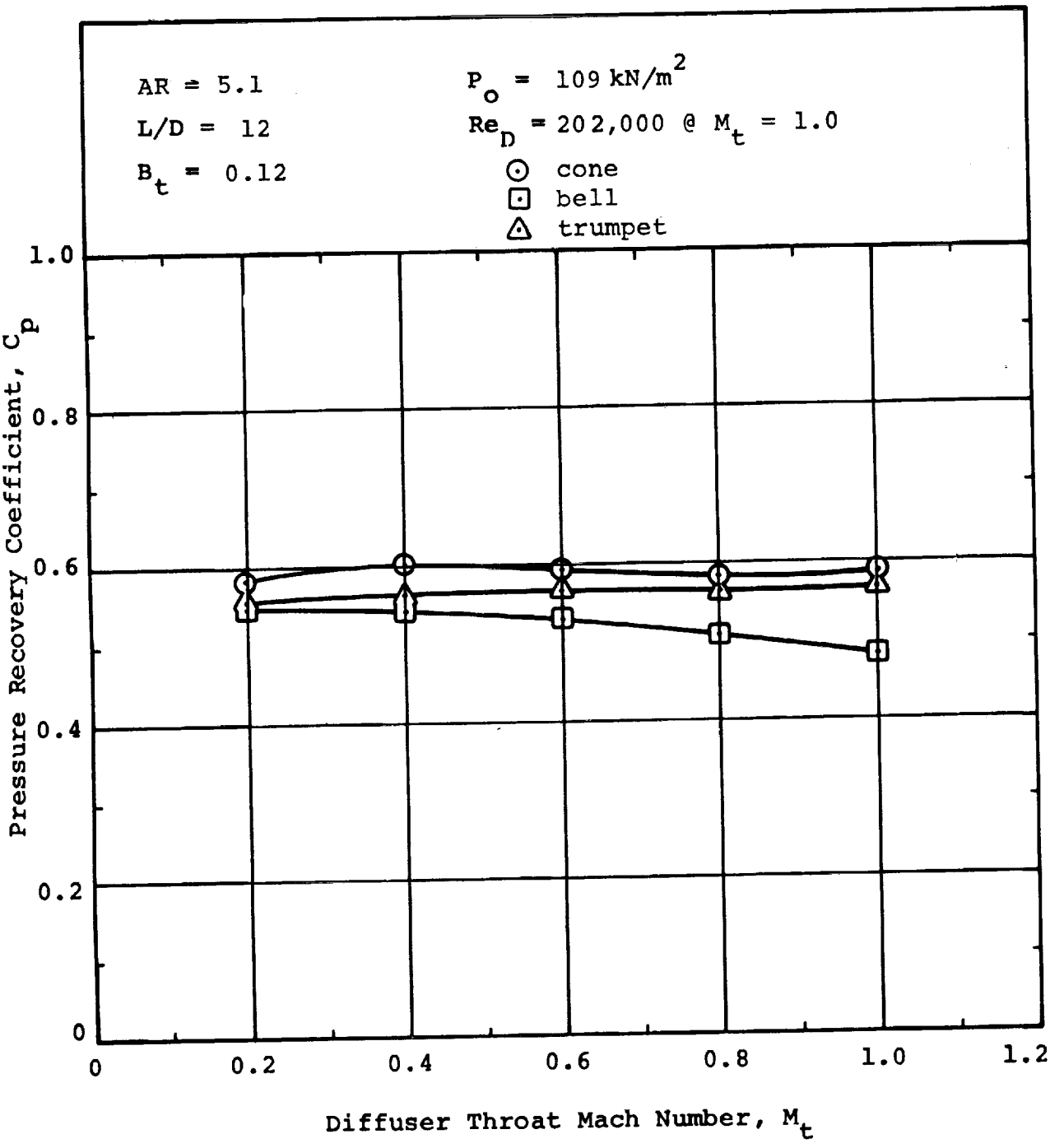


Figure 89 Non-Conical Diffuser Performance
AR = 5.1, $B_t$ = 0.12

In the case of the L/D = 12 diffusers, the bell again shows a decreasing $C_p$ as $M_t$ is increased. And, as $B_t$ is increased the level of performance of the bell drops much more rapidly than for the other diffusers. At $B_t$ = 0.12, the bell demonstrates the poorest performance at all Mach numbers. Again, the cone and trumpet exhibit nearly "flat" performance curves, as for the L/D = 8 data.

Other investigators (Reference 4) have made measurements on various classes of diffusers in which the wall shape has been varied, but the full performance maps for these generic types of diffusers are not available. Thus, it is difficult to know if the changes in performance are the result of an improved (or poorer, as the case may be) class of diffuser design or whether they merely reflect a change in the performance map contours.

To our knowledge, the only other reasonably detailed evaluation of the effects of wall shape on subsonic diffuser performance is that reported by Carlson, et al (Reference 6). In that program, the pressure recovery performance of two-dimensional diffusers was measured for a wide range of geometries, covering the unstalled and stalled flow regimes. The major conclusions drawn in that program related the performance of the contoured wall diffusers to the behavior of the flow.

Although flow behavior was not specifically investigated in the present program, we can infer the location of the "stall line" for conical diffusers from their performance maps. From examination of the maps we see that conical diffusers having L/D = 8 and 12 and AR = 3.4 and 5.1, respectively, lie in the unstalled to lightly stalled flow regimes. Then, by analogy with the two-dimensional work of Carlson, et al, we can say that the bell and trumpet geometries tested also lie close to their respective stall lines, the location of the line being determined in large part by the inlet flow conditions, particularly blockage.

Several conclusions drawn in the two-dimensional study also apply to the results of the present investigation.

a) The bell-shaped diffuser gives slightly better performance in unstalled and lightly stalled

flows than either the straight-wall or trumpet-shape.

b) For fully stalled flows (higher $B_t$ and longer L/D) the highest recovery is attained with the straight-walls, i.e. the conical diffuser.

c) There is little advantage, in terms of gains in pressure recovery, in contouring the walls of diffusers of circular cross section.

## CONCLUSIONS

Pressure recovery performance maps for the conical diffuser have been presented. These data include a range of diffuser geometries sufficient to show the ridge of optimum recovery and to indicate the maximum pressure recovery attainable. Inlet Mach numbers from incompressible flow ($M_t$ = 0.2) to choke ($M_t$ = 1.0) are surveyed over the range of Reynolds numbers and inlet blockage of interest to centrifugal compressor diffuser design.

As in the study of diffusers of other types, inlet blockage is the most significant parameter controlling diffuser pressure recovery. Fifteen to twenty points in pressure recovery can be lost in going from $B_t$ = 0.03 to 0.12 for a given diffuser configuration, all other conditions being held constant.

Mach number and Reynolds number have a small effect, compared to blockage effects, on the pressure recovery map contours.

Conical and single-plane-divergence, plane-wall diffusers have almost identical pressure recovery performance when compared on the basis of maximum pressure recovery coefficient for identical conditions of inlet blockage, throat Mach number and throat Reynolds number.

No significant gain in performance is realized as a result of contouring the walls of the conical diffuser to the bell and trumpet shapes.

The results displayed in this report provide a firm base for the design of conical diffusers and the data should be applicable to a range of fluid dynamic problems.

## APPENDIX A

## CONVERSION FROM MEASURED PRESSURE RECOVERY TO CALCULATED PRESSURE RECOVERY

The definitions of measured and calculated pressure recovery coefficient are given below:

$$C_{pm} = \frac{p_e - p_t}{p_{ot} - p_t} \tag{25}$$

and,

$$C_{pc} = \frac{p_e - p_t}{\bar{p}_{ot} - p_t} \tag{26}$$

where:

$C_{pm}$ and $C_{pc}$ are the measured and calculated pressure recovery coefficients, respectively

$p_e$ is the diffuser exit plane static pressure

$p_t$ is the static pressure at the diffuser throat

$p_{ot}$ is the throat total pressure as measured by the inlet plenum total (static) pressure

$\bar{p}_{ot}$ is a "mass-averaged" throat total pressure defined as the total pressure required to pass the actual mass flow through the given throat geometric area at a specified total temperature.

Then,

$$\frac{C_{pc}}{C_{pm}} = \frac{p_{ot}/p_t - 1}{\bar{p}_{ot}/p_t - 1} \tag{27}$$

Assuming an isentropic flow:

$$\frac{p_{ot}}{p_t} = \left(1 + \frac{k-1}{2} M_t^2\right)^{\frac{k}{k-1}} \tag{28}$$

and,

$$\frac{\bar{p}_{ot}}{p_t} = \left(1 + \frac{k-1}{2}\bar{M}_t^2\right)^{\frac{k}{k-1}} \tag{29}$$

where:

$M_t$ is the throat center line or maximum Mach number

$\bar{M}_t$ is a "mass-averaged" throat Mach number.

We can also express the mass flow in terms of $\bar{M}_t$ and $M_t$:

$$\dot{m}_{actual} = p_t (1 - B_t) A_t \sqrt{\frac{kR}{T_{ot}}} M_t \sqrt{1 + \frac{k-1}{2} M_t^2} \tag{30}$$

and,

$$\dot{m}_{actual} = p_t A_t \sqrt{\frac{kR}{T_{ot}}} \bar{M}_t \sqrt{1 + \frac{k-1}{2} \bar{M}_t^2} \tag{31}$$

Equating (30) and (31) and rearranging gives:

$$(\bar{M}_t)^2 = -\left(\frac{1}{k-1}\right) + \sqrt{\left(\frac{1}{k-1}\right)^2 + M_t^2 (1-B_t)^2 \left(\frac{2}{k-1} + M_t^2\right)} \tag{32}$$

Thus it is seen that $\bar{M}_t$ is a function only of $M_t$ and $B_t$ and so the relation between $C_{pc}$ and $C_{pm}$ can be expressed as a function of $M_t$ and $B_t$. Figure 90 shows this relation.

Given the measured performance $C_p$ ($C_{pm}$) for a diffuser with the throat blockage $B_t$ and centerline (maximum) Mach number $M_t$, the calculated pressure recovery coefficient $C_{pc}$ may be determined, without the need to present a second complete set of performance maps.

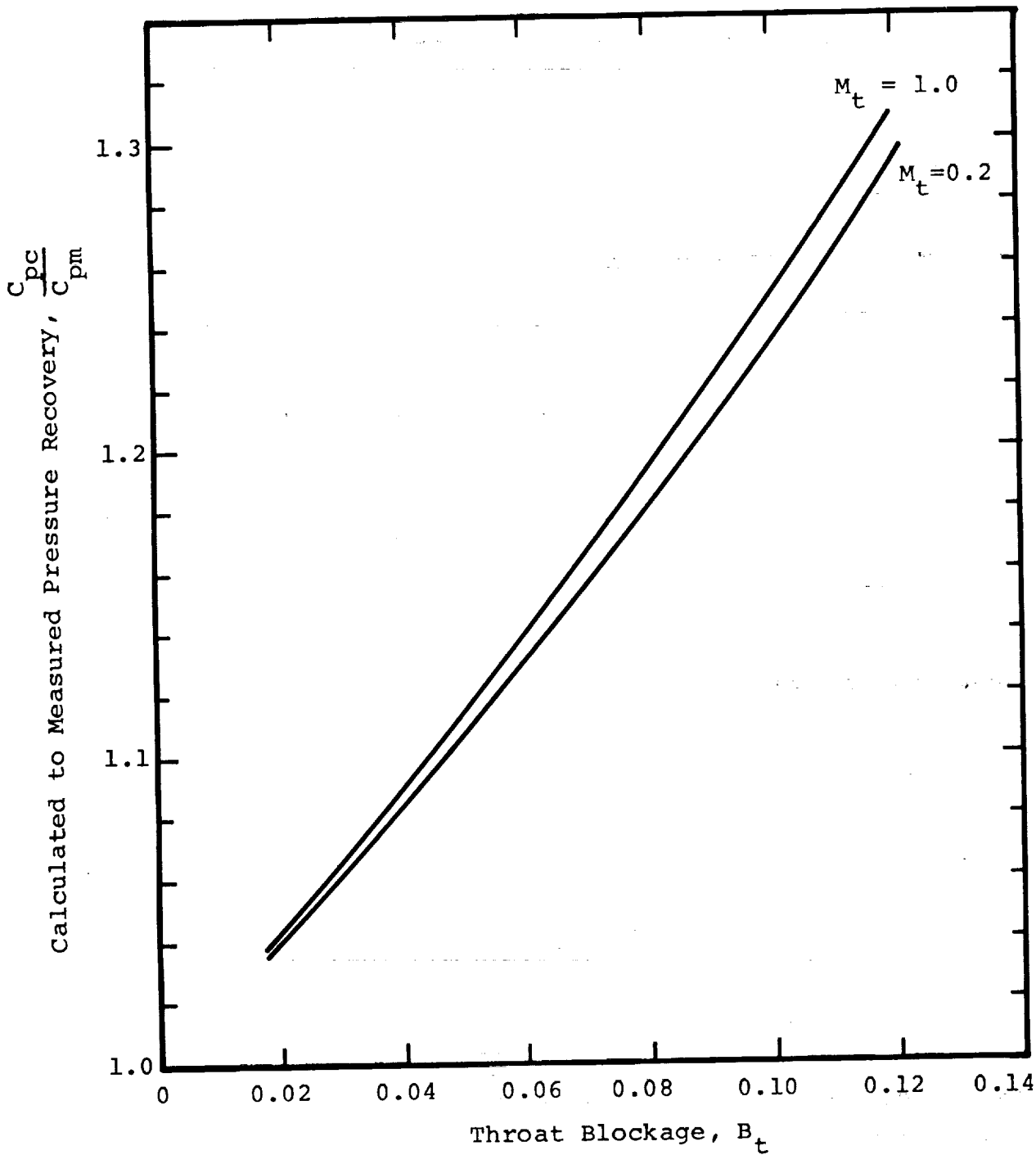


Figure 90 - Comparison Between Calculated and Measured Pressure Recovery

## APPENDIX B

## SPECIAL TREATMENT AND INTERPRETATION OF BLOCKAGE DATA

Diffuser throat blockage is the single most important inlet parameter investigated in this program affecting the performance of the conical diffuser. Consequently, the blockage data have been carefully examined for accuracy, and special tests and calculations were performed in order that the correct interpretations be made when using these results.

The analysis of the blockage data falls into three main areas:

1) averaging of measured blockage data to obtain mean values for given inlet conditions,

2) comparing theoretical predictions with measured performance, and

3) correlating blockage data to determine the nature of the boundary layer at the throat.

### Data Averaging

For all tests in which the diffuser inlet conditions are similar ($p_{ot}$, $T_{ot}$, $M_t$ and geometry) the boundary layer growth, hence the blockage, is expected to be equal. In practice, instrumentation and operator error can result in some scatter in the measured variables. Assuming that this scatter is random in nature (there is no justification for any other assumption) we can use statistical techniques to determine the mean values of the blockage data and to say something about the uncertainty in these mean values.

The measured blockage data for identical inlet conditions were averaged to determine a mean value, and the uncertainty (at 20:1 odds) calculated as twice the standard deviation. This was done for each combination of the inlet geometry, $p_{ot}$, and $M_t$ used, and the results are shown in Figures 6, 7 and 8. Each mean value is the average of some 16 to 25 data points, depending on the number of diffuser geometries tested and the number of repeat runs. These blockage data are plotted at the

mean values of throat Mach number, since the scatter in $M_t$ at each nominal value is small.

The calculated uncertainty intervals are indicated by the bars around the mean values. As may be seen, the maximum spread in any of these data is approximately plus or minus 1.5 points in blockage (0.015). In general, the scatter decreases with increasing $M_t$. This trend is expected, since the two pressure readings which affect $B_t$ to the greatest extent, flow meter differential and throat pressure referenced to $p_{ot}$, increase with $M_t$ thereby decreasing the effect of small, fixed errors.

For the purposes of cross-plotting pressure recovery as a function of blockage, $B_t$, values were extracted from the $B_t$ vs $M_t$ curves at $M_t$ = 0.2, 0.4, 0.6, 0.8 and 1.0 for fixed inlet conditions. In only a few cases was it necessary to interpolate between $M_t$ values to get the average throat blockage, and the uncertainty from this is assumed to be small since the interpolations in $M_t$ were very small.

Of greater consequence was the need to extrapolate the $C_p$ vs $B_t$ curves in order to obtain $C_{p_2}$ data at $B_t$ = 0.03. For example, in Figure 6 ($p_{ot}$ = 54.5 kN/m$^2$) the blockage for the shortest inlet length varies from about 0.075 at $M_t$ = 0.2 to 0.05 at $M_t$ = 1.0. This means that extrapolations as large as 4.5 points in blockage were needed at the lowest Mach numbers. In order to minimize the extent of extrapolation here, a series of sixteen tests were run to measure performance and blockage at $p_{ot}$ = 54.5 kN/m$^2$, with a modified inlet geometry. For these tests the boundary layer "trip" block was removed, and the diffuser throat block was directly coupled to the discharge of the inlet nozzle. The results of these tests are shown as the single mean value of $B_t$ = 0.0534 at $M_t$ = 0.2.

Fortunately, the trends in $C_p$ vs $B_t$ were usually quite clear and so the uncertainty associated with this extrapolation

is believed to be small. By drawing several curves through each set of data for which the extrapolation was questionable, the "spread" in $C_p$ at $B_t = 0.03$ was estimated. Using this method, it has been estimated that the maximum uncertainty in $C_p$ associated with the extrapolation is plus or minus 0.75 points in recovery (0.0075) for the $p_{ot} = 54.5$ kN/m$^2$ data. For the two higher $p_{ot}$ levels (109 and 218 kN/m$^2$) the spread is less than plus or minus 0.5 points (0.005) in recovery. These uncertainties apply only for data at $B_t = 0.03$.

## Theoretical Blockage Calculations

From the theory of the growth of turbulent boundary layers, blockage would be expected to decrease with increasing Mach number (actually increasing $Re_D$ with $p_{ot}$ and $T_{ot}$ fixed) for a constant inlet length. As may be seen in the $C_p$ vs $B_t$ data (Figures 6, 7 and 8) several curves show $B_t$ increasing with $M_t$, counter to the expected trend. Instrumentation errors were considered as a possible cause for this behavior, but review of the raw data, transducer calibrations and the data acquisition procedures eliminated this possibility. If the problem had been caused by instrumentation errors, the same general shape would be evident in the $B_t$ vs $M_t$ curves for all inlet lengths at the same $p_{ot}$. The basis for this reasoning is that the same combination of transducers is used at any Mach number, independent of inlet length.

The only other plausible explanation for these trends is that the boundary layer was not always turbulent (or fully turbulent) at the inlet to the diffusers. That is, for some combinations of inlet length and $p_{ot}$, a laminar boundary layer persists up to the throat of the diffuser at low $M_t$. And as $M_t$ is increased, transition of the boundary layer from laminar to turbulent flow occurs in the inlet section, resulting in a higher blockage at the throat, since a turbulent boundary layer grows faster than a laminar one for the same conditions.

In order to verify this conclusion, a compressible, laminar and turbulent boundary layer calculation program was used to predict the effect of transition on the throat blockage. Built into this program was a routine for predicting the onset of boundary layer transition as a function of turbulence level and pressure gradient. This transition criterion is based on methods proposed by Dunham (Reference 10).

Figure 91 compares the results of the calculations with the experimentally determined values of blockage, for $p_{ot}$ = 54.5 kN/m$^2$. Similar results were obtained for calculations at the other $p_{ot}$ levels. The $B_t$ vs $M_t$ contours in Figure 91 all have the same general shape, i.e. $B_t$ decreasing with increasing $M_t$ and then an increase in $B_t$ when the boundary layer undergoes transition, followed by a second region of decreasing $B_t$. For the inlet length of 15.5 cm, the increase in measured $B_t$ over the range of $M_t$ = 0.2 to $M_t$ = 0.4 is very pronounced, but is not as evident for the other lengths. However, because data were taken only at $M_t$ values of 0.2, 0.4, 0.6, 0.8 and 1.0, it is conceivable that the data spanned this transition point because of the fixed $M_t$ acquisition intervals. This fact is also indicated from the theoretical $B_t$ curves.

To further verify the existence of the "bumps" in the $B_t$ vs $M_t$ contours, several special tests were run for the longest inlet length (15.5 cm), at $p_{ot}$ = 54.5 and 218 kN/m$^2$ and $M_t$ = 0.1, 0.2, 0.3 and 0.4. Three replications were made for each setup. The results of these tests are shown in Figure 92, along with the previously shown theoretical and experimental $B_t$ vs $M_t$ data. Good agreement is seen between the theory and the experimental results.

Based on these results, it is obvious that putting a "best fit" curve through the $B_t$ vs $M_t$ data would likely lead to an incorrect interpretation of the blockage data. Thus, use of these data is limited to the throat Mach number values at which it was acquired and any attempt to interpolate

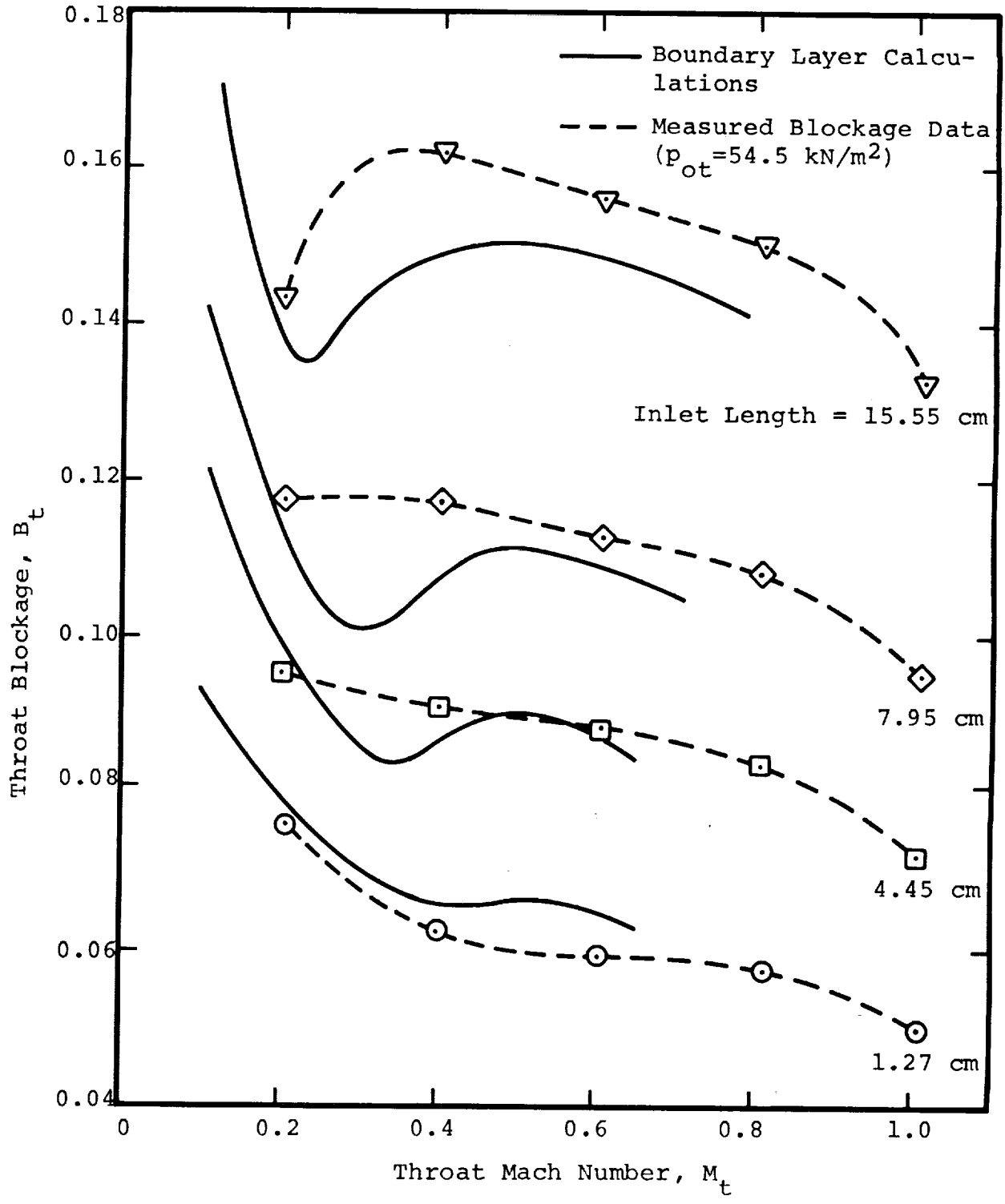


Figure 91 - Comparison Between Theoretical and Measured Blockage Data - $p_{ot}$ = 54.5 kN/m$^2$

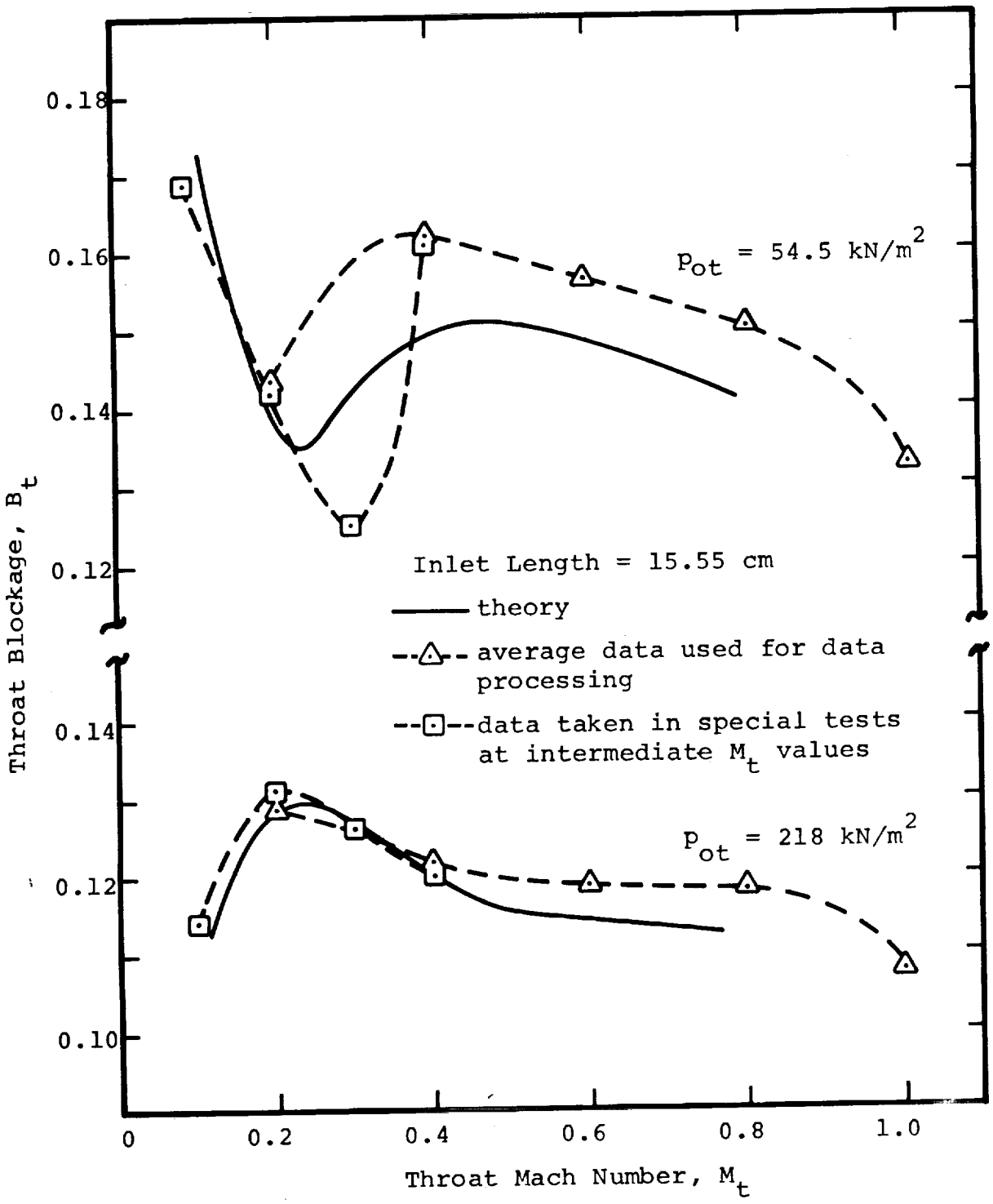


Figure 92 - Comparison Between Theoretical and Measured Blockage Data at Intermediate Mach Numbers

between these points could be misleading.

## Interpretation of Data

Another consequence of this inlet boundary layer transition phenomenon is that the boundary layer at the diffuser throat is apparently laminar for some cases and turbulent in others. For those cases in which transition has not occurred upstream of the geometric throat, the sudden area change there would promote transition and give a turbulent boundary layer in the diffusing passage. Figure 75 shows the range of $B_t$ vs $M_t$ values at which the transition occurs for the three $p_{ot}$ levels. These curves are based on results from predictions of boundary layer growth which most nearly approximated the measured blockage data. It is seen that all $C_p$ data for which $M_t$ is greater than 0.7 are for a turbulent boundary layer at the diffuser throat.

## APPENDIX C

## SYMBOLS

| | |
|---|---|
| $A$ | cross-section area, $m^2$ |
| $A_{effective}$ | "one-dimensional" flow area, $m^2$ |
| $A_{geometric}$ | throat geometric area, $m^2$ |
| AR | area ratio = $(D_e/D_t)^2$ |
| AS | aspect ratio = b/W |
| B | blockage = 1 - $A_{effective}/A_{geometric}$ |
| b | diffuser depth, m |
| $C_d$ | flow nozzle discharge coefficient, dimensionless |
| $C_p$ | pressure recovery coefficient = $(p_e-p_t)/(p_{ot}-p_t)$ |
| $C_{pc}$ | "calculated" pressure recovery coefficient (eqs.13&26) |
| $C_{pm}$ | "measured" pressure recovery coefficient = $C_p$ |
| $C_{pmax}$ | maximum pressure recovery |
| D | diameter, m |
| d | diameter, m (eq. 3, also flow meter throat diameter) |
| k | ratio of specific heats, dimensionless |
| L | diffuser centerline length, m |
| $M_t$ | throat Mach number (eq. 8) |
| $\dot{m}_{actual}$ | measured mass flow = $\dot{m}_a$, kg/sec |
| $\dot{m}_{ideal}$ | "ideal" mass flow = $\dot{m}_i$, kg/sec (eq. 10) |
| n | exponent (eqs. 5 and 24) |
| p | static pressure, $kN/m^2$ |
| $p_{atm}$ | atmospheric pressure, $kN/m^2$ |
| $p_{inlet}$ | flow nozzle inlet pressure, $kN/m^2$ |
| $p_o$ | stagnation pressure, $kN/m^2$ |

| | |
|---|---|
| $\bar{p}_o$ | "mass-averaged" stagnation pressure, $kN/m^2$ (eq.13) |
| R | gas constant, J/kg °K |
| $Re_{crit}$ | critical transition Reynolds number = $x_{crit}V/\nu$ |
| $Re_D$ | diffuser throat Reynolds number = $DV/\nu$ |
| $Re_d$ | flow nozzle Reynolds number = $dU/\nu$ |
| $Re_x$ | unit length Reynolds number = $xV/\nu$ |
| $T_{inlet}$ | flow nozzle inlet temperature, °K |
| $T_o$ | total temperature, °K |
| U | flow meter velocity, m/sec |
| V | throat centerline "core" velocity, m/sec (eq.12) |
| W | diffuser width, m |
| x | axial distance along flow centerline, m |
| $x_{crit}$ | axial length at transition, m |
| y | coordinate system axis, m (eq. 3) |
| $\Delta p_{nozzle}$ | flow nozzle differential pressure, $kN/m^2$ |
| $\alpha$ | shape factor for non-conical diffusers, dimensionless (eq. 6) |
| $\delta^*$ | boundary layer displacement thickness, m |
| $2\theta$ | diffuser divergence angle, degrees |
| $\nu$ | fluid kinematic viscosity, $m^2/sec$ |
| $\pi$ | 3.14159... |
| $\sigma$ | standard deviation, dimensionless |

Subscripts

| | |
|---|---|
| a | actual |
| c | calculated |
| e | exit |
| i | ideal |
| m | measured |

| | |
|---|---|
| o | stagnation |
| t | throat |

## REFERENCES


1. Dean, Robert C., Jr.; THE FLUID DYNAMIC DESIGN OF ADVANCED CENTRIFUGAL COMPRESSORS; TN-153, Creare Incorporated, September 1972.

2. Means, James L., Glance, Paul C. and Klassen, Hugh A.; ANALYTICAL INVESTIGATION OF CONICAL DIFFUSERS; NASA TMX-2605, August 1972.

3. Runstandler, Peter W.,Jr.; PRESSURE RECOVERY PERFORMANCE OF STRAIGHT-CHANNEL SINGLE-PLANE DIVERGENCE DIFFUSERS AT HIGH MACH NUMBERS; TN-88, Creare Incorporated, USAAVLABS TR 69-56, AD865300, October 1969

4. Rohlik, Harold E., Kofskey, Milton G. and Nusbaum, William, J.; RADIAL INFLOW TURBINE PERFORMANCE WITH AN EXIT DIFFUSER DESIGNED FOR LINEAR STATIC PRESSURE VARIATION; NASA TMX-52890, September 1970.

5. American Society of Mechanical Engineers; FLUID METERS - THEIR THEORY AND APPLICATION; Fifth Edition, 1959.

6. Carlson, J. J., Johnston, J. P. and Sagi, C. J.; EFFECTS OF WALL SHAPE ON FLOW REGIMES AND PERFORMANCE IN STRAIGHT,TWO-DIMENSIONAL DIFFUSERS; Journal of Basic Engineering, Transactions of the ASME, Series D, Vol. 89, 1967, pp. 151-160.

7. Dean, Robert C,Jr.; AERODYNAMIC MEASUREMENTS; Gas Turbine Laboratory, Massachusetts Institute of Technology, 1953 (out of print, available from University Microfilms, Ann Arbor, Michigan).

8. Reneau, L.R., Johnston, J.P. and Kline, S. J.; PERFORMANCE AND DESIGN OF STRAIGHT, TWO-DIMENSIONAL DIFFUSERS; ASME Paper No. 66-FE-10, 1966.

9. Launder, Brian, E.; LAMINARIZATION OF THE TURBULENT BOUNDARY LAYER; Massachusetts Institute of Technology, Gas Turbine Laboratory, Report No. 77, November 1964.

10. Dunham, J.; PREDICTIONS OF BOUNDARY LAYER TRANSITIONS ON COMPRESSOR BLADING; National Gas Turbine Establishment, September 1971, AGARD, Paris, 1972.

11. Sovran, Gino and Klomp, Edward D.; Experimentally Determined Optimum Geometries for Rectilinear Diffusers with Rectangular, Conical or Annular Cross-Section; FLUID MECHANICS OF INTERNAL FLOW; Gino Sovran, Editor, Elsevier Publishing Co., 1967.

*U.S. GOVERNMENT PRINTING OFFICE: 1973-738-151/9